

**MICROFLUIDIC SYSTEM FOR DETECTING
MALARIA-INFECTED RED BLOOD CELLS
USING IMPEDANCE MEASUREMENT
COUPLED WITH ELECTROMAGNETIC FORCE**



A Thesis Submitted in Partial Fulfillment of the Requirements
for the Degree of Master of Engineering in Biomedical Engineering
Common Course
FACULTY OF ENGINEERING
Chulalongkorn University
Academic Year 2020
Copyright of Chulalongkorn University

ระบบของไหลจุลภาคเพื่อการตรวจเซลล์เม็ดเลือดแดงที่ติดเชื่อมมาลาเรีย
โดยใช้การตรวจวัดอิมพีแดนซ์ร่วมกับแรงแม่เหล็กไฟฟ้า



วิทยานิพนธ์นี้เป็นส่วนหนึ่งของการศึกษาตามหลักสูตรปริญญาวิศวกรรมศาสตรมหาบัณฑิต
สาขาวิชาวิศวกรรมชีวเวช ไม่สังกัดภาควิชา/เทียบเท่า
คณะวิศวกรรมศาสตร์ จุฬาลงกรณ์มหาวิทยาลัย
ปีการศึกษา 2563
ลิขสิทธิ์ของจุฬาลงกรณ์มหาวิทยาลัย

ประเภทพรรณ สอนฤทธิ์ : ระบบของไหลจุลภาคเพื่อการตรวจเซลล์เม็ดเลือดแดงที่ติดเชื้อมาลาเรียโดยใช้การตรวจวัดอิมพีแดนซ์ร่วมกับแรงแม่เหล็กไฟฟ้า. (MICROFLUIDIC SYSTEM FOR DETECTING MALARIA-INFECTED RED BLOOD CELLS USING IMPEDANCE MEASUREMENT COUPLED WITH ELECTROMAGNETIC FORCE) อ.ที่ปรึกษาหลัก : รศ. ดร.อลงกรณ์ พิมพ์พิณ, อ.ที่ปรึกษาร่วม : รศ. น.สพ. ดร.มรกต แก้วธรรมสอน

มาลาเรียเป็นหนึ่งในโรคที่คุกคามชีวิตมนุษย์มากที่สุดโรคหนึ่งที่เกิดจากปรสิตมีชื่อว่าพลาสโมเดียม มาลาเรียสามารถป้องกันและรักษาได้ ด้วยการติดตามความรุนแรงของโรคอย่างใกล้ชิดจะช่วยจัดการการแพร่กระจายโรคได้ด้วยและการตรวจจับอย่างรวดเร็วด้วยความแม่นยำสูงจะช่วยให้กระบวนการกำจัดโรคมีประสิทธิภาพมากขึ้น ในงานวิจัยนี้ เราแนะนำเทคนิคใหม่ซึ่งใช้ระบบของไหลจุลภาคที่อาศัยการควบคุมการเคลื่อนที่ของเซลล์เม็ดเลือดด้วยแรงแม่เหล็กไฟฟ้า ร่วมกับการวัดอิมพีแดนซ์เพื่อใช้ตรวจวัดระดับความรุนแรงของโรค โดยเปรียบเทียบค่าอิมพีแดนซ์ที่ระยะสมมาตรจากทางเข้าของช่องทางออก 2 ทาง ซึ่งหนึ่งในนั้นใช้สนามแม่เหล็กไฟฟ้าเพื่อดึงเซลล์ติดเชื้อมาลาเรียให้ไหลออกมากกว่า ดังนั้นค่าอิมพีแดนซ์ของทั้งสองฝั่งจะมีค่าแตกต่างกัน การเปลี่ยนแปลงของอิมพีแดนซ์ที่เกิดขึ้นน่าจะบ่งบอกถึงระดับความรุนแรงของโรคหรือค่าพาราไซต์ที่เมียได้ จากการทดลองเบื้องต้น เราพบว่าระบบสามารถแบ่งจำนวนอนุภาคและปริมาตรของไหลเท่ากันสำหรับทั้งสองช่องทางไหล เมื่อเราใส่สนามแม่เหล็กไฟฟ้าใกล้ช่องทางออกหนึ่ง จำนวนเม็ดแม่เหล็กที่ด้านที่ถูกดึงด้วยสนามแม่เหล็กไฟฟ้าจะมากกว่าอีกช่องทางออกหนึ่ง ในขณะที่การทดลองเม็ดพลาสติกให้ผลลัพธ์เท่ากันในทั้งสองด้าน นอกจากนี้เรายังทดสอบการวัดอิมพีแดนซ์ด้วยความหนาแน่นของเม็ดพลาสติกต่างๆ ซึ่งอยู่ที่ 2×10^5 , 3×10^5 และ 6×10^5 เม็ด/มิลลิลิตร ในการทดสอบแบบสถิต (หยดของเหลวบนอิเล็กโทรด) และ 6×10^5 , 7.5×10^5 และ 1.5×10^6 เม็ด/มิลลิลิตร ในการทดสอบแบบพลวัต (ของไหลไหลต่อเนื่อง) ผลการวิจัยพบว่าความต้านทานเพิ่มขึ้นอย่างมาก ในขณะที่ค่ารีแอกแตนซ์จะเพิ่มขึ้นเล็กน้อยเมื่อเราเพิ่มความหนาแน่นของอนุภาคพลาสติก ในทำนองเดียวกัน เราใช้เลือดของหนูเมาส์ปกติ เลือดที่ติดเชื้อมาลาเรีย 10% และเลือดที่ติดเชื้อมาลาเรีย 44% เป็นตัวอย่างการทดลองของการทดสอบทั้งแบบสถิตและแบบพลวัต ผลการวิจัยพบว่าเราสามารถแยกความแตกต่างของสัญญาณระหว่างเลือดของหนูปกติกับเลือดที่ติดเชื้อมาลาเรียได้ และเมื่อเราใส่สนามแม่เหล็กไฟฟ้าที่ 15V และ 24V ในกรณีของเลือดที่ติดเชื้อมาลาเรีย 44% พบว่ามี การเปลี่ยนแปลงความต้านทานและค่ารีแอกแตนซ์อย่างมากโดยเฉพาะด้านที่ไม่ใส่สนามแม่เหล็ก ในอนาคตเราเชื่อว่าจะสามารถหาอัตราส่วนที่แตกต่างกันเพื่อใช้ระบุความรุนแรงของโรคหรือค่าพาราไซต์ที่เมียได้จากระบบที่พัฒนานี้

จุฬาลงกรณ์มหาวิทยาลัย
CHULALONGKORN UNIVERSITY

สาขาวิชา วิศวกรรมชีวเวช
ปีการศึกษา 2563

ลายมือชื่อนิสิต
ลายมือชื่อ อ.ที่ปรึกษาหลัก
ลายมือชื่อ อ.ที่ปรึกษาร่วม

6170384221 : MAJOR BIOMEDICAL ENGINEERING

KEYWORD: Microfluidics, Parasitemia, Malaria, Impedance, Electromagnetic

Prapapan Sonridhi : MICROFLUIDIC SYSTEM FOR DETECTING MALARIA-INFECTED RED BLOOD CELLS USING IMPEDANCE MEASUREMENT COUPLED WITH ELECTROMAGNETIC FORCE. Advisor: Assoc. Prof. Dr. ALONGKORN PIMPIN, Ph.D. Co-advisor: Assoc. Prof. Dr. MORAKOT KAEWTHAMASORN, (D.V.M.,M.Sc.,Ph.D)

Malaria is one of the most life-threatening diseases caused by Plasmodium parasite. Malaria is preventable and curable, mainly due to the factor of time and management of the spread. In other words, a rapid detection with high accuracy will contribute to more effective treatment process. In this research, we introduced the new technique implemented microfluidics, dealing with the manipulation of blood cells using magnetic force, and impedance measurement measuring the signal changes of electrical impedance between a couple of electrodes. According to the distinct magnetic properties of normal red blood cells and malaria-infected red blood cells, the experiment was designed to compare the impedance of these two blood types at the symmetrical distance along two outlets. One of which used electromagnetic field to pull malaria cells to flow into more than the other. By the capability of distinguishing the signal resolution, the differentiation of changes in impedance would refer to discriminated percentage parasitemia of malaria. From the preliminary experiment, our microfluidic channel could divide similar number of beads and amount of fluid volume for both outlets. When we applied electromagnetic field on only the side near one outlet, the number of magnet beads on that side is greater than the other. Moreover, impedance measurement was tested with various plastic bead density which is at 2×10^5 , 3×10^5 , and 6×10^5 beads/ml in static test, and 6×10^5 , 7.5×10^5 , and 1.5×10^6 beads/ml in dynamic test. These results shared the same trend that the resistance was greatly increased, while the reactance was gradually increased when the density was increased. Similarly, we used normal mouse blood, 10% and 44% parasitemia malaria-infected blood to be our experiment samples in both static and dynamic test. The results showed that the difference of signal between normal mouse blood, 10% and 44% malaria-infected blood could be discriminated when we applied electromagnet at 15V and 24V. In case of 44% malaria-infected blood, significant change in resistance and reactance was found which specially increased in the outlet where magnetic force was not applied. When applied magnetic field, the outlet without the magnetic force had less infected blood cells and lower cell density that has two countering effects on the impedance in such a way that higher and lower resistance would be obtained, respectively. From our experiments, the results suggested the stronger influence of blood type on the impedance as the total resistance increases at this outlet. In the future, after the further development, we hope that the impedance different ratio would more precisely translate into the percentage parasitemia.

CHULALONGKORN UNIVERSITY

Field of Study: Biomedical Engineering
Academic Year: 2020

Student's Signature
Advisor's Signature
Co-advisor's Signature

ACKNOWLEDGEMENTS

I would like to express my deep and sincere gratitude to my advisor Associate Professor Dr. Alongkorn Pimpin who gave me the opportunity to do research and providing invaluable guidance throughout this research. His guidance helped me in all the time of research and writing of this thesis. I cannot express enough thanks to my co-advisor Associate Professor Dr. Morakot Kaewthamasorn who generously gave me knowledge and place to conduct malaria experiments. I would like to express my deepest appreciation to Assistant Professor Dr. Pakpum Somboon for his support, motivation, enthusiasm, and immense guidance. I would like to express my special thanks of gratitude to Assistant Professor Dr. Suramate Chalermwisutkul for his insightful comments to complete this thesis.

Secondly, I would like to special thanks to all members of MEMS & Nanotech Laboratory: Assoc. Dr. Werayut Srituravanich, Dr. Nattapol Damrongplasit, and Dr. Sarita Morakul for their helpful feedback comments. I am also grateful to all my lab mates for supporting me and teaching me how to do proper experiments in order to gain the reliable test results, especially Mr. Pachara Noosawad and Dr.Thammawit Suwannaphan. I would like to thanks to Ms. Apinya Arnuphapprasert from Parasitology unit for helping with malaria culturing.

Finally, I am extremely grateful to my parents for their love, caring and sacrifices for educating and preparing me for my future.

Prapapan Sonridhi

TABLE OF CONTENTS

| | Page |
|--|-------------|
| ABSTRACT (THAI) | iii |
| ABSTRACT (ENGLISH)..... | iv |
| ACKNOWLEDGEMENTS | v |
| TABLE OF CONTENTS..... | vi |
| FIGURE CONTENTS | ix |
| TABLE CONTENTS..... | xii |
| CHAPTER 1 INTRODUCTION..... | 1 |
| 1.1 State of problems..... | 1 |
| 1.2 Objectives | 8 |
| 1.3 Scopes of the study..... | 8 |
| 1.4 Expected outcomes..... | 8 |
| CHAPTER 2 LITERATURE REVIEWS..... | 9 |
| 2.1 Severe malaria | 9 |
| 2.2 Microfluidics for malaria diagnosis..... | 10 |
| 2.2.1 Microfluidic impedance spectroscopy..... | 10 |
| 2.2.1.1 Single-cell microfluidic impedance spectroscopy..... | 11 |
| 2.2.1.2 Bulk suspension microfluidic impedance spectroscopy..... | 17 |
| 2.2.2 Microfluidic coupled with electromagnetic forces..... | 21 |
| 2.3 Summary..... | 24 |
| CHAPTER 3 METHODOLOGY | 25 |
| 3.1 Concepts | 25 |
| 3.2 System designs..... | 26 |
| 3.2.1 Overview | 26 |
| 3.2.2 Components..... | 27 |

| | |
|--|-----------|
| 3.2.2.1 3D-printed connector..... | 27 |
| 3.2.2.2 PDMS microchannel | 29 |
| 3.2.2.3 PCB | 30 |
| 3.2.2.4 Laser-cut acrylic plates..... | 32 |
| 3.2.2.5 Syringe, needle, and tubes | 32 |
| 3.2.3 Equipment | 33 |
| 3.2.3.1 Electromagnet..... | 34 |
| 3.2.3.2 DG8SAQ Vector Network Analyzer..... | 35 |
| 3.3 Summary..... | 36 |
| CHAPTER 4 CALIBRATION AND PRELIMINARY RESULTS | 37 |
| 4.1 Calibration | 37 |
| 4.2 Proof of concept | 42 |
| 4.2 Preliminary Results | 42 |
| 4.3 Summary | 44 |
| CHAPTER 5 RESULTS | 45 |
| 5.1 Plastic test..... | 46 |
| 5.1.1 Static impedance measurement | 46 |
| 5.1.2 Dynamic impedance measurement..... | 47 |
| 5.2 Normal and malaria-infected mouse blood..... | 48 |
| 5.2.1 Static impedance measurement | 50 |
| 5.2.1.1 Normal mouse blood | 50 |
| 5.2.1.2 10% malaria-infected blood | 50 |
| 5.2.2 Dynamic impedance measurement..... | 51 |
| 5.2.2.1 Normal mouse blood | 51 |
| 5.2.2.2 10% malaria-infected blood | 52 |
| 5.2.2.3 44% malaria-infected blood | 53 |
| 5.2.3 Different ratio of infection | 55 |
| 5.3 Summary..... | 58 |

| | |
|--|----|
| CHAPTER 6 CONCLUSION AND FUTURE WORK | 59 |
| 6.1 Conclusion..... | 59 |
| 6.2 Future work | 61 |
| APPENDIX..... | 62 |
| REFERENCES | 68 |
| VITA..... | 71 |



FIGURE CONTENTS

| | | |
|--------------------|---|----|
| Figure 1.1 | Life cycle of malaria | 1 |
| Figure 1.2 | Malaria diagnosis | 2 |
| Figure 1.3 | Hemozoin | 4 |
| Figure 1.4 | Examples of impedance spectroscopy | 5 |
| Figure 1.5 | The overview of microfluidic system for detecting malaria-infected red blood cells using impedance measurement coupled with electromagnetic force | 7 |
| Figure 1.6 | Schematic diagram of cell enrichment part and impedance measurement part | 7 |
| Figure 1.7 | Schematic diagram of impedance measurement part | 8 |
| Figure 2.1 | The impedance of a cell as a function of frequency | 11 |
| Figure 2.2 | The single-shelled spherical model | 12 |
| Figure 2.3 | Foster and Schwan's simplified circuit model for a single cell in suspension | 13 |
| Figure 2.4 | Single cell impedance measurements | 13 |
| Figure 2.5 | Example of single cell measurement | 14 |
| Figure 2.6 | Schematic of the MIC system | 15 |
| Figure 2.7 | The dielectric properties at different hpi (h post-invasion) | 15 |
| Figure 2.8 | Electric impedance microflow cytometry (EIMC) | 16 |
| Figure 2.9 | Dielectric properties in suspension | 17 |
| Figure 2.10 | 3D schematic diagram of the device structure and top view of sensing area | 18 |
| Figure 2.11 | Impedance values in suspension | 18 |
| Figure 2.12 | Portable impedance analyzer developed for malaria diagnosis | 19 |
| Figure 2.13 | Nyquist diagrams obtained for the different assays tested with the proposed impedance analyzer in laboratory conditions (25 °C,2%RH)..... | 20 |
| Figure 2.14 | Dominant forces on a particle in a flow field | 22 |
| Figure 2.15 | Separation paramagnetic and diamagnetic particles/cells | 23 |
| Figure 2.16 | Malaria-infected RBC separation using a high magnetic field gradient | 23 |
| Figure 3.1 | The cell enrichment technique schematic diagram | 25 |
| Figure 3.2 | The part of the system | 26 |
| Figure 3.3 | The components of system | 27 |
| Figure 3.4 | The design of connector | 28 |
| Figure 3.5 | How to gather all components | 28 |
| Figure 3.6 | The size of 3D-printed connector..... | 29 |
| Figure 3.7 | The design of PDMS microchannel | 29 |
| Figure 3.8 | The PDMS microchannel and mold..... | 30 |
| Figure 3.9 | The design of PCB..... | 31 |

FIGURE CONTENTS (Cont.)

| | |
|---|----|
| Figure 3.10 The PCB..... | 31 |
| Figure 3.11 The design of laser-cut acrylic plate | 32 |
| Figure 3.12 The laser-cut acrylic plates | 32 |
| Figure 3.13 The sizes of syringe, needle, and tubes..... | 33 |
| Figure 3.14 The outer and inner diameters of needle and tubes | 33 |
| Figure 3.15 The equipment connection | 34 |
| Figure 3.16 MGE30 specs from misumi | 34 |
| Figure 3.17 The measurement of magnetic induced | 35 |
| Figure 3.18 DG8SAQ VNWA 3 | 35 |
| Figure 3.19 SDR-Kits VNWA model matrix | 36 |
| Figure 4.1 Premium FEMALE SMA SOL 4 pcs Calibration Kit of 12 GHz Parts | 37 |
| Figure 4.2 Female calibration step | 37 |
| Figure 4.3 RC circuit with VNWA Testboard Kit | 38 |
| Figure 4.4 Impedance and Resistance-Reactance signal of resistor 47 Ohms and capacitor 68 pF | 39 |
| Figure 4.5 Impedance and Resistance-Reactance signal of resistor 1 kOhms and capacitor 68 pF | 40 |
| Figure 4.6 Impedance and Resistance-Reactance signal of resistor 10 kOhms and capacitor 68 pF | 41 |
| Figure 4.7 Proof of concept | 42 |
| Figure 4.8 Results in volume of two sides (from repeating 3 times/condition) | 43 |
| Figure 4.9 Results in number of two sides (from repeating 3 times/condition) | 44 |
| Figure 5.1 The impedance measurement part | 45 |
| Figure 5.2 Resistance-Reactance of plastic static test at 100 kHz-10 MHz | 46 |
| Figure 5.3 Resistance-Reactance of plastic static test at 4-10 MHz | 47 |
| Figure 5.4 Resistance-Reactance of plastic dynamic test at 100 kHz-10 MHz | 47 |
| Figure 5.5 Resistance-Reactance of plastic dynamic test at 4-10 MHz | 48 |
| Figure 5.6 How to induce percentage parasitemia in mouse | 48 |
| Figure 5.7 Resistance-Reactance of static test of normal mouse blood at 0x, 5x, and 10x dilution in PBS | 50 |
| Figure 5.8 Resistance-Reactance of static test of 10% malaria-infected blood at 0x, 5x, and 10x dilution in PBS | 51 |
| Figure 5.9 Resistance-Reactance of dynamic test of normal mouse blood at 0V, 15V, and 24V | 52 |
| Figure 5.10 Resistance-Reactance of dynamic test of 10% malaria-infected blood at 0V, 15V, and 24V | 52 |
| Figure 5.11 Resistance-Reactance of dynamic test of 44% malaria-infected blood at 0V, 15V, and 24V | 53 |

FIGURE CONTENTS (Cont.)

| | |
|---|----|
| Figure 5.12 Comparison of normal mouse blood, 10% Malaria-Infected blood, and 44% Malaria-Infected blood when not applied electromagnetic field | 54 |
| Figure 5.13 Comparison of normal mouse blood, 10% Malaria-Infected blood, and 44% Malaria-Infected blood when applied electromagnetic field at 15V | 54 |
| Figure 5.14 Comparison of normal mouse blood, 10% Malaria-Infected blood, and 44% Malaria-Infected blood when applied electromagnetic field at 24V | 55 |
| Figure 5.15 Difference of resistance and reactance at 24V compared each side with average resistance and reactance at 0V | 56 |
| Figure 5.16 Difference of resistance and reactance at 0V and 15V compared both sides | 57 |
| Figure 5.17 Difference of resistance and reactance at 0V and 24V compared both sides | 57 |
| Appendix Figure 1 The previous version of connector | 62 |
| Appendix Figure 2 Smith chart of 10 kHz-10 MHz calibration | 63 |
| Appendix Figure 3 Counting number method | 64 |
| Appendix Figure 4 Giemsa stain procedure | 64 |
| Appendix Figure 5 All fields of 10% parasitemia red blood cells | 65 |
| Appendix Figure 6 All fields of 44% parasitemia red blood cells | 66 |

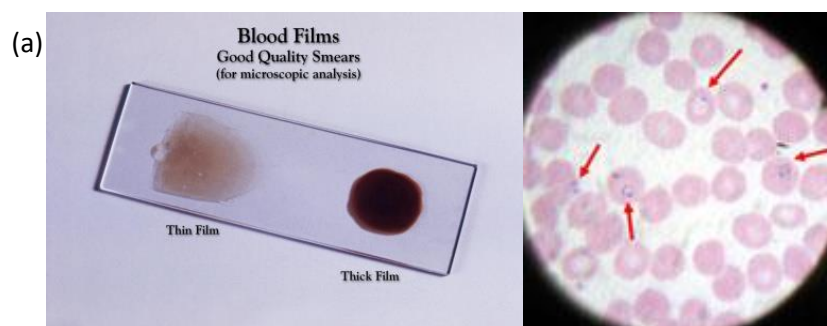
TABLE CONTENTS

| | |
|--|----|
| Table 1.1 Relative magnetic susceptibilities of each type of RBC to water | 4 |
| Table 1.2 Dielectric properties of iRBC and hRBC | 5 |
| Table 2.1 Dielectric properties of i-RBCs and parasite | 16 |



waste substances such as hemozoin pigment, the product of consuming hemoglobin of malaria parasites, and other toxic factors. When malaria-infected red blood cells (iRBCs) in schizont (a last stage of infected red blood cells) split, these toxic substances will trigger mechanisms of managing alien objects to produce the chemicals that lead to fever and other uncomfortable symptoms. Moreover, it may cause other severe malaria-associated pathophysiology [2]. The symptoms of uncomplicated malaria are fever, headaches and body pain, vomiting, and nausea, that will appear within 10 days to 4 weeks after getting infected. However, it is hard to recognize as malaria when the symptoms are absent or mild. If malaria is left untreated after 24 to 48 hours, *P. falciparum* malaria can turn to severe malaria and often lead to death when organs begin to work abnormally and fail. The manifestations of severe malaria include the following: severe anemia (due to destruction of red blood cells), respiratory distress (resulting from pulmonary edema), cerebral malaria (impairment of consciousness, seizures, coma, or other neurologic abnormalities with abnormal behavior), kidney or liver failure, and other complication. Severe malaria is a medical emergency and should be treated immediately and aggressively.

The gold standard of malaria diagnosis is microscopy, which sample is prepared in forms of thick or thin blood film stained with a Giemsa or Wright stain. Medical workers who are responsible for examine malaria, must pass the training before they can work. Therefore, this task requires only well trained and well supervised technicians. Microscopic method can find species identification and percentage parasitemia that play an important role for assessing treatment; but it takes a lot of time (~60 min/slide) as shown in figure 1.2(a). Most importantly, microscopy needs laboratory preparation. Thus, it is not suitable for using in field. In malaria-endemic areas, such as Sub-Saharan Africa and Indian subcontinent, malaria rapid diagnostic tests (RDTs) is presented for faster tests (2-15 minutes) and the ease of use when dealing with a numerous test samples and lacking experts. RDT detects specific malaria antigens in blood to tell us whether suspected patients get infected or not as shown in figure 1.2(b); but it cannot point out stage and percentage parasitemia. The other effective malaria diagnosis is polymerase chain reaction (PCR). PCR is the most sensitive and specific method because it detects malaria cells at the DNA level, even in very small amount of sample as shown in figure 1.2(c). However, this method requires extremely difficult steps that can only test in fully equipped laboratories. For this reason, PCR test is very expensive. For all the above, many scientists try to find the new malaria diagnosis methods to perform faster and more effective test in lower price.



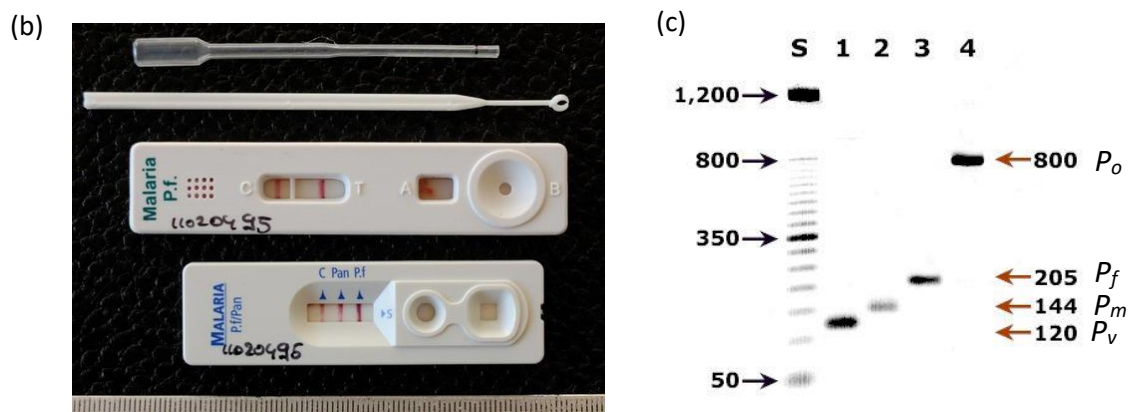


Figure 1.2 Malaria diagnosis. (a) Microscopic diagnosis [3]. (b) malaria rapid diagnostic tests (RDTs) [3]. (c) polymerase chain reaction (PCR) [4].

Microfluidics is the well-known method in order to deal with the fluid in micro- and nanoscales. Therefore, it uses only few microliters of sample and takes just a little time to run the test. Microfluidics plays an important role for malaria diagnosis in terms of analyzing time, portable use, and improving sensitivity. There are many researches of microfluidics, focusing on improving existing diagnostics [5], and developing new microfluidics or paper-fluidics [6] strategies, carry out experiments protein-based tests, nucleic acid tests (NATs), and cell-based detection [7]. Similar to enzyme-linked immunosorbent assays (ELISA) or RDTs, microfluidics using protein-based tests are looking for detecting HRP-2 antigen in malaria cells [5]. On the other hand, microfluidics using nucleic acid tests use molecule techniques, like PCR, to identify specific species of *Plasmodium* parasites [8]. Lastly, microfluidics using cell-based detection utilize the differentiation of malaria-infected red blood cells (iRBCs) developing in 48-multi-h cycles in order to detecting malaria cells.

According to the component of infected red blood cells (iRBCs), there is one substance named hemozoin pigment (or malaria pigment) that occurs when malaria parasites successfully invade in healthy red blood cells (hRBCs), and begin to consume hemoglobin (the protein molecule in red blood cells that carries oxygen or carbon dioxide for exchanging gas between tissue and lung) and leave high quantities of heme (a prosthetic group consisting of an iron) as shown in figure 1.3 [9]. Hemozoin is an insoluble crystalline containing a lot of heme that causes infected red blood cells (iRBCs) to have a stronger magnetic property depends on the developmental stage of the parasite as shown in table 1.1 [10]. Many researchers use this principle in order to manipulate or separate infected red blood cells (iRBCs) and healthy red blood cells (hRBCs). There have many works of this method to increase concentration of malaria cells that will give a better chance for detecting malaria [11]. For example, microscopic malaria tests and RDTs have many false negative test if patient's infection is in initial stage because of few number of infected cell; therefore, increasing number of infected cell is helpful to help the staff finding disease and giving the patient a treat on time. Nevertheless, the significant disadvantage of this method is that the magnetic field decays so fast depending on distance; thus, magnet needs to be close to malaria cells as much as possible.

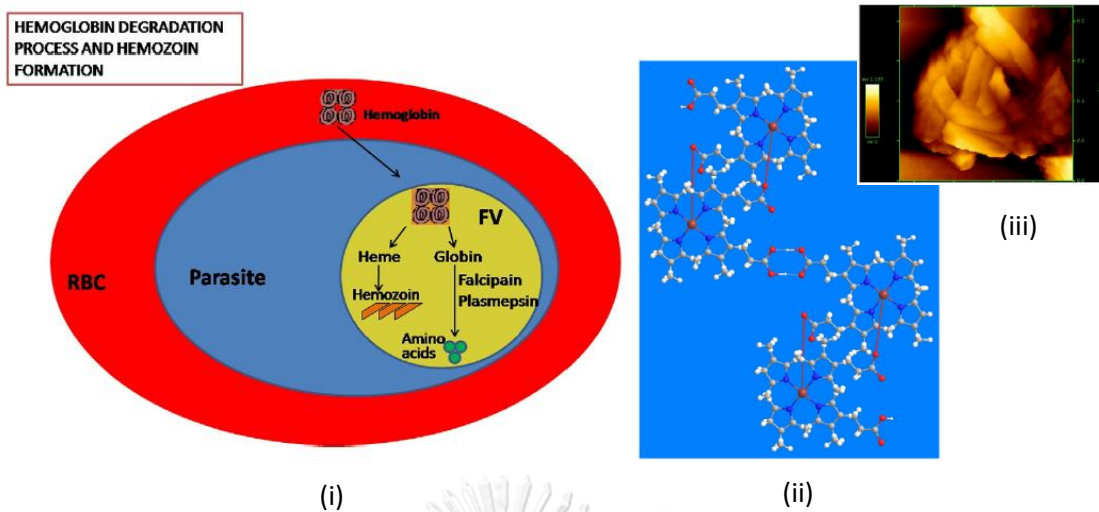


Figure 1.3 Hemozoin. (i) Diagram of hemoglobin degradation and formation of hemozoin inside *P. falciparum* infected erythrocytes. (ii) Chemical arrangement of hemozoin. A) Monomers of hemozoin with iron, shown in gray, will join to form a dimer. B) Crystal moiety with the dimers forming H-bonds with oxygen atoms (red) of contiguous ones. (iii) Atomic force microscopy (AFM) image of *P. falciparum* hemozoin [9].

Table 1.1 Relative magnetic susceptibilities of each type of RBC to water [10].

| Type of RBC | Relative magnetic susceptibilities ($\Delta\chi$) 10^{-6} |
|-----------------------|--|
| hRBC | 0.01 |
| Early ring from-iRBC | 0.82 |
| Late trophozoite-iRBC | 0.91 |
| Schizont-iRBC | 1.80 |

Malaria parasites change not only a size, elasticity, roughness, but also dielectric properties [10] that effect impedance value as shown in table 1.2. One of cell-based detection microfluidics for malaria diagnosis is using impedance analytic technique in order to differentiate the signals of healthy red blood cells (hRBCs) and infected red blood cells (iRBCs), especially the signals of different stages of developing malaria cells and cell counting [12]. Impedance analytic method normally uses the electrode with Impedance measurement instruments or LCR meter (Inductance (L), Capacitance (C), and Resistance (R) meter) to measure impedance value of single cell or bulk suspension (many cells) as shown in figure 1.4. The advantage of single cell impedance measurement is the impedance value of individual cells that we can know exactly stages of malaria cell and its number [13]. Nonetheless, the disadvantages of this measurement are the preparation of single cell suspension that usually has a blood coagulation, the high noise because of containing all individual data, and the

complexity of system. On the other hand, a bulk suspension impedance measurement is easier than single cell suspension for cell preparation and no blood clotting. Furthermore, this measurement can reduce the noise of data because it measures the average impedance value of many cells in sensing area [14]. That is why we cannot know about the stages of infection.

Table 1.2 Dielectric properties of iRBC and hRBC. [10].

| Cell type | Position | Electrical conductivity (S/m) | | Relative dielectric permittivity | |
|-----------|----------|-------------------------------|---------------|----------------------------------|------------|
| | | Host | Parasite | Host | Parasite |
| iRBC | Membrane | $7 \pm 2 \times 10^{-5}$ | $< 10^{-6}$ | 9.03 ± 0.82 | 8 ± 4 |
| | Interior | $(0.95 \pm 0.05)\sigma_m$ | 1.0 ± 0.4 | 58 ± 10 | 70 ± 5 |
| hRBC | Membrane | $< 10^{-6}$ | - | 4.44 ± 0.45 | - |
| | Interior | 0.31 ± 0.03 | - | 59 ± 6 | - |

Remark: σ_m is the electrical conductivity of the suspension medium

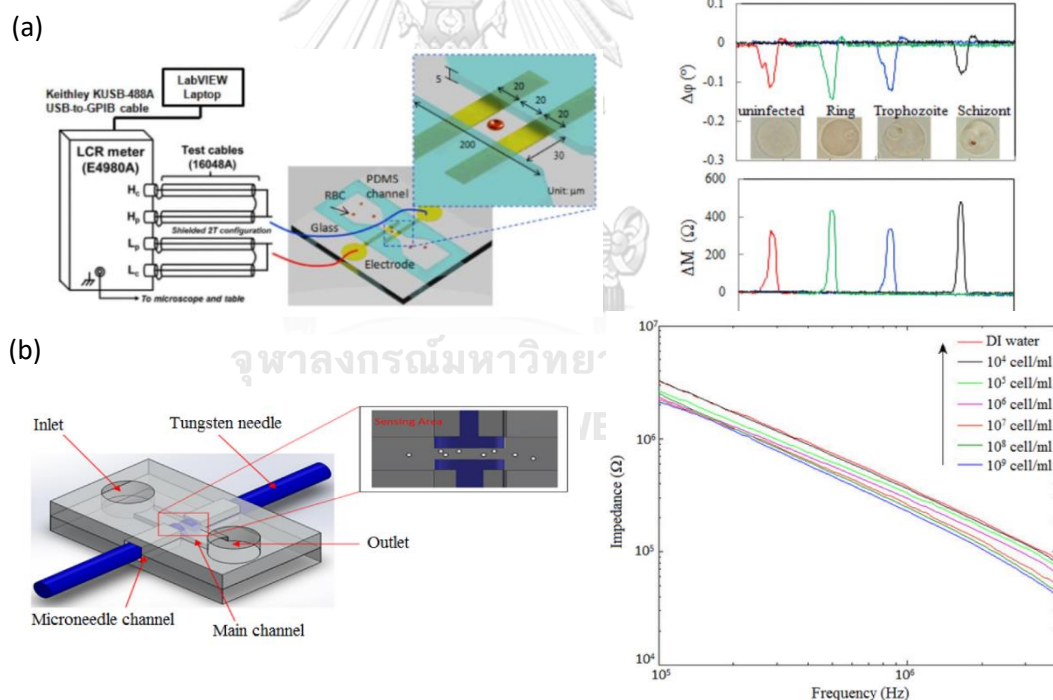


Figure 1.4 Examples of impedance spectroscopy. (a) Single-cell microfluidic impedance spectroscopy [13]. (b) Bulk suspension microfluidic impedance spectroscopy [14].

Compare between the single cell impedance measurement and the bulk suspension impedance measurement, there are different advantages and disadvantages depends on what we want to observe. For instance, if we want to observe the characteristic of impedance in each infection stages, the single cell impedance measurement is the

answer for this task. If we want to just detect whether there are malaria cells or not and approximate number of cells, the bulk suspension impedance measurement is more appropriate for this task. For this research, we have some limitation of production because we want to develop a low-cost system. Therefore, many components of system are commercial-available product, such as electromagnet and Printed Circuit Board (PCB), that are limited sizes. The smallest electrodes that PCB can make is $50\ \mu\text{m}$ (approximately 10 times compared to red blood cells). Thus, we are focusing on bulk suspension impedance measurement. However, like other malaria diagnosis method, if the patients just begin to get infected, the bulk suspension impedance measurement might not be able to find infected cells because of no significant different between infected cells and normal cells. That is the reason why we need to find the other methods to increase concentration of malaria cells for seeing the differences.

This research aims for detecting infected red blood cells (iRBCs) and percentage parasitemia to tell the state of infection by using impedance measurement method combined with electromagnetic force by electromagnet in microfluidic system as shown in figure 1.5. These techniques suit our research in terms of using electromagnetic field that requires the closest distance between electromagnet and the flow of cells, and using impedance analyzer that requires the smallest area of sensing area. In this research, we want to test the malaria infection of suspected patients and the severity of malaria if these patients really get infected. Thus, we choose to use the bulk suspension impedance measurement to be a detector of malaria. Accordingly, we design a one-inlet-and-two-outlet microfluidic microchannel to divide the flow in two ways and identically place microelectrode in Printed Circuit Board (PCB) along these two ways in same sizes and distance. Then, we use electromagnet, that can vary the electromagnetic field by adjusting the current of power supply, to contact in one side of inlet for pulling malaria cells in either way of outlets (as shown in figure 1.6) in order to increase the concentration of malaria cells in one side. The result is supposed to figure out the different impedance value between two outlets that can refer to the infection of malaria and the percentage parasitemia. Furthermore, the difference of electromagnetic field can tell us the state of infection. E.g. when we test samples, we can gradually increase the magnitude of electromagnetic field until seeing the different impedance value. If the sample is low parasitemia, we will use very strong electromagnetic fields in order to see a little different impedance value, similar to non-malaria patients (figure 1.7(a)). On the other hand, if the sample is high parasitemia, we will find some different impedance value at beginning of applying electromagnet and huge difference when using very strong electromagnetic fields as shown in figure 1.7(b).

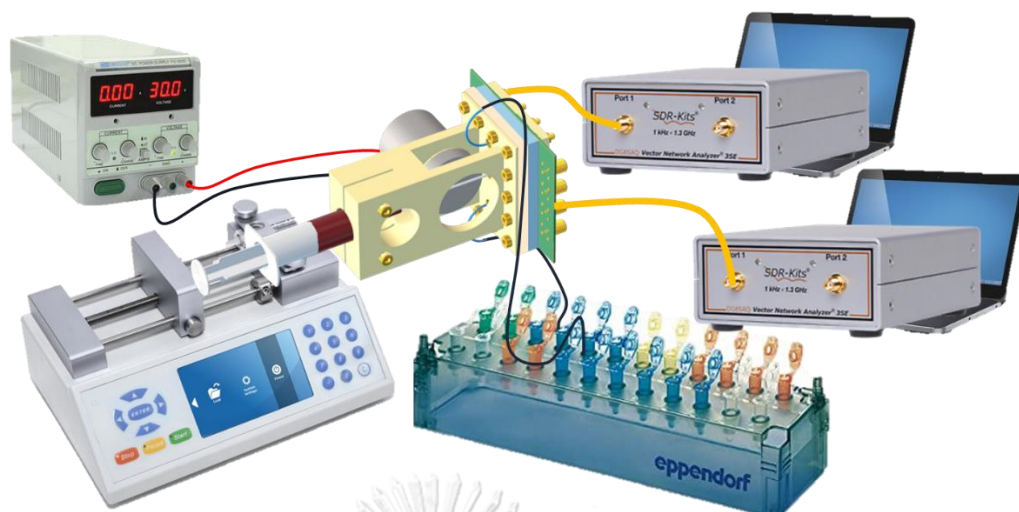


Figure 1.5 The overview of microfluidic system for detecting malaria-infected red blood cells using impedance measurement coupled with electromagnetic force.

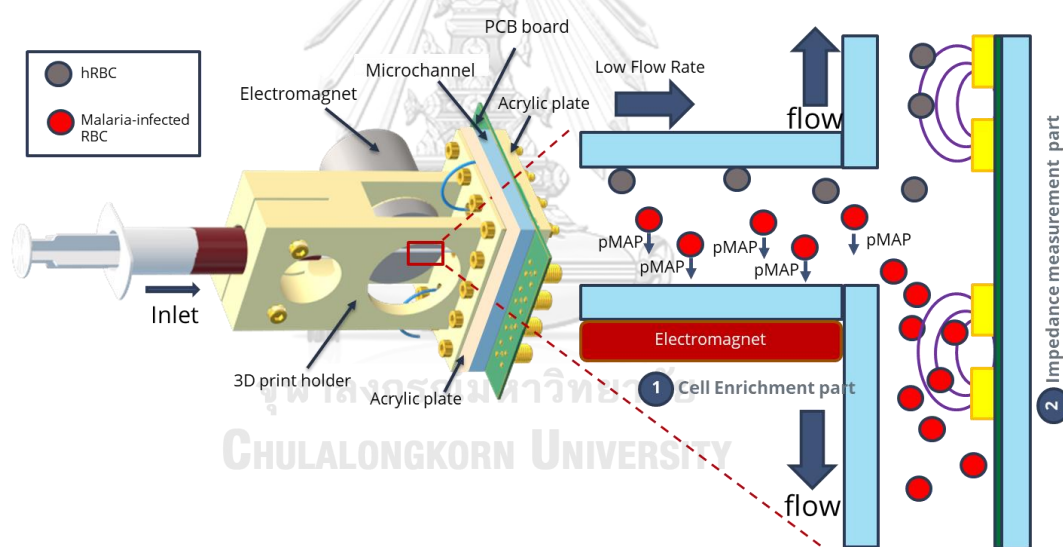


Figure 1.6 Schematic diagram of cell enrichment part and impedance measurement part.

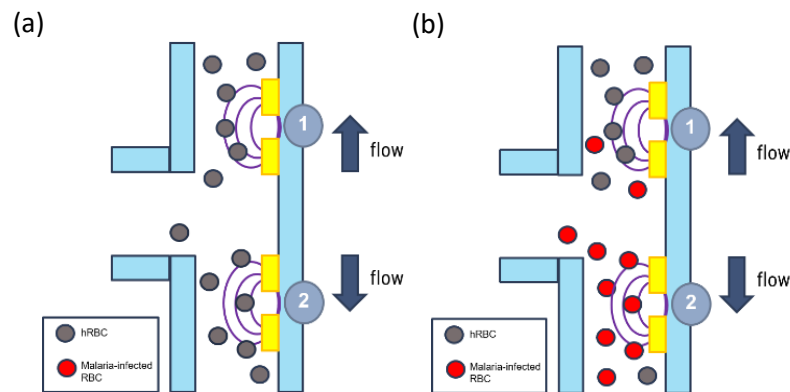


Figure 1.7 Schematic diagram of impedance measurement part (a) Schematic diagram when suspected patients have no parasite. (b) Schematic diagram when suspected patients have high parasitemia.

1.2 Objectives

To develop a system to distinguish the state of malaria infection by impedance of cell suspension and cell-enrichment using electromagnetic force.

1.3 Scopes of the study

- Introducing an idea for distinguishing the state of malaria infection that is faster and cheaper than the existing methods by detecting the different changes of signal at two identical outlets
- Developing and improving the system, by fabricating T-shaped PDMS microchannel articulated with PCB's microelectrodes and designing 3D printing plastic model to fix all parts
- Testing with plastic beads (representing healthy red blood cells (hRBCs)) and magnetic beads (representing malaria-infected red blood cells (iRBCs)) to proof of concept
- Testing with malaria cells to study the possibility of system and the proper parameters for detecting malaria-infected red blood cells (iRBCs) using impedance measurement coupled with electromagnetic force

1.4 Expected outcomes

This research can detect the infection of malaria and tell us the severity of disease by finding percentage parasitemia.

CHAPTER 2

LITERATURE REVIEWS

2.1 Severe malaria

Severe malaria [15] is the complicated symptom of malaria disease. It occurs exclusively with *P. falciparum* (rarely with *P. vivax* or *P. knowlesi*) and is associated with delay in detection and treatment. A general overview of the features of severe malaria is shown as follows:

Clinical features of severe malaria

- impaired consciousness (including unrousable coma)
- prostration, i.e. generalized weakness so that the patient
- is unable to sit, stand or walk without assistance
- multiple convulsions: more than two episodes within 24h
- deep breathing and respiratory distress (acidotic breathing)
- acute pulmonary oedema and acute respiratory distress syndrome
- circulatory collapse or shock, systolic blood pressure
- < 80mm Hg in adults and < 50mm Hg in children

Note: these symptoms can occur singly or, more commonly, in combination in the same patient

Hyperparasitemia (> 5% infected red blood cells or > 250,000 parasites/ μ l) is a risk factor for deaths from *P. falciparum* malaria. However, the severity of diseases depends on transmission areas. In low-transmission areas, the deaths from *P. falciparum* malaria have parasite densities over 100,000/ μ l (~2.5% parasitaemia), whereas in high transmission area, the deaths from *P. falciparum* malaria have much higher parasite densities. Moreover, there are other finding criteria of severe malaria as follows:

Laboratory and other findings

- hypoglycaemia (< 2.2mmol/l or < 40mg/dl)
- metabolic acidosis (plasma bicarbonate < 15mmol/l)
- severe normocytic anaemia (haemoglobin < 5g/dl, packed cell volume < 15% in children; < 7g/dl, packed cell volume < 20% in adults)
- haemoglobinuria
- hyperlactataemia (lactate > 5mmol/l)

- renal impairment (serum creatinine > 265 μ mol/l)
- pulmonary oedema (radiological)

The risk of severe malaria also relies on transmission areas. In low-transmission areas, severe malaria is more evenly distributed across all age groups, whereas in high transmission area, severe malaria is greater distributed among children and visitors (with all age groups). The risk will increase in pregnant women, patients with HIV/AIDS, and people who have undergone splenectomy as follows:

- High transmission area: hyperendemic or holoendemic area in which the prevalence rate of *P. falciparum* parasitaemia is over 50% most of the year among children aged 2–9 years. In these areas, virtually all exposed individuals have been infected by late infancy or early childhood.
- Moderate transmission area: mesoendemic area in which the prevalence rate of *P. falciparum* parasitaemia is 11–50% during most of the year among children aged 2–9 years. The maximum prevalence of malaria occurs in childhood and adolescence, although it is not unusual for adulthood to be attained before an infection is acquired.
- Low transmission area: hypoendemic area in which the prevalence rate of *P. falciparum* parasitaemia is 10% or less during most of the year among children aged 2–9 years. Malaria infection and disease may occur at a similarly low frequency at any age, as little immunity develops and people may go through life without being infected.

2.2 Microfluidics for malaria diagnosis

Microfluidics or lab-on-a-chip technique is the key techniques to do an experiment in microscales that is the same scales of particles or cells. It allows us to manage the experiment and the behavior control of test particles better. Therefore, this technique performs a complicated test faster and uses less reagents. Because of the small size of overall system and cheap production, microfluidic is also the popular method for point-of-care malaria diagnosis by detecting malaria-infected red blood cells (iRBCs).

After invading into healthy red blood cells (hRBCs), malaria parasites bring many changes to the normal cells [16], including the loss of discoid shape, increased rigidity of the membrane [17], increased permeability of magnetic [10], and changed dielectric property [10]. Microfluidics for malaria diagnosis utilizes many fields of sciences such as impedance spectroscopy and magnetophoretic principle to detect the different changes.

2.2.1 Microfluidic impedance spectroscopy

Impedance is a measure of the frequency-dependent ratio between the two fundamental electrical parameters that is voltage and current, or the dielectric properties (permittivity and conductivity) of the system. It offers a non-invasive method identifying the different of malaria cells that detect the changes in cell morphology after invasion by malaria parasites and cell counting detecting by means

of impedance when a different of number of cells refer to a difference of the impedance of the sensor at different scales of sensors. There are two experimental methods that widely use in measuring impedance in microfluidics: single-cell measurement and bulk suspension measurement.

2.2.1.1 Single-cell microfluidic impedance spectroscopy

Electrical impedance is defined as the ratio between excitation voltage and response current of cell in suspension as follow:

$$Z^* = \frac{V^*}{I^*} \quad (1)$$

where Z^* is electrical impedance (Ohm), V^* is excitation voltage (Volt) and I^* is current response (Amp) and superscript * denotes complex number [18].

In 2010, T. Sun and H. Morgan [12] reviewed single-cell microfluidic impedance cytometry. Impedance spectroscopy measures the complex impedance as a function of frequency of a cell. It reveals information about different aspects of cells depending on the frequency: cytoplasm and subcellular components at high frequencies, membrane capacitance at medium frequencies, and size at low frequency, as shown in figure 2.1.

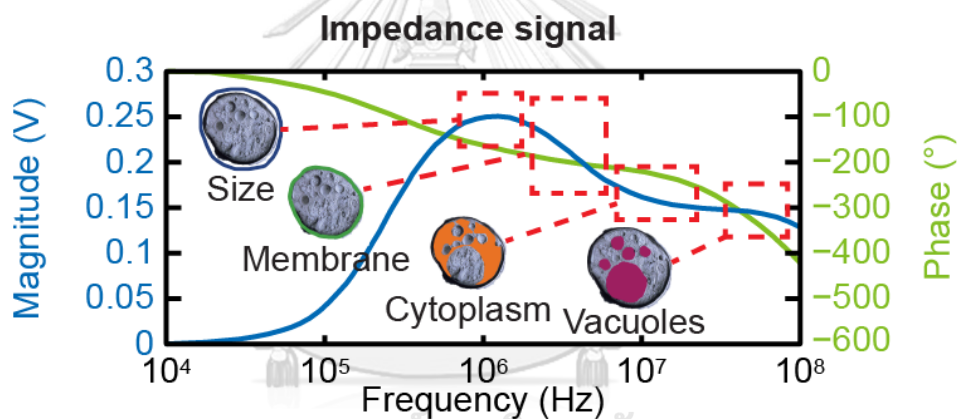


Figure 2.1 The impedance of a cell as a function of frequency [12].

In 2012, D. Holmes and B. L. J. Webb [19] presented an electrical impedance cytometry that use Maxwell's mixture theory [20] to explain a dielectric behavior of particles in suspension related to the complex permittivity of the suspension and particles in terms of mediums and the volume fraction. The single-shelled spherical model is used to describe a cell in suspension shows the spherical model of a cell including the dielectric and geometrical parameters as shown in figure 2.2(a)

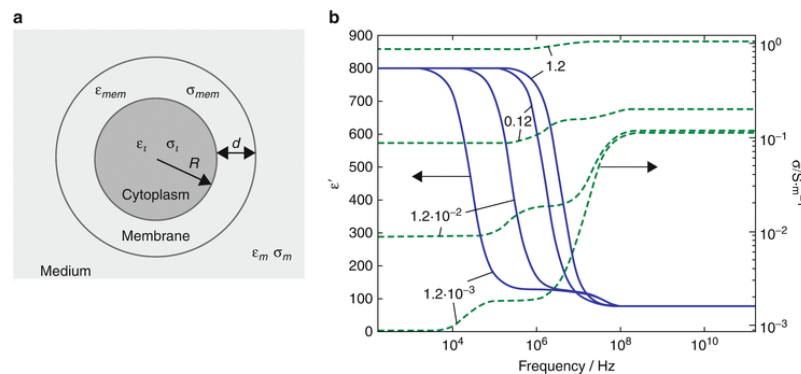


Figure 2.2 The single-shelled spherical model. (a) Single-shell electrical model of the spherical cell in suspension. (b) Plot showing the real and imaginary parts of the Clausius–Mossotti factor. The following parameters were used: $\epsilon_o = 8.854 \times 10^{-12}$ F.m⁻², $R = 3 \times 10^{-6}$ m, $d = 5 \times 10^{-9}$ m, $\epsilon_m = 80 \times \epsilon_o$, $\epsilon_{mem} = 5 \times \epsilon_o$, $\sigma_{mem} = 10^{-8}$ S.m⁻¹, $\epsilon_i = 60 \times \epsilon_o$, $\sigma_i = 0.4$ S.m⁻¹ and the medium conductivity varied between $\sigma_m = 1.2 \times 10^{-3}$ S.m⁻¹ and 1.2 S.m⁻¹ [19].

The impedance of a suspension of particles can be calculated where the equivalent complex permittivity $\tilde{\epsilon}_{mix}$ of a mixture of particles and medium is given by:

$$\tilde{\epsilon}_{mix} = \tilde{\epsilon}_m \frac{1+2\Phi\tilde{f}_{CM}}{1-\Phi\tilde{f}_{CM}} \quad (2) \quad \text{where} \quad \tilde{f}_{CM} = \frac{\tilde{\epsilon}_p - \tilde{\epsilon}_m}{\tilde{\epsilon}_p + 2\tilde{\epsilon}_m} \quad (3)$$

and $\tilde{\epsilon} = \epsilon - j\sigma/\omega$ (the complex permittivity), $j^2 = -1$, ω is the angular frequency, \tilde{f}_{CM} is the Clausius-Mossotti factor and Φ is the volume fraction. $\tilde{\epsilon}_m$ is the complex permittivity of medium and $\tilde{\epsilon}_p$ is the complex permittivity of particle (or cell).

$\tilde{\epsilon}_p$ combines the dielectric properties of membrane $\tilde{\epsilon}_{mem}$ and cytoplasm $\tilde{\epsilon}_{cyto}$, and cell geometry (where R is the inner radius and d is the membrane thickness) given by:

$$\tilde{\epsilon}_p = \tilde{\epsilon}_{mem} \frac{\gamma^3 + 2 \left(\frac{\tilde{\epsilon}_{cyto} - \tilde{\epsilon}_{mem}}{\tilde{\epsilon}_{cyto} + 2\tilde{\epsilon}_{mem}} \right)}{\gamma^3 - \left(\frac{\tilde{\epsilon}_{cyto} - \tilde{\epsilon}_{mem}}{\tilde{\epsilon}_{cyto} + 2\tilde{\epsilon}_{mem}} \right)} \quad (4) \quad \text{where} \quad \gamma = \frac{R+d}{R} \quad (5)$$

Maxwell's mixture theory is only valid for dilute suspensions ($\Phi < 10\%$). For higher concentrations, the interaction between the particles will get involved. The mixture theory can be extended to high volume fractions:

$$1 - \Phi = \left(\frac{\tilde{\epsilon}_{mix} - \tilde{\epsilon}_p}{\tilde{\epsilon}_m - \tilde{\epsilon}_p} \right) \left(\frac{\tilde{\epsilon}_m}{\tilde{\epsilon}_{mix}} \right)^{1/3} \quad (6)$$

Therefore, the impedance of the system including complex permittivity as the following:

$$\tilde{Z}_{mix} = \frac{1}{j\omega\tilde{\epsilon}_{mix}G_f} \quad (7)$$

where G_f is a geometric constant (the ratio of electrode area to gap A/g (m)).

There are two equivalent circuit models that described the cell [21], as shown in figure 2.3. Firstly, simplified circuit model describes cytoplasm as a resistor and membrane as a capacitor when cell membrane resistance is much greater than the reactance of the membrane and cell cytoplasm capacitance is much greater than the cell cytoplasm resistance (figure 2.3(a)). This model used in single cell impedance measurements as shown in figure 2.4. Secondly, the complete circuit model includes

the resistance of the membrane and the capacitance of the cytoplasm when the cell membrane conductance and cytoplasm capacitance have different values and cannot be ignored (figure 2.3(b)).

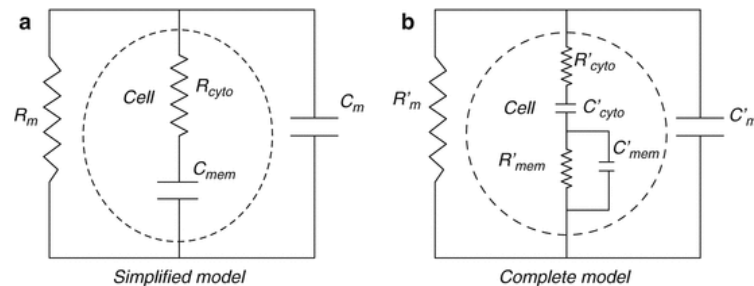


Figure 2.3 Foster and Schwan's simplified circuit model for a single cell in suspension. (a) The cell is modeled as a resistor R_{cyto} (cytoplasm) and a capacitor C_{mem} (membrane) in series, with the suspending medium modeled as a resistor R_m and capacitor C_m . (b) The complete circuit model for a single-shelled particle in suspension. The particle is modeled as a resistor R'_{cyto} and a capacitor C'_{cyto} in series (cytoplasm) in combination with a resistor R'_{mem} and a capacitor C'_{mem} in parallel (membrane) [12].

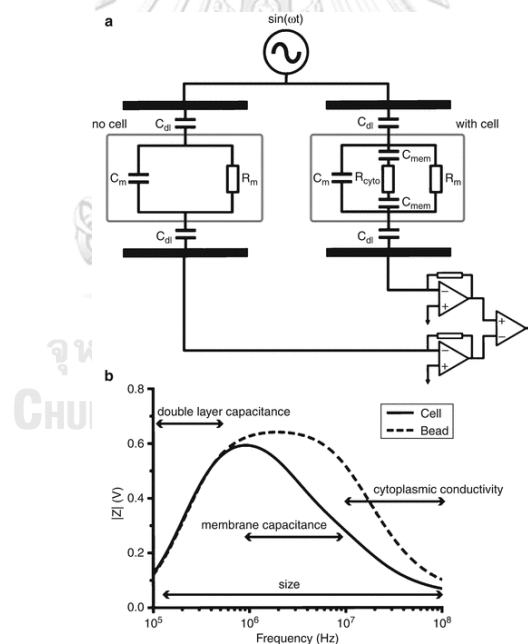


Figure 2.4 Single cell impedance measurements. (a) Simplified schematic of the impedance detection system shows the differential detection system. The electrode pair on the left illustrates the equivalent circuit model with no cell between the electrodes; the right electrode pair has the cell between the electrodes. R_m and C_m are the equivalent resistance and capacitance of the medium, respectively, C_{mem} is the equivalent capacitance of the cell membrane, R_{cyto} is equivalent resistance of the cell cytoplasm. C_{dl} represents the electrical double layer capacitance at the electrode-liquid interface. (b) The frequency-dependent impedance magnitude from a polymer bead (i.e., an insulating particle) and a cell of the same diameter [19].

In 2017, C. Phetchakup et al. [18] reviewed advanced single-cell impedance cytometry for biomedical applications. In terms of electrode designs, there are three commonly used in microfluidic impedance cytometry: coplanar electrodes (as shown in figure 2.5(a)), parallel electrodes (as shown in figure 2.5(b)), and constriction channel (as shown in figure 2.5(c)). Even these designs are created differently, the detection principle is almost the same. According to figure 2.5(a), when a cell flows between a pair of electrodes (point A and C), it will disrupt the electric field between these electrodes and effect the current changes at point A. Impedance values will acquire by measured the current at this point combining impedance of cells and suspension media.

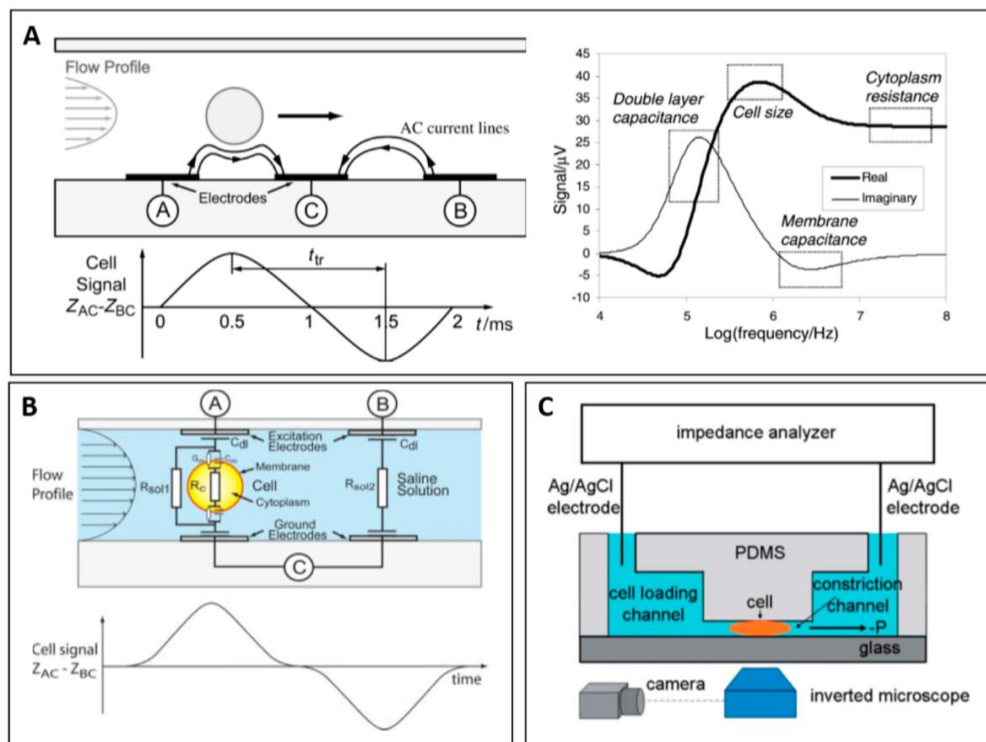


Figure 2.5 Example of single cell measurement. (A) (Left) Illustration of coplanar electrodes design and impedance signal response when a cell flows through the detection region. (Right) Impedance response at different frequencies carries different information regard the cell. (B) Illustration of parallel electrodes design. (C) Illustration of constriction channel design [18].

In 2018, C. Honrado et al. [22] presented the system to find Dielectric characterization of *P. falciparum*-infected red blood cells using microfluidic impedance cytometry. Microfluidic impedance cytometry is used to measure the dielectric properties of malaria-infected red blood cells (iRBCs) at specific time points and use green fluorescent protein (GFP) emission to identify inside each malaria cell (figure 2.6). The dielectric properties at different hpi (h post-invasion) are shown in figure 2.7 and the values are shown in table 2.1.

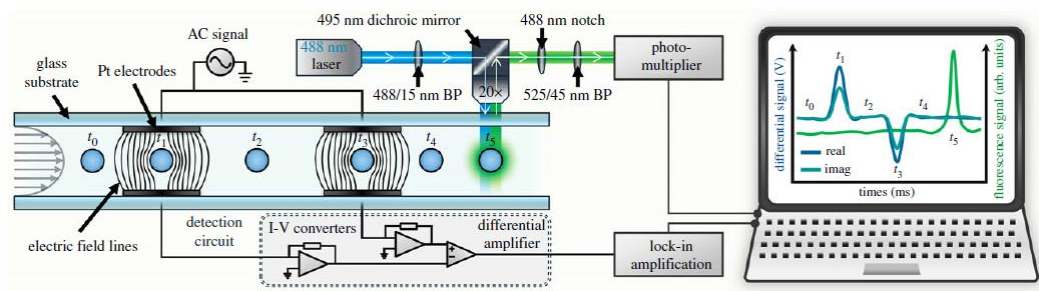


Figure 2.6 Schematic of the MIC system, showing impedance and fluorescence detection sections. Particles flow through the microchannel, between pairs of electrodes and the fluorescence detection region. The fluorescence from cells is measured simultaneously with impedance, allowing direct correlation of electrical and fluorescent properties of single cells [22].

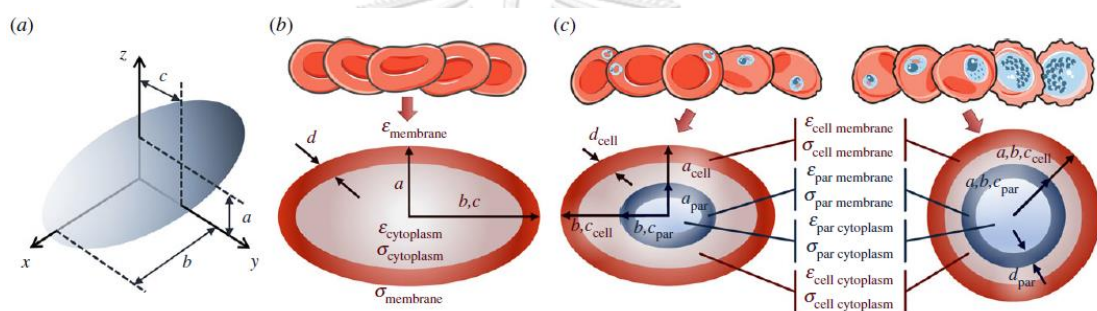


Figure 2.7 The dielectric properties at different hpi (h post-invasion). (a) Ellipsoidal model, with semi-axes a – c . (b) Oblate spheroid model implemented for u-RBCs, with semi-axes $a < b = c$ (based on the ellipsoidal model), membrane thickness d and dielectric properties modelled are represented. (c) Models implemented for i-RBCs: oblate spheroid model for early-stage i-RBCs and spherical model for late-stage i-RBCs, with semi-axes $a = b = c$ (based on the ellipsoidal model). Membrane thickness of cell (d_{cell}) and parasite (d_{par}), and dielectric properties modelled are represented [22].

Table 2.1 Dielectric properties of i-RBCs and parasite estimated using MMT modelling, during the parasite intraerythrocytic life cycle (hours post-invasion, hpi). Values are mean estimates (N = 3 TCs) with s.d. [22].

| properties | period of intraerythrocytic development of parasite | | | | | | |
|--|---|--------------------|--------------------|-----------|-----------|-----------|-----------|
| | 6 hpi | 12 hpi | 18 hpi | 24 hpi | 30 hpi | 36 hpi | 42 hpi |
| $\epsilon_{\text{cell membrane}}$ | 4.58±0.28 | 5.38±0.36 | 6.43±0.50 | 7.40±0.43 | 7.99±0.80 | 8.32±0.45 | 7.80±1.40 |
| $\epsilon_{\text{cell cytoplasm}}$ | 60 (fixed value) | 60 (fixed value) | 60 (fixed value) | 66.7±9.4 | 83.3±4.7 | 86.7±4.7 | 86.7±4.7 |
| $\epsilon_{\text{par membrane}}$ | 3.03±0.40 | 3.33±0.47 | 5.83±0.24 | 5.67±0.47 | 5.67±1.70 | 3.50±0.41 | 4.00±0.82 |
| $\epsilon_{\text{par cytoplasm}}$ | 60 (fixed value) | 60 (fixed value) | 60 (fixed value) | 76.7±9.4 | 76.7±4.7 | 86.7±4.7 | 86.7±4.7 |
| $\sigma_{\text{cell cytoplasm}} (\text{S m}^{-1})$ | 0.51±0.03 | 0.52±0.02 | 0.55±0.04 | 0.53±0.05 | 0.74±0.04 | 0.97±0.07 | 1.24±0.04 |
| $\sigma_{\text{par cytoplasm}} (\text{S m}^{-1})$ | 0.40 (fixed value) | 0.40 (fixed value) | 0.40 (fixed value) | 0.50±0.09 | 0.44±0.04 | 0.47±0.01 | 0.50±0.03 |
| $C_{\text{cell membrane}} (\text{mF m}^{-2})$ | 8.1±0.50 | 9.1±0.47 | 11.4±0.88 | 13.1±0.77 | 14.1±1.42 | 14.8±0.83 | 13.8±2.47 |

In 2013, E. Du et al. [13] measured electric impedance of the stages of malaria-infected red blood cells (iRBCs) by using electric impedance microflow cytometry (EIMC) platform. For identifying characteristics of the disease states of single cell, this platform will be a microfluidic device for a label-free and cell-counting assay through electric impedance sensing. This paper studied the different impedance values of iRBCs that developing the stages of infection during 48-hour cycle of *P. falciparum*. The system and measurement method illustrates as shown in figure 2.8(a) and impedance values results illustrates as shown in figure 2.8(b).

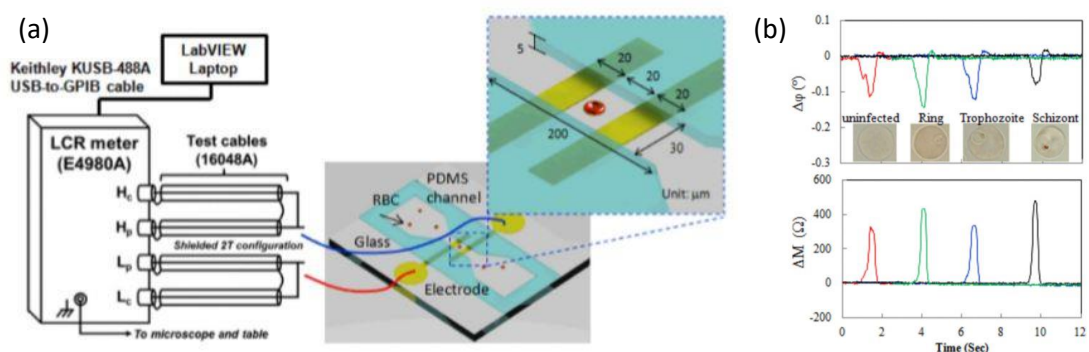


Figure 2.8 Electric impedance microflow cytometry (EIMC). (a) Experimental EIMC system setup for Pf-iRBC detection using a microfluidic device. (b) EI transitions measured as uninfected RBCs and Pf-iRBCs crossed over the electrode probe. Measurement conditions: 2 MHz 1 V and 0.2% w/v BSA-PBS [13].

2.2.1.2 Bulk suspension microfluidic impedance spectroscopy

With the same principles of single-cell microfluidic impedance spectroscopy, bulk suspension microfluidic impedance spectroscopy measures the complex impedance as a function of frequency of many cells. The result is the average impedance of all cells in detection area at the same period of time. In 2017, M. I Altaf and A. Ahmad [23] measured dielectric properties of malaria parasite infected human blood in suspension: dielectric constant (as shown in figure 2.9(a)), dielectric loss (as shown in figure 2.9(b)), and electrical conductivity (as shown in figure 2.9(c)).

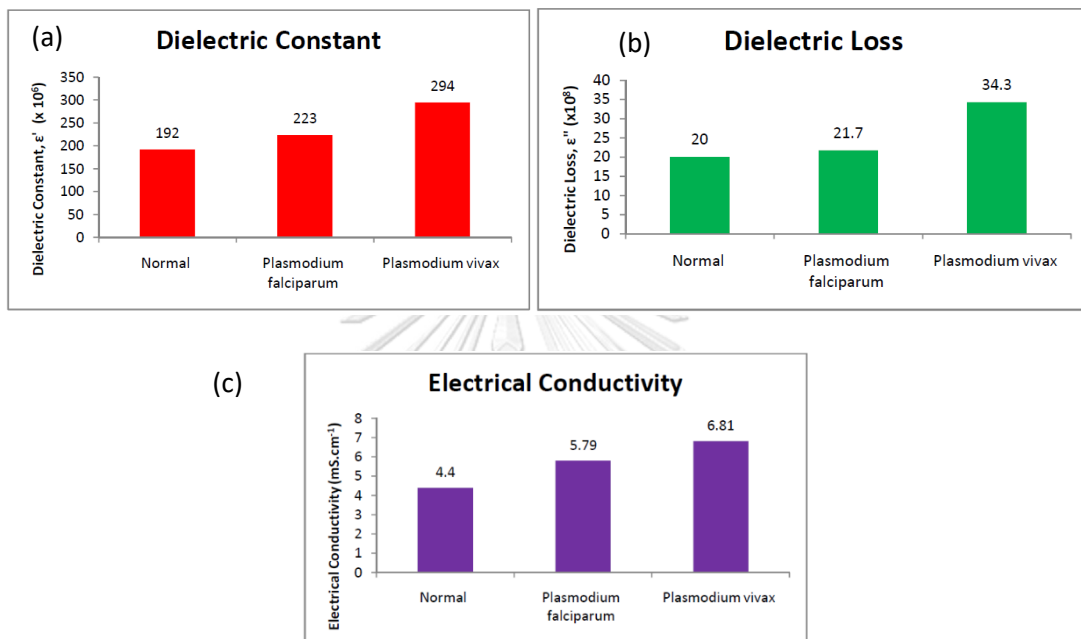


Figure 2.9 Dielectric properties in suspension. (a) A comparison of dielectric constant of normal and malaria infected human blood. (b) A comparison of dielectric loss of normal and malaria infected human blood. (c) A comparison of electrical conductivity of normal and malaria infected human blood [23].

In 2012, M. A. Mansor et al [14] carried out the experiment about electrical impedance spectroscopy for detection of cells in suspensions using microfluidic device with integrated microneedles. They tried to save the cost and time of electrode fabrication by using commercial Tungsten microneedles as electrodes, which can reusable. The two microneedles are located at the half height of the microchannel for cell detection and electrical measurement as shown in figure 2.10. Using *Saccharomyces cerevisiae* cells as a model for proof of concepts, this paper focused on detecting impedance in different cell concentration. The results are show in figure 2.11.

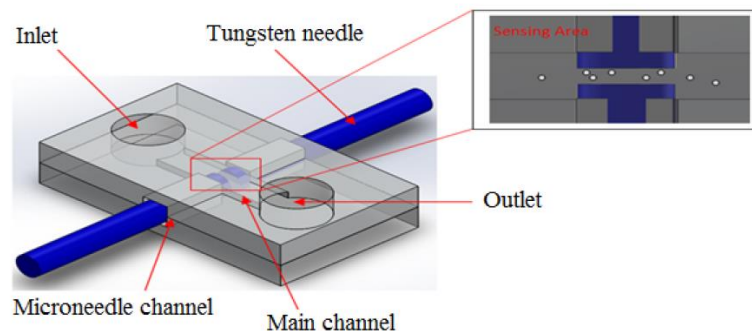


Figure 2.10 3D schematic diagram of the device structure and top view of sensing area [14].

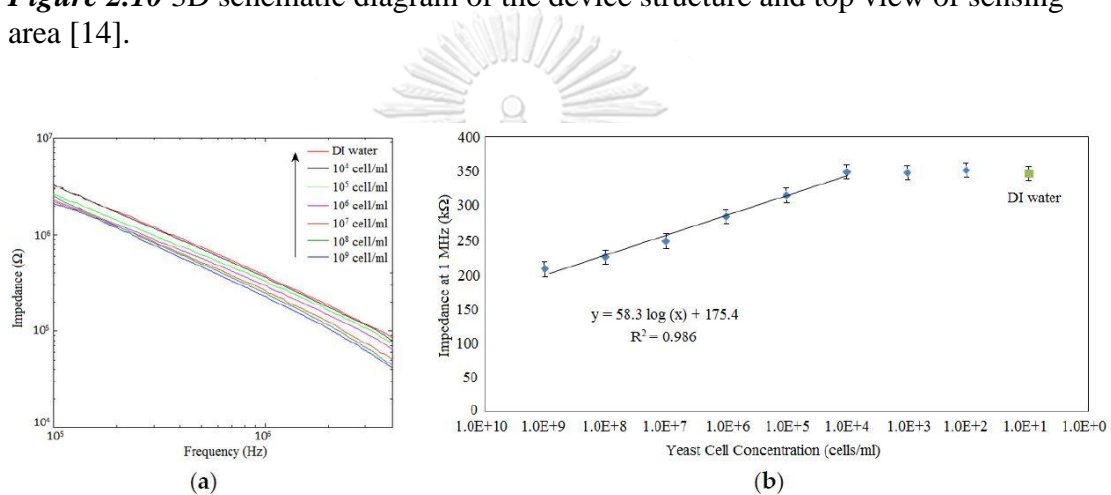
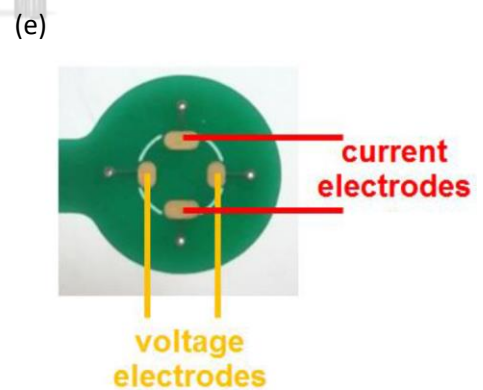
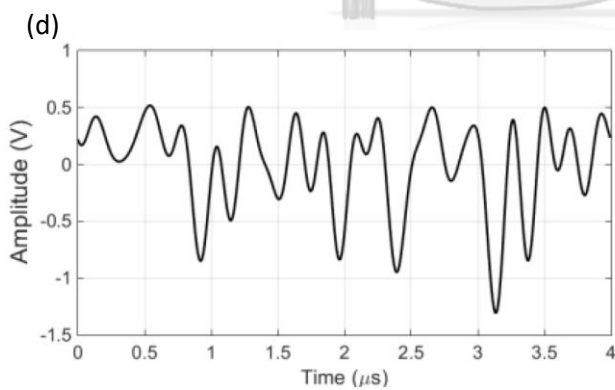
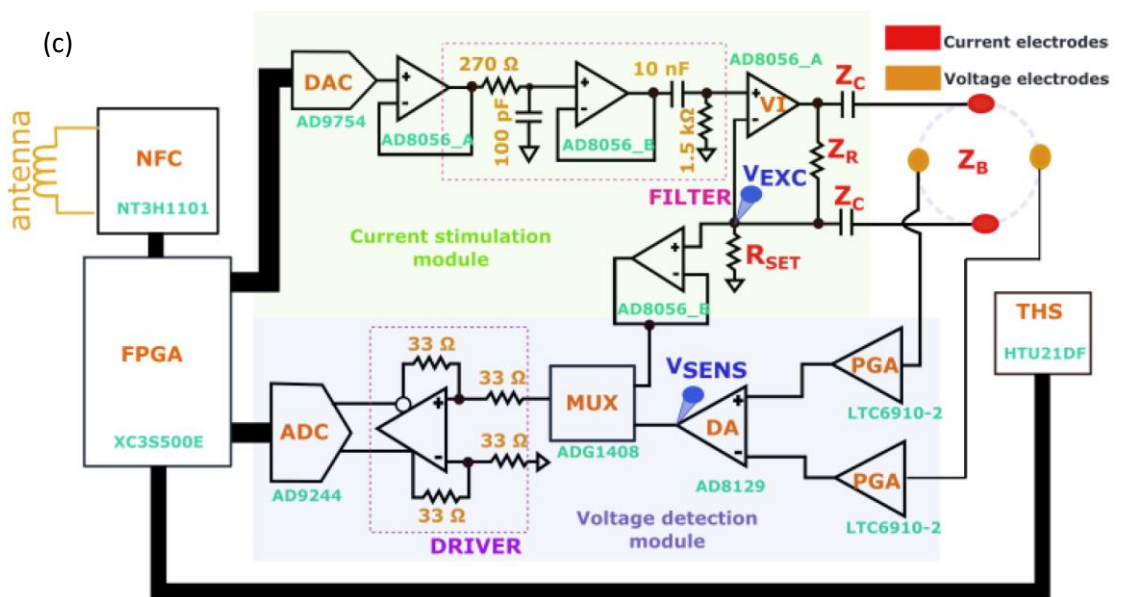
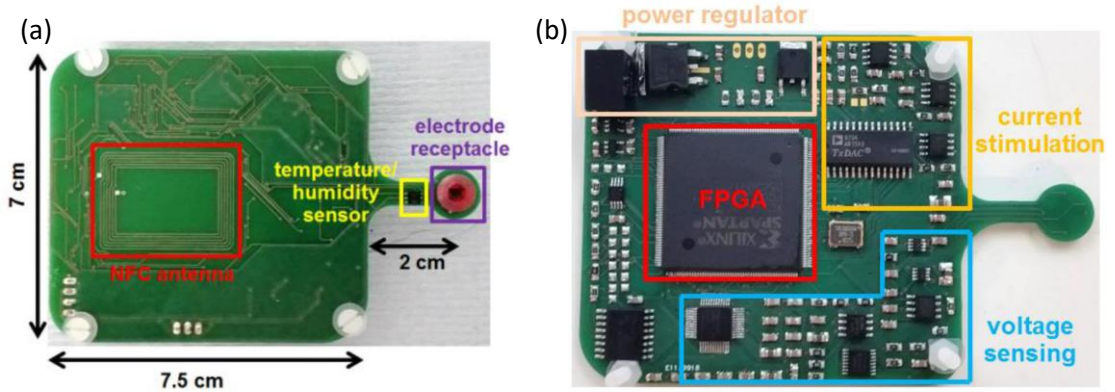


Figure 2.11 Impedance values in suspension. (a) Impedance spectra of yeast cells in water with cell concentrations ranging from 10^2 to 10^9 cfu/mL, along with DI water as control. (b) The linear relationship between the logarithmic value of the concentration of yeast cells and the impedance measured at 1 MHz. Error bars are standard deviations of 5 measurements [14].

In 2020, B. M. G. Rosa and G. Z. Yang [24] carried out the experiment about portable impedance analyzer as a rapid screening tool for early forms of *Plasmodium falciparum* detection. They developed a tetrapolar electrode system located at the bottom of the receptacle for blood impedance measurements ($\varnothing = 5$ mm) in order to drop the sample on electrode, process the impedance signal by FPGA, and send the results to mobile's app through NFC antenna as shown in figure 2.12. Minimum parasitemia level discriminated they can measure was 0.0078% (or, equivalently 390 parasites/ μ l), which closely approaches the international standard set to 200 parasites/ μ l. The results are show in figure 2.13.



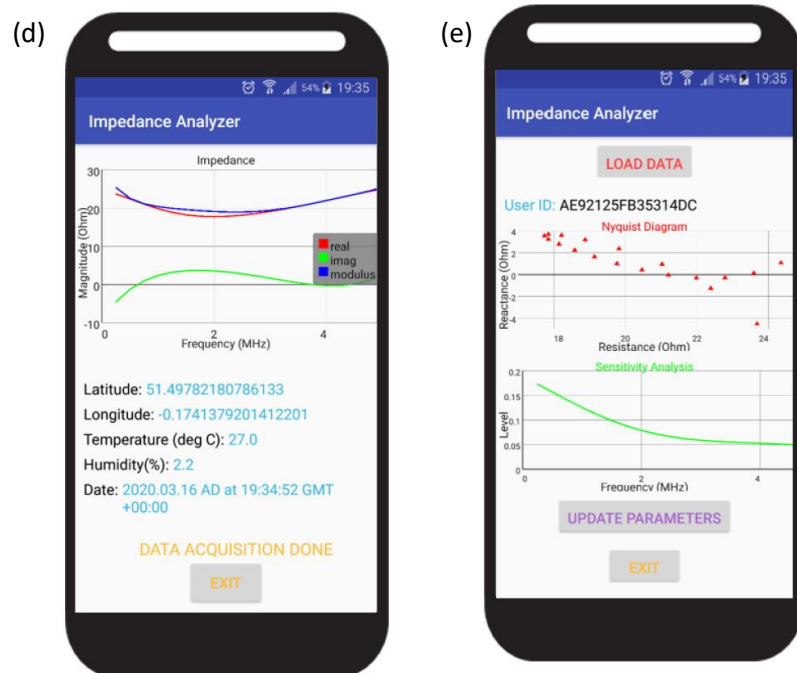
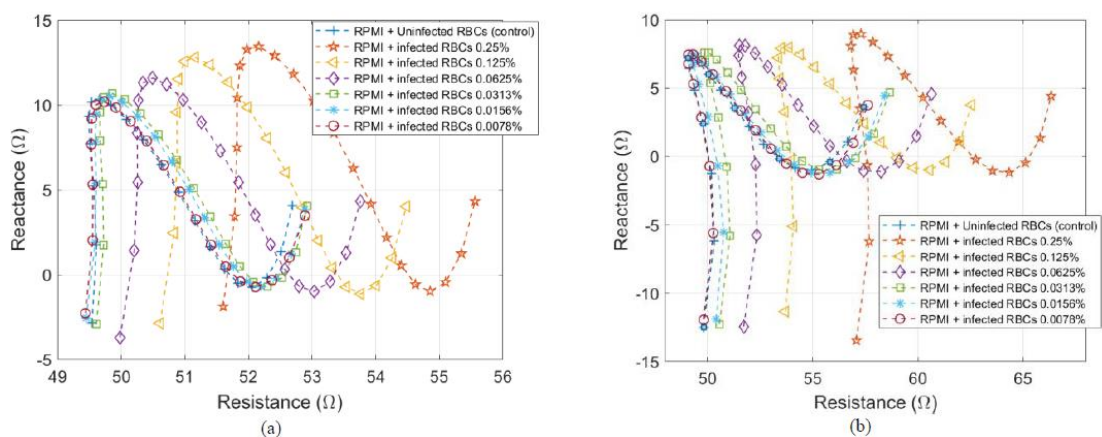


Figure 2.12 Portable impedance analyzer developed for malaria diagnosis. a) Top layer of the device containing the NFC antenna and electrode receptacle for blood samples. b) Bottom layer containing the assembled components for current stimulation, voltage sensing, power regulation and central control unit (FPGA). c) Simplified electronic schematic of the impedance analyzer with main functional blocks. d) Multi-tone waveform signal employed for current stimulation. e) Tetrapolar electrode system located at the bottom of the receptacle for blood impedance measurements ($\varnothing = 5$ mm). f) Mobile phone's app developed for contactless reception of the impedance parameters sent over the NFC protocol, with ambient temperature, humidity and geolocation included. g) Different menu of the app responsible for data sensitivity analysis and update of the control parameters [24].



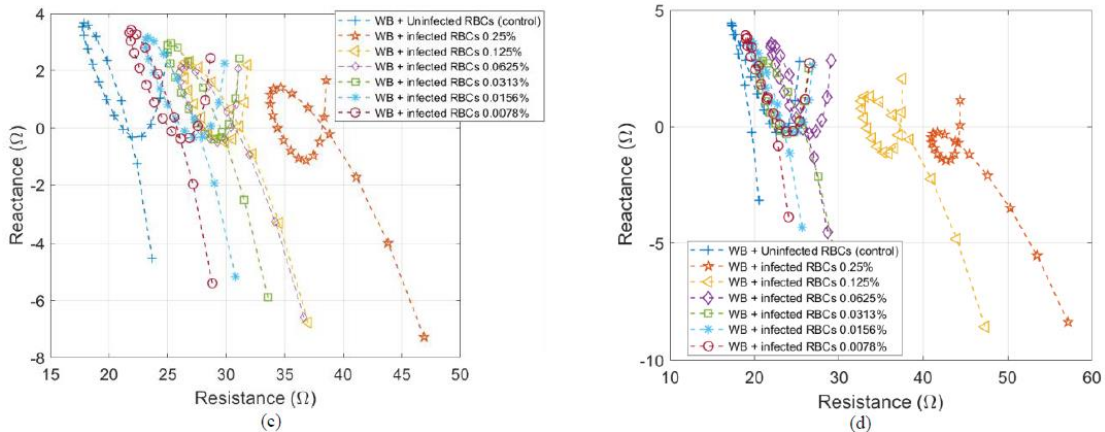


Figure 2.13 Nyquist diagrams obtained for the different assays tested with the proposed impedance analyzer in laboratory conditions (25o C, 2% RH). a) Unsynchronized RPMI (assay 1A). b) Ring-synchronized RPMI (assay 2A). c) Unsynchronized WB (assay 3A). d) Ring-synchronized WB (assay 4A) [24].

2.2.2 Microfluidic coupled with electromagnetic forces

According to the key substance of malaria cells, Hemozoin, that has a stronger magnetic than normal red blood cells, magnets and electromagnets are applied for microfluidics in order to separate between infected cells and normal cells for drug testing or increasing concentration of malaria cells. The relative magnetic susceptibilities of malaria-infected red blood cells (iRBCs) will increase during the stage development of the parasite.

In 2015, M. Hejazian et al [25] reviewed the fundamental physics involved in using magnetic force to separate particles, and identifies the parameters and methods for increasing the magnetic force. There are key forces (figure 2.14) that affect the particle trajectory while passing through the microfluidic device: the magnetic force, drag force, gravity force, Brownian force, and lift force (Eq. 8).

$$m_p \frac{du_p}{dt} = F_m + F_g + F_d + F_B + F_L \quad (8)$$

where m_p is the mass of particles, u_p is the particle velocity, F_m is the magnetic force, F_d is drag force, F_g is gravity force, F_B is Brownian force, and F_L is lift force.

The magnetic force is the force effecting magnetic particles in magnetic fields. The equation is:

$$F_m = \frac{V_p \cdot \Delta\chi}{\mu_0} (B \cdot \nabla) B \quad (9)$$

where F_m is the magnetic force (N), V_p is the volume of the particle (m^3), $\Delta\chi = \chi_p - \chi_f$ is the difference between magnetic susceptibilities of the particles χ_p and the base fluid χ_f (dimensionless), B is the magnetic induction (T(Tesla) or Wb/m²), and $\mu_0 = 4\pi \times 10^{-7}$ (T mA⁻¹) is the permeability of the vacuum.

The gravitational force can be expressed as:

$$F_g = -V_p(\rho_p - \rho_f)g \quad (10)$$

where F_g is the gravitational force, V_p is the volume of the particle, ρ_p is the density of the particle, ρ_f is the density of the fluid and g is the acceleration due to gravity.

The drag force is estimated from the Stokes' law and the relative velocity:

$$F_d = 3\eta d_c(u_f - u_p) \quad (11)$$

where η is the dynamic viscosity of the fluid, u_f is the velocities of the fluid and u_p is the velocities of the particles. The diameter d_c can be estimated based on the relative size ratio between the magnetic particles and the biological particles (figure 2.14(b)).

There are two types of lift forces on particles relies on the position of the particle: shear gradient-induced lift force and boundary layer lift force. The first force is the shear gradient-induced lift force:

$$F_{L,s} = \frac{\pi}{8} \rho_f \omega u d_p^3 \quad (12)$$

Another one is the boundary layer lift force:

$$F_{L,b} = 9.22 \left(\frac{9U^2}{4h^2} \right) \rho_f d_p^4 \quad (13)$$

where $F_{L,s}$ is the shear gradient induced lift force and $F_{L,b}$ is the boundary layer lift forces, d_p is the diameter of the particle, ρ_f is the density of the fluid, and ω is the vorticity of the flow, U is the average velocity of the particle, and h is the channel height.

Brownian motion is a random movement. The Brownian force can be estimated as:

$$F_B = \zeta \sqrt{\frac{6\eta k_B T d_p}{\Delta t}} \quad (14)$$

where the parameter ζ is a Gaussian random number with zero mean and unit variance. k_B is the Boltzmann constant, η is the fluid viscosity, T is the absolute temperature, and Δt is the magnitude of the characteristic time step.

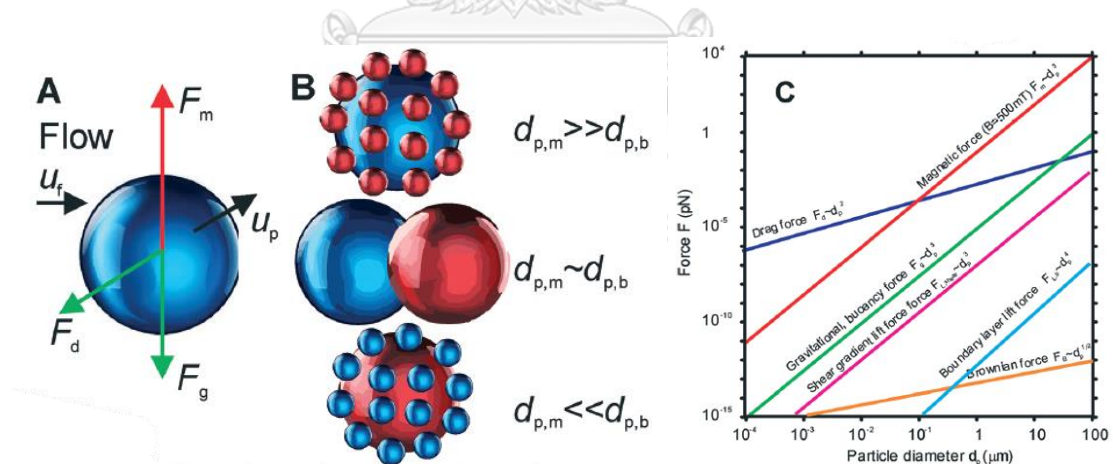


Figure 2.14 Dominant forces on a particle in a flow field: (A) representative illustration of force and velocity components (the directions of F_m and F_g are arbitrary). (B) relative sizes between magnetic particles (blue) and diamagnetic (biological) particles (red). (C) orders of magnitude of different forces as functions of characteristic particle diameters (at a typical velocity of 1 mm s^{-1} and channel width and depth of $100 \text{ }\mu\text{m}$) [25].

In 2017, S. Huang et al [26] reviewed advances of particles/cells magnetic manipulation in microfluidic chips using the concept of particles/cells separation with

different criteria, such as sizes, shapes, and magnetic properties to do a separation, concentration, capture, arrangement, and assembly. They reviewed the separation of paramagnetic and diamagnetic particles/cells using magnet, and 3-way outlet (as shown in figure 2.15(a)) and T-shaped channel (as shown in figure 2.15(b)).

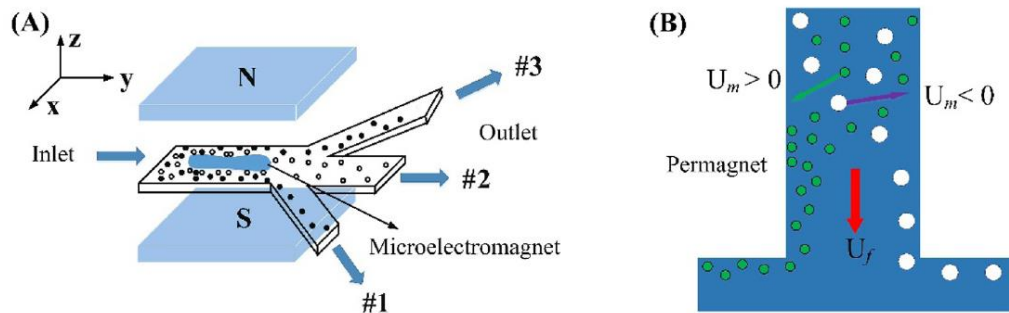


Figure 2.15 Separation paramagnetic and diamagnetic particles/cells: (A) Separation of white blood cells and red blood cells. (B) Separation of paramagnetic and diamagnetic particles in a T-shaped channel [26].

In 2013, J. Nam et al [27] presented magnetic separation of malaria-infected red blood cells in various developmental stages that can separate not only late-stage iRBCs, but also early-stage iRBCs with low paramagnetic characteristics using magnetophoretic force. A polydimethylsiloxane (PDMS) microchannel was fabricated and integrated with a ferromagnetic wire fixed on a glass slide as shown in 2.16.

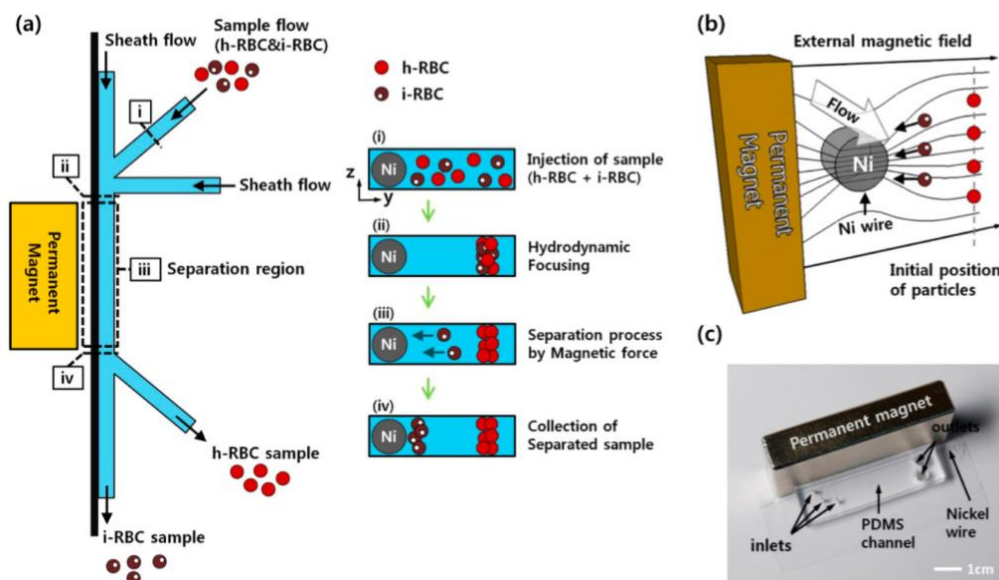


Figure 2.16 Malaria-infected RBC separation using a high magnetic field gradient. (a) Schematic diagram of iRBC separation using the paramagnetic characteristics of hemozoin in iRBCs. (b) Working principle of magnetophoretic separation with a ferromagnetic nickel wire in an external magnetic field. (c) Photograph of the permanent magnet for applying an external magnetic field in the microchannel and a microfluidic device consisting of the PDMS microchannel and a nickel wire [27].

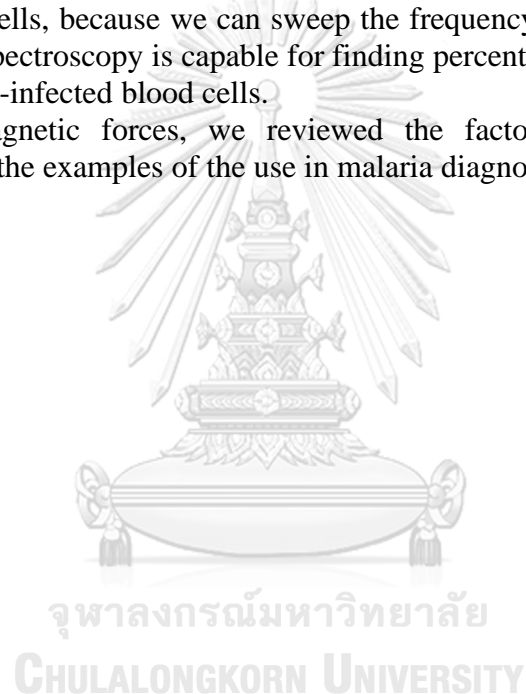
2.3 Summary

From all above, we introduced severe malaria about clinical features, laboratory and other findings, and the risk of severe malaria. Then, the microfluidics technology in malaria diagnosis that utilize many techniques, focusing on impedance spectroscopy and electromagnetic forces.

According to impedance spectroscopy, there are two different methods to detect different objectives: single-cell impedance spectroscopy and bulk suspension spectroscopy. Single-cell impedance spectroscopy is suit for identifying the characteristics of each cell, such as identifying the characteristics of each stage of malaria-infected red blood cells. The result will be the different impedance signals of each cell.

Whereas bulk suspension spectroscopy is suit for more detailed information about the group of cells, such as the effect in impedance when measure at different concentration of cells, because we can sweep the frequency in long range. Moreover, bulk suspension spectroscopy is capable for finding percentage parasitemia by sensing number of malaria-infected blood cells.

For electromagnetic forces, we reviewed the factors of magnetic force in microfluidics and the examples of the use in malaria diagnosis.



CHAPTER 3 METHODOLOGY

3.1 Concepts

This research is focusing on malaria detection and classification of the states of infection from uncomplicated symptoms (mild) to complicated symptoms (severe). The goal of this research is to identify malaria-infected red blood cells (iRBCs), even in early-stage malaria cells or very low parasitemia. Moreover, the system should differentiate percentage parasitemia in order to proper assessment treatment on time.

Microfluidic System for Detecting Malaria-Infected Red Blood Cells Using Impedance Sensor Coupled with Electromagnetic Force utilizes many principles that are widely used for novel malaria diagnosis tools nowadays, such as microfluidics, magnetic separation, and impedance spectroscopy. We are developing a non-invasive system that examines the external characteristics of cells from an external force and measurement. These techniques play an important role for reducing analyst time and reducing the complication of existing malaria diagnosis method. It is also helpful for reducing cost of production and available for mass productive in order to fight the malaria in high-transmission areas.

The system divides into two parts according to the application that we want to apply for iRBCs. Firstly, we begin with cell enrichment techniques by using paramagnetic property of iRBCs that allows us to use magnet or electromagnet to generate magnetic field. In this work, we choose electromagnet because of its features that can turn-on or turn-off when it needs by applying input voltage. Moreover, we expect for the ability to classify the states, and to see the immediately responses from the signal when we turn on the electromagnet. Acting to infected red blood cells, electromagnet is used for pulling malaria cells to itself. This technique will make a different to the 2-way identical outlets in terms of the variety and density of cells (figure 3.1), which normally, in mixed cells, two outlets are supposed to get the similar numbers and types of cells. Therefore, we can investigate these differences by using impedance spectroscopy.

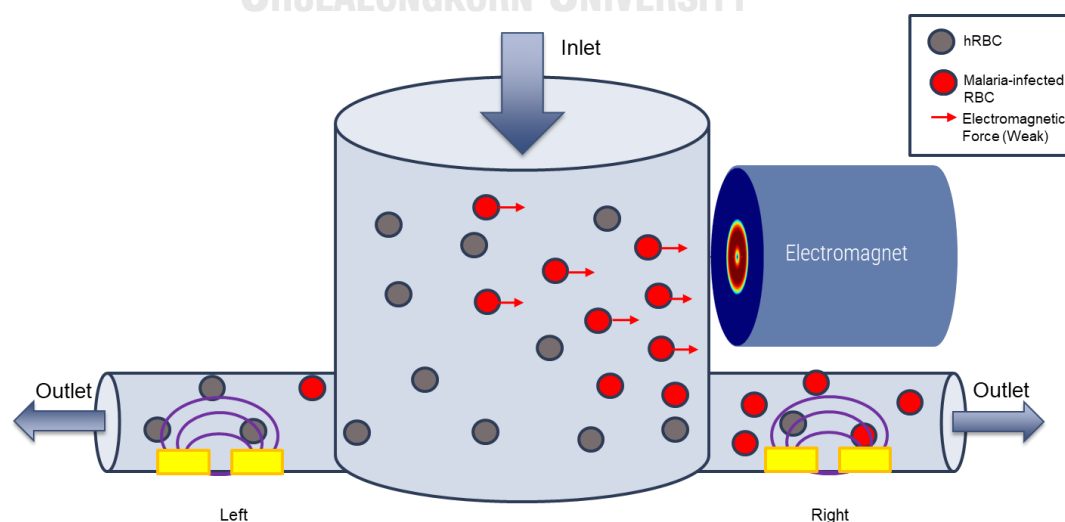


Figure 3.1 The cell enrichment technique schematic diagram.

Secondly, we use impedance techniques to identify the changes between two outlets, which we increase concentration of malaria cells in just one-sided outlets. In terms of low-cost fabrication, we choose to make electrodes from Printed Circuit Board (PCB) that is coplanar electrode or electrodes that located in the same plane. The PCB is also good for the custom-made circuits that we can design the suitable circuit for our system. Moreover, we can select the materials for electrode. In this research, we select the high proportion of gold in copper material to increase the conductivity and sensitivity of electrodes. One disadvantage of PCB is the limitation of fabrication that cannot be smaller than 3 mils (approximately $76\ \mu\text{m}$). The smallest sensing area is $330\ \mu\text{m}$ (two electrode widths and one gap) $\times 400\ \mu\text{m}$. When there are a cell passing through a pair of electrodes that much bigger than itself, the current signal does not change. The signal will change if there are a huge number of cells. Not alike as our work, we introduced the novel method that detects malaria from comparison the differences of impedance values that we are already make both outlets unequally and the cells, between normal cells and infected cells, have different dielectric property. We will use the ratio between the impedance values of two outlets to be an indicator of numbers of percentage parasitemia by using the normalized different between before applied electromagnetic field and after applied electromagnetic field of each outlet or normalized different between two outlets. Here is our hypothesis, the ratio that is not much different means the suspected patients have low parasitemia. On the other hand, if the ratio that is much different means the suspected patients have high parasitemia.

3.2 System designs

3.2.1 Overview

Microfluidic System for Detecting Malaria-Infected Red Blood Cells Using Impedance Sensor Coupled with Electromagnetic Force was design based on two main principles: 1. Cell enrichment, and 2. Impedance measurement. Firstly, part of cell enrichment used for increasing density of malaria cells in system by bringing electromagnet into close contact of needle to generate electromagnetic field. Secondly, part of impedance measurement used for detecting the differentiate signal of each pair of electrodes on PCB. The system part is shown in figure 3.2.

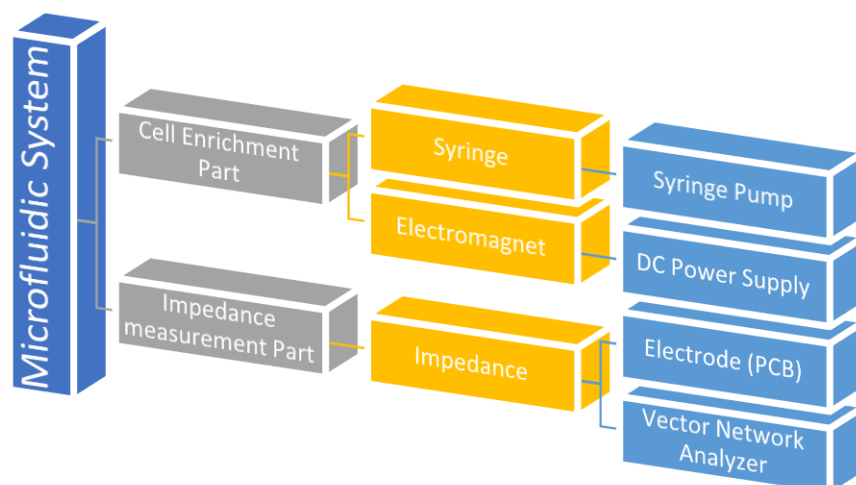


Figure 3.2 The part of the system.

3.2.2 Components

To meet the physical expectation of system's principles, we created many components to fit our system as shown in figure 3.3.

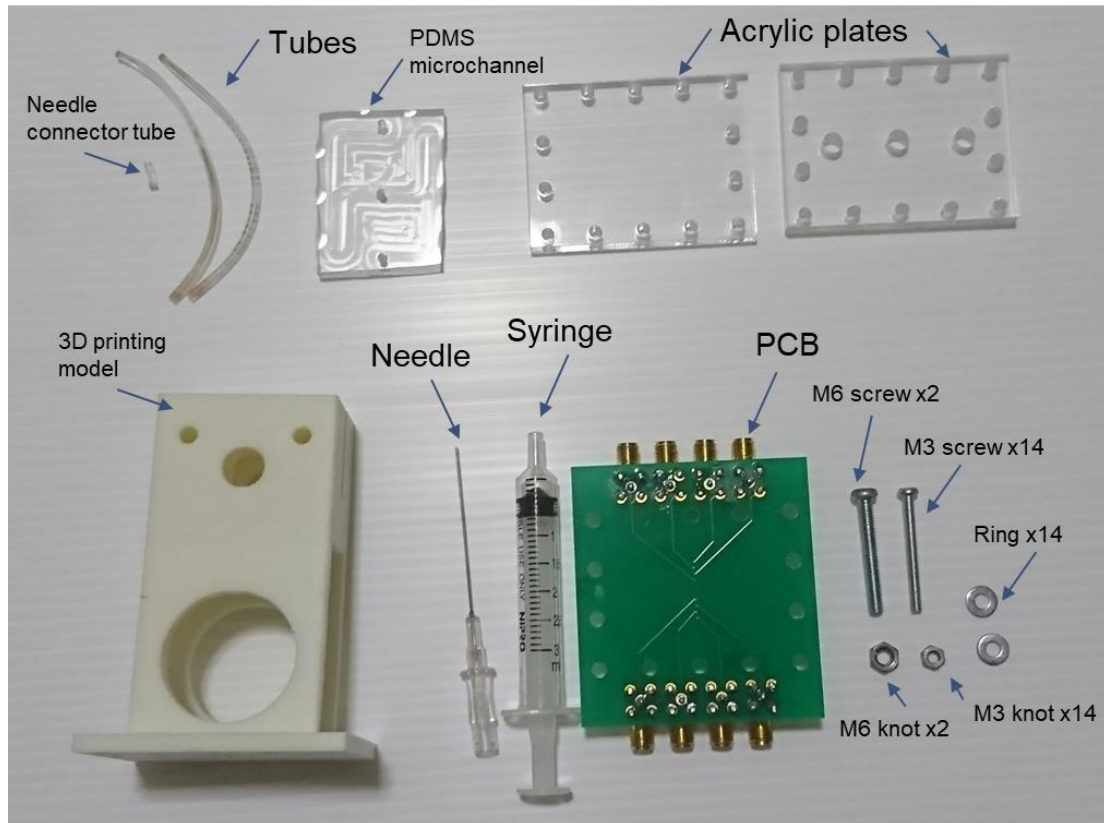


Figure 3.3 The components of the system.

However, there are many limitations of how to design this system. For example, we have made electromagnet attach to the needle because of the gradient of magnetic fields will rapidly decline depending on the distance. Therefore, we must design the connector that will put electromagnet and needle together, including other components. There are many components that we have to design in this system, as follows.

3.2.2.1 3D-printed connector

The connector needs to be as lighter weight as possible because the weight is on the syringe, and we already have electromagnet that is quite heavy. There are many designs until now (Appendix Figure 1), the connector is shown in figure 3.4. and how to gather with other components (figure 3.5). After finished the design, we chose 3D printing using Acrylonitrile Butadiene Styrene (ABS) with 200 μm resolution. The total width of connector is 47.3 mm, total length is 59.8 mm, and total height is 81.8 mm with 11-mm hole for syringe and two 6-mm hole for M6 screws to fix the syringe. Moreover, there are two 30-mm hole for electromagnet and fourteen 3-mm hole for M3 screws to fix with other part of system as shown in figure 3.6.

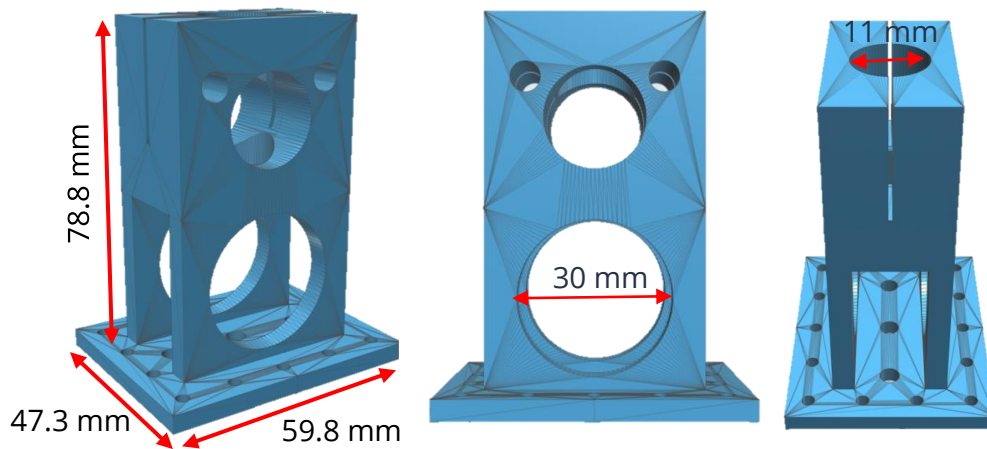


Figure 3.4 The design of connector.

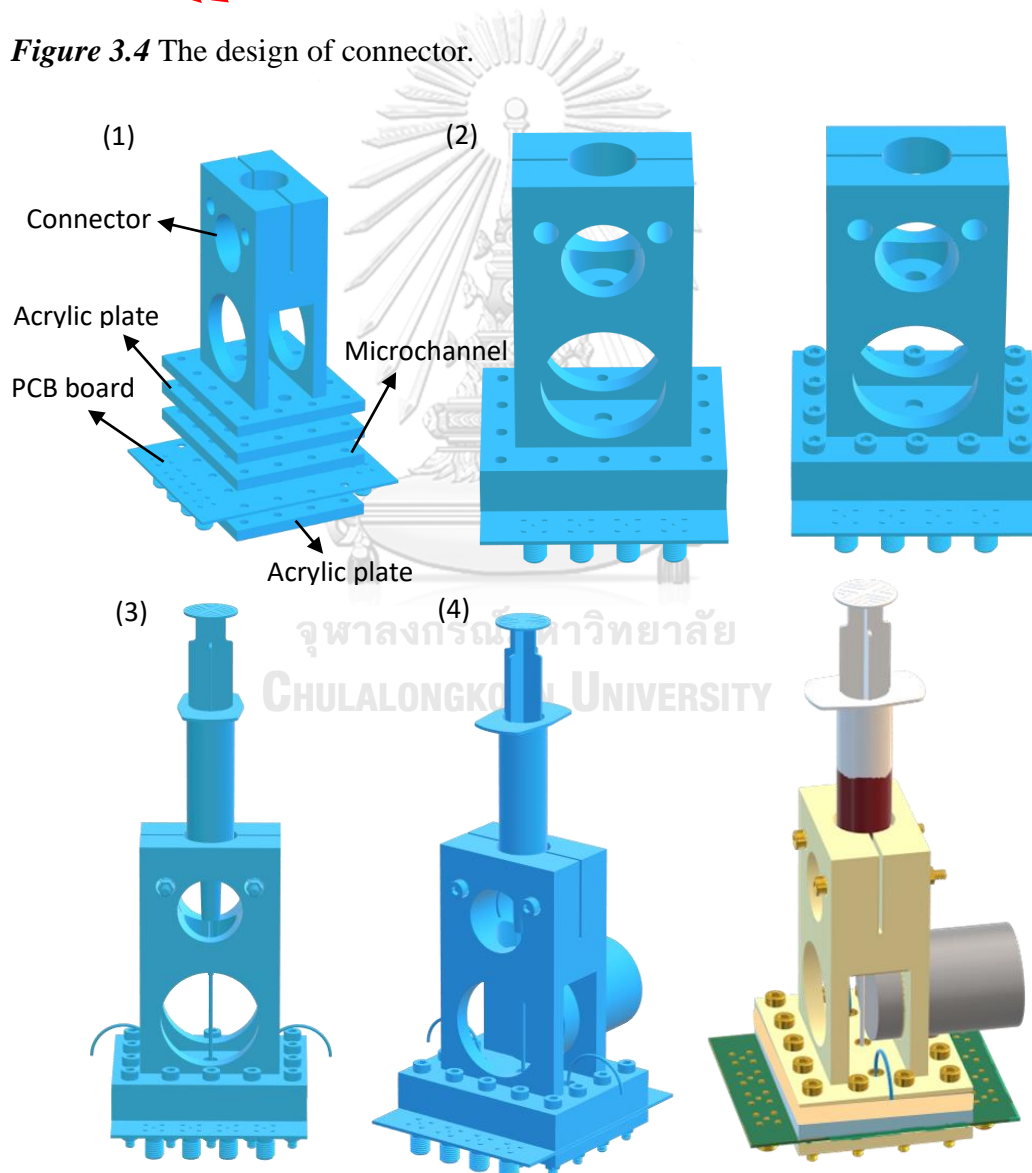


Figure 3.5 How to gather all components: (1) The components of system, (2) Arrange all components and fix position with screw, (3) Put syringe and outlet tube, and (4) Put electromagnet.

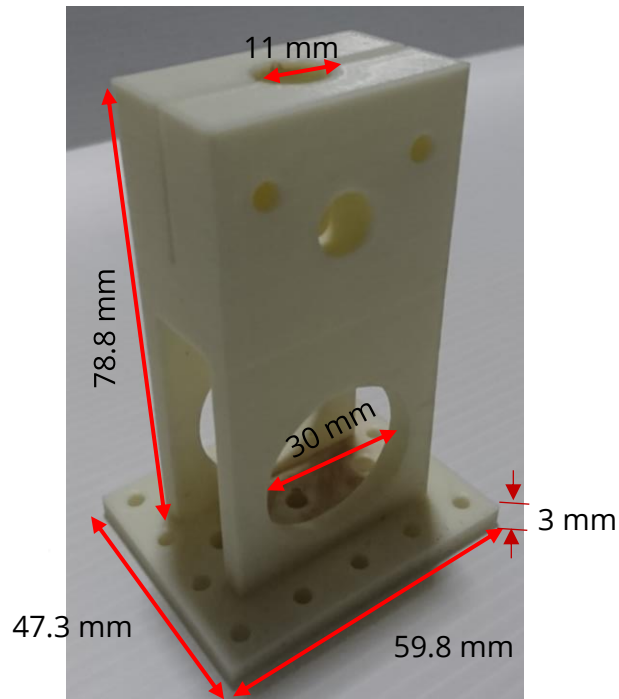
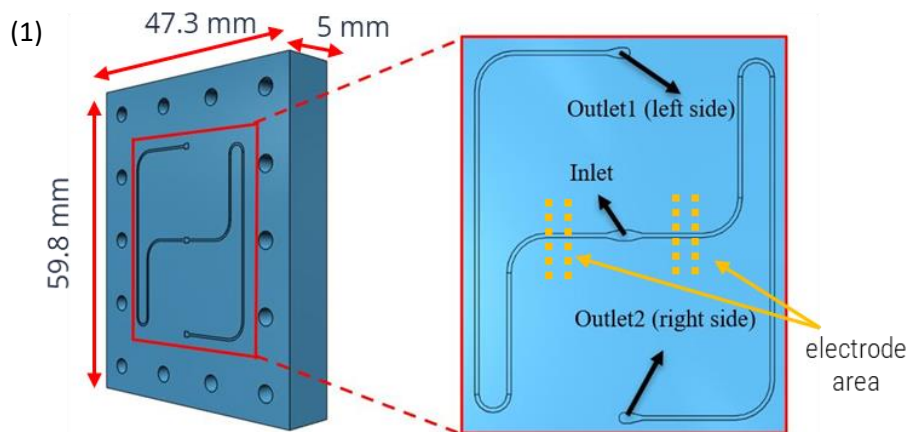


Figure 3.6 The size of 3D-printed connector

3.2.2.2 PDMS microchannel

The PDMS microchannel have to be exactly symmetrical flow of both outlets; likewise, the pressure of outlet will be different and causes pressure to drop that the flow will be flow only one outlet. For preventing the significant fabrication error that causes pressure drop, we design the channel to be long for reducing the risk of fabrication error. Microchannel had 40- μm height and 400- μm width with around 77- μm length for both outlets. The design of PDMS microchannel and mold are shown in figure 3.7. The mold was made of aluminium because of good heat conduction. After we made the mold, we fabricated our microchannel by using Polydimethylsiloxane (PDMS) to have approximately 5-mm height. The PDMS microchannel and mold are shown in figure 3.8. Unfortunately, we cannot peel our microchannel around the pillars. The finished microchannel is 33.3 mm x 43.3 mm with 5-mm height.



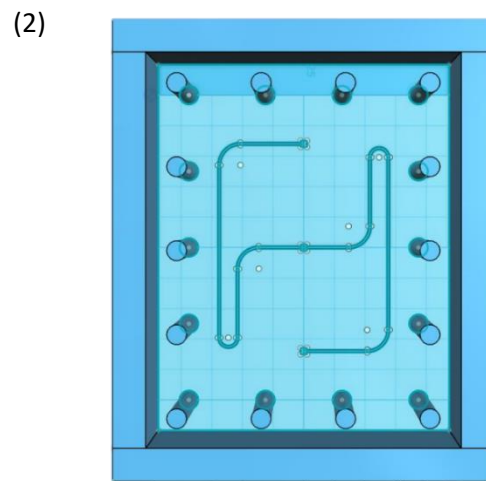


Figure 3.7 The design of PDMS microchannel. (1) PDMS microchannel. (2) PDMS mold.

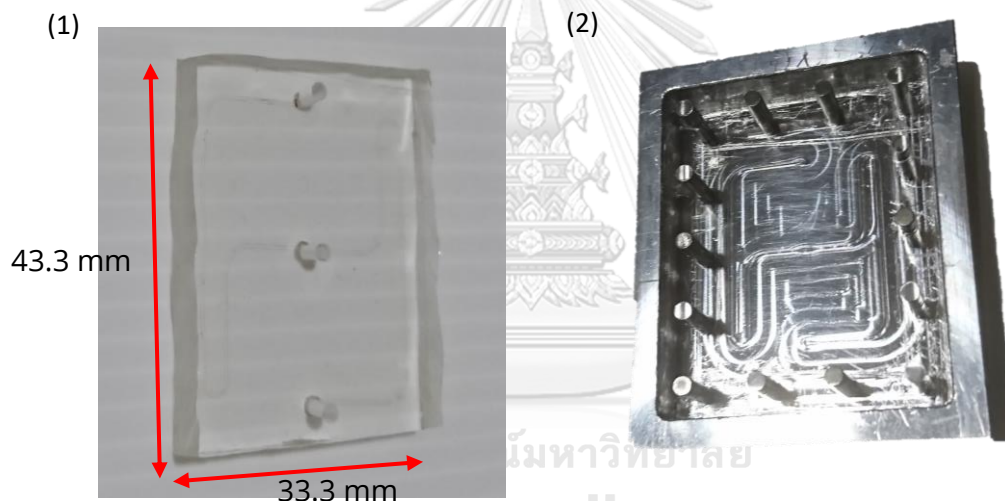


Figure 3.8 The PDMS microchannel and mold. (1) PDMS microchannel. (2) PDMS mold.

3.2.2.3 PCB

Typically, the electrodes for cell impedance measurement used microfabrication which is capable to form similar in size to the cell. That is difficult to make and expensive as well. In this research, we measured the impedance of a group of cells that required at most $300\text{-}\mu\text{m}$ area matched the smallest electrode size of PCB. Thus, we chose to fabricate our electrode on PCB for easily reproduction. There are 8 pair of electrodes which is divided to be 4 pair located each side of microchannel outlets symmetrically with $330 \times 400 \mu\text{m}$ sensing area (figure 3.9). The PCB sensing area coated by insulator, except sensing area. Moreover, we connected SMA connectors to the end of electrodes in order to link Vector Network Analyzer during an experiment. The finished PCB is shown in figure 3.10.

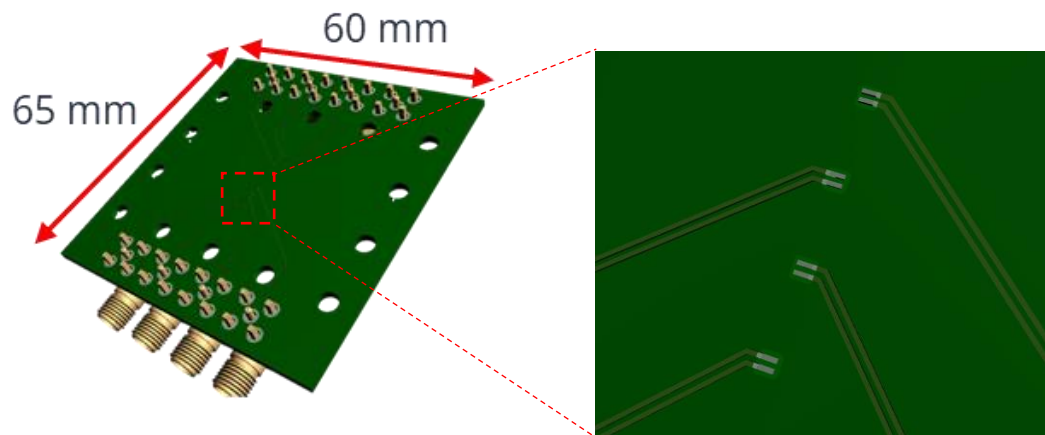


Figure 3.9 The design of PCB.

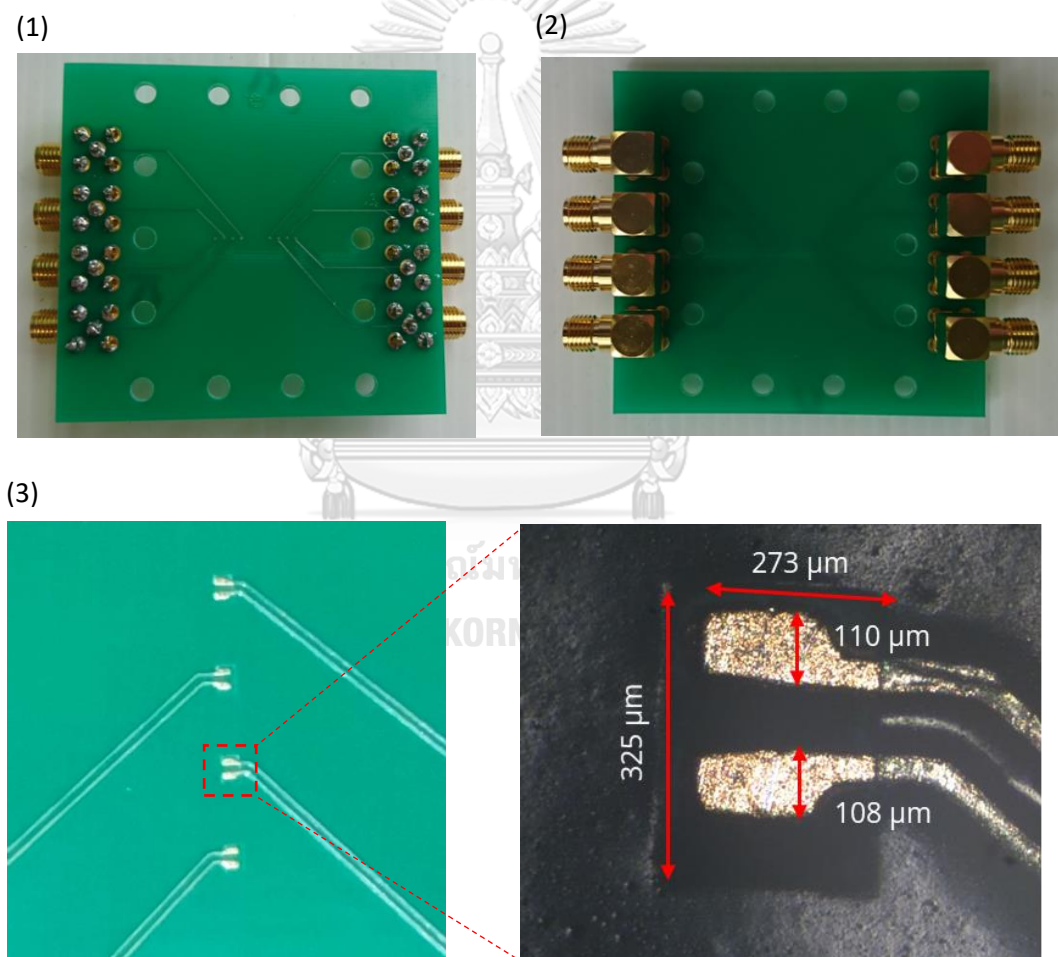


Figure 3.10 The PCB. (1) Front of PCB. (2) Back of PCB. (3) Size of Electrode.

3.2.2.4 Laser-cut acrylic plates

Laser-cut acrylic plates are the part to thicken the microchannel and electrodes on PCB together. Because of its smooth surface and rigid body, it let our channel flow smoothly and has no leaking. There are two plates: top plate and bottom plate with 6-mm thick. The top plate is the part between 3D-printing connector and PDMS microchannel which requires the holes for one inlet and two outlets. On the other hand, the bottom plate needs only the holes for connecting all part. The picture in figure 3.11 shows the design for laser-cut acrylic pattern and the finished acrylic plates are shown in figure 3.12.

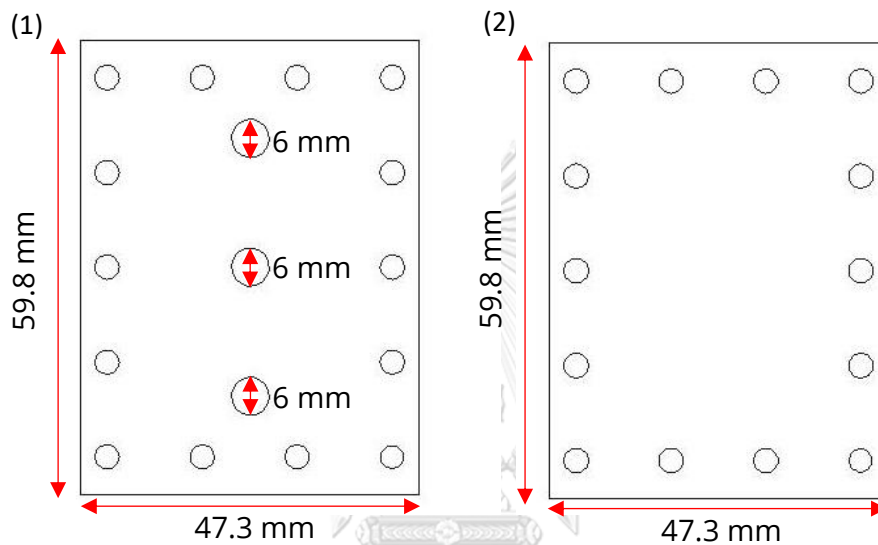


Figure 3.11 The design of laser-cut acrylic plate. (1) Top plate. (2) Bottom plate.

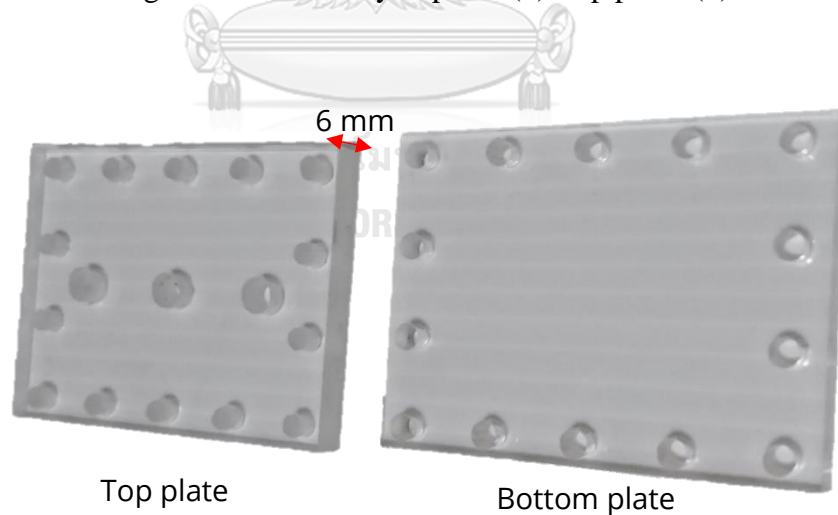


Figure 3.12 The laser-cut acrylic plates.

3.2.2.5 Syringe, needle, and tubes

We used the 3mL syringe to contain our test sample and blunted IV catheters safelet cath 20G x 1 ¼" needle which has 43-mm length covered all electromagnetic diameter and 152- μ m thick between electromagnetic field and test sample. Moreover,

we used one 6.5-mm-length tube to be inlet and two 80-mm-length tubes to be outlets connected to PDMS microchannel. The sizes of syringe, needle, and tubes are shown in figure 3.13. In addition, the outer and inner diameters of needle and tubes are shown in figure 3.14.

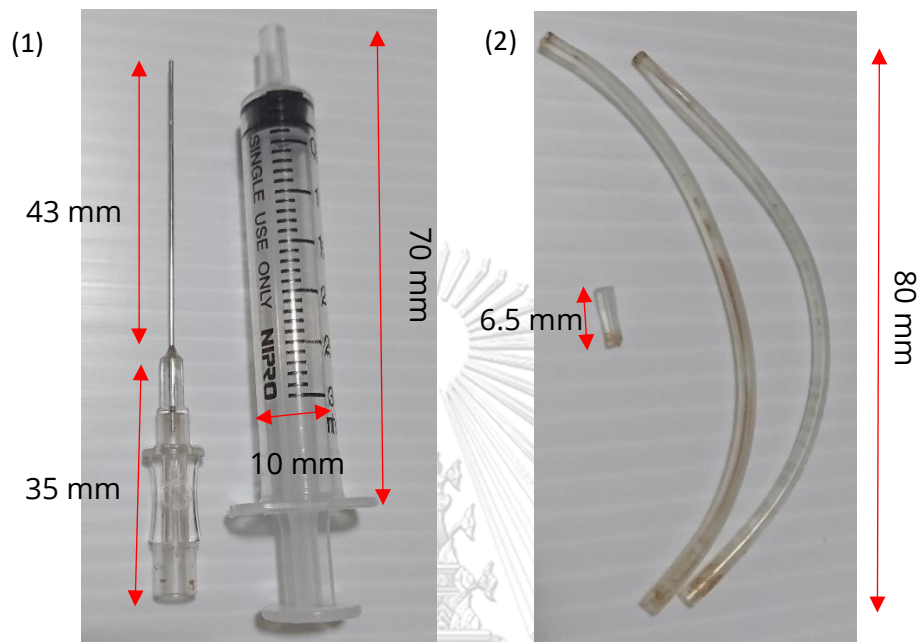


Figure 3.13 The sizes of syringe, needle, and tubes. (1) Syringe and needle. (2) Tubes

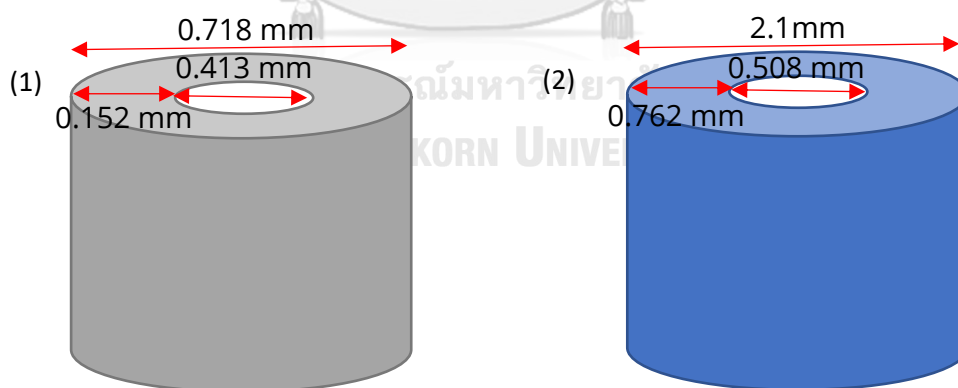


Figure 3.14 The outer and inner diameters of needle and tubes. (1) Diameter of needle. (2) Diameter of tube.

3.2.3 Equipment

After we combined every component together, we connected our system to tools followed by the principle of our system as shown in figure 3.15.

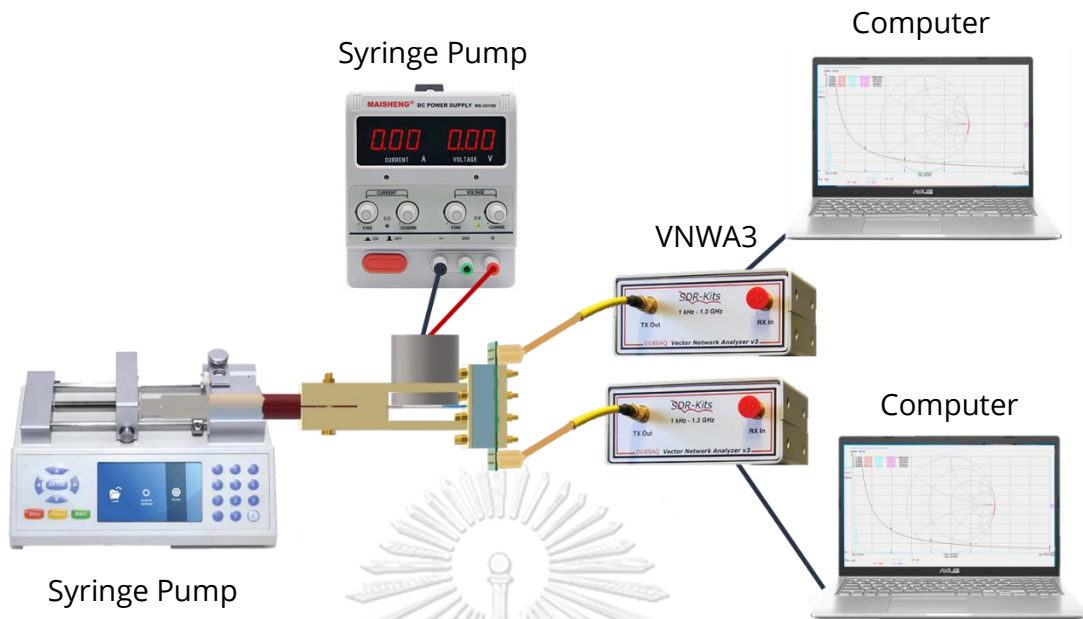
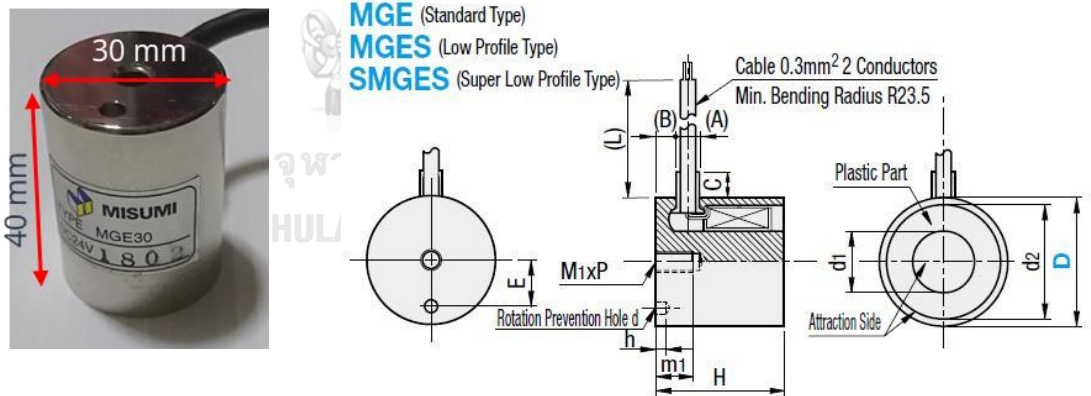


Figure 3.15 The equipment connection.

3.2.3.1 Electromagnet

We choose electromagnet from misumi (MGE30), as shown in figure 3.16. The magnetic induced (T) of this electromagnet is shown in 3.17.



| Part No. | | H | d ₁ | d ₂ | (A) | (B) | C | M _{1xP} | m ₁ | d | h | E | (L) | V | A | Mass (g) |
|----------|----|----|----------------|----------------|-----|-----|----|------------------|----------------|---|---|----|-----|----|------|----------|
| Type | D | | | | | | | | | | | | | | | |
| MGE | 30 | 40 | 13 | 27 | 7.2 | 6 | 10 | 6 × 1.0 | 12 | 4 | 3 | 10 | 700 | 24 | 0.17 | 200 |

Figure 3.16 MGE30 specs from misumi.

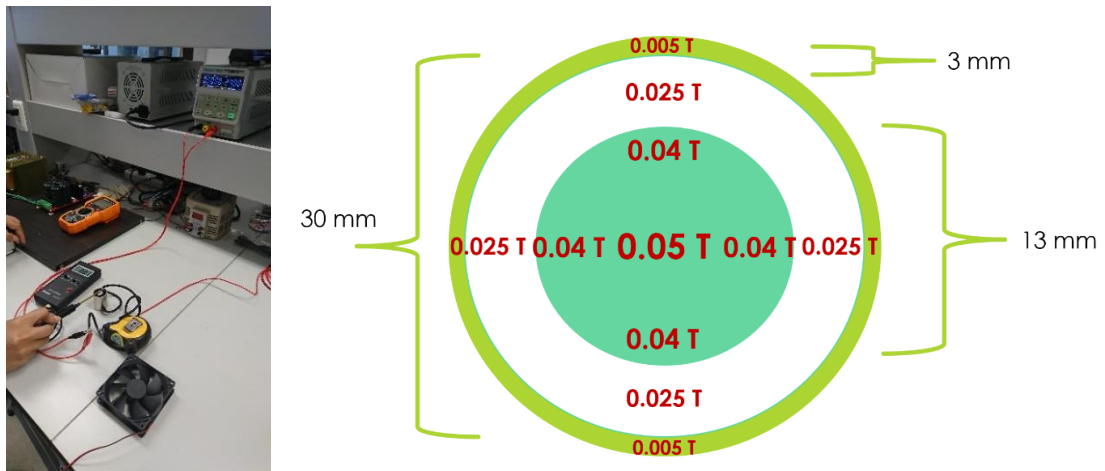


Figure 3.17 The measurement of magnetic induced.

3.2.3.2 DG8SAQ Vector Network Analyzer

We chose the DG8SAQ VNWA 3 Low Cost 1.3 GHz Vector Network Analyzer (figure 3.18) to measure impedance signal because it is cheap and frequency range up to 1.3 GHz that can response the biological cells. The DG8SAQ VNWA 3 offers all VNWA hardware on a single PCB for maximum reliability, high stability 12 MHz +/- 0.5 ppm Analogue TCXO from which all clock signals are obtained, and supplied fully assembled and tested. The more information is shown in figure 3.19.



Figure 3.18 DG8SAQ VNWA 3.

| SDR-Kits VNWA Model Matrix | | | | |
|---|-----------------------------|------------------------|------------------|------------------|
| Model | VNWA3 | VNWA3E | VNWA3SE-SMA | VNWA3SE-N |
| Description | original 1 port VNWA Design | Expansion board fitted | 2 Port Automatic | 2 Port Automatic |
| Front Connectors type | 2 x SMA | 2 x SMA | 2 x SMA | 2 x N-Connector |
| S-Parameter switch fitted - automatic 2 Port Measurements | No | No | Yes | Yes |
| S11 and S21 measurements in single sweep supported | No | Yes | Yes | Yes |
| External Clock connector & RJ12 | No | Yes | Yes | Yes |
| Control options fitted | No | Yes | Yes | Yes |
| Basic Calibration kit option 1 3pc SOL + Thru Cable | Yes | Yes | Yes | Optional order |
| VNWA Case + 4 pcs Cal kit + Thru Cable | Yes | Yes | Yes | Optional order |
| VNWA Case _ 4 pcs Premium Cal kit + 1 Thru cable | No | Yes | Yes | Optional order |
| VNWA Options: | | | | |
| Magi-Cal® Automatic Calibrator | Supported | Supported | Supported | No |
| VNWA 3 Expansion Board | Available | Fitted | Fitted | Fitted |
| VNWA 2 port upgrade kit | Available | Available | Fitted | Fitted |
| Simple BNC Bracket upgrade | Available | Available | No | No |
| Simple N Bracket upgrade kit | Available | Available | No | Not Required |
| VNWA Presentation Case | Available | Available | Yes 09/20 | Yes 09/20 |
| Low Jitter 1pps GPSDO Ext Clock | Optional | Fitted | Fitted | Fitted |
| 3 pc SMA SOL Cal Kit | Available | Available | Available | No |
| 4 pcs SOLT Cal Kit SMA or N | Available | Available | Available | Available |
| 4 or 5 pc Premium SOLT Cal Kit | Available | Available | Available | Yes 5pc planned |

Figure 3.19 SDR-Kits VNWA model matrix.

3.3 Summary

Our concept is to develop the system that can differentiate percentage parasitemia by measuring impedance of two symmetrically located electrodes that we use electromagnetic field for cell enrichment. We developed the system that contained 7 main components: 1. 3D-printed connector, 2. PDMS microchannel, 3. PCB's electrode, 4. laser-cut acrylic plates, 5. syringe, 6. needle, and 7. tubes. Our system connected to electromagnet with DC power supply for cell enrichment and DG8SAQ VNWA 3 for impedance measurement.

Next, the experiment will be conduct in proof-of-concept by using plastic beads as a representative of healthy red blood cells (hRBCs) and magnetic beads as a representative of malaria-infected red blood cells (iRBCs) in order to find suitable parameters. Then, we will test with mouse malaria cells in order to test the hypothesis that our system will generate the symmetrical flow and only iRBCs respond to electromagnetic field to enrich cells in one side. The results should be the little different impedance changes in low parasitemia samples and high different impedance changes in high parasitemia samples that we can find the ratio between the impedance values of two outlets to be an indicator of numbers of percentage parasitemia.

CHAPTER 4

CALIBRATION AND PRELIMINARY RESULTS

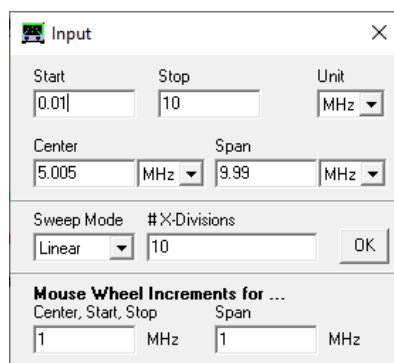
4.1 Calibration

First of all, we have to check the reliability of DG8SAQ Vector Network Analyzer in order to be our tool to measure impedance signal. The first step is equipment calibration (figure 4.2) by calibrating 10 kHz – 10MHz through SMA 50 ohms cable with Female SMA SOL 4 pieces Calibration Kit of 12 GHz Parts: (1) 50 Ohm 1 Watt Jack (female) load, (2) 0 Ohm Short Jack (female), (3) SMA Jack - Jack (Female-Female) Open connector & Adapter, and (4) SMA Plug - Plug (Male-Male Open) connector & Adapter as shown in figure 4.1. The results of calibration are shown as Smith graph (Appendix Figure 2).

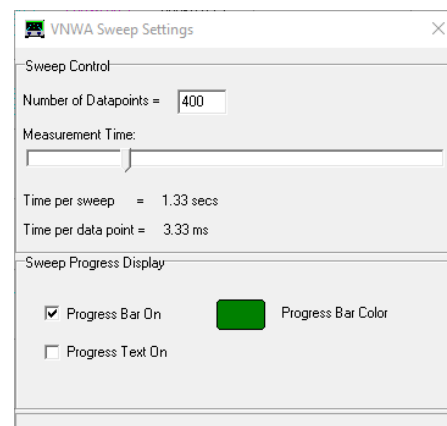


Figure 4.1 Premium FEMALE SMA SOL 4 pcs Calibration Kit of 12 GHz Parts.

(1)



(2)



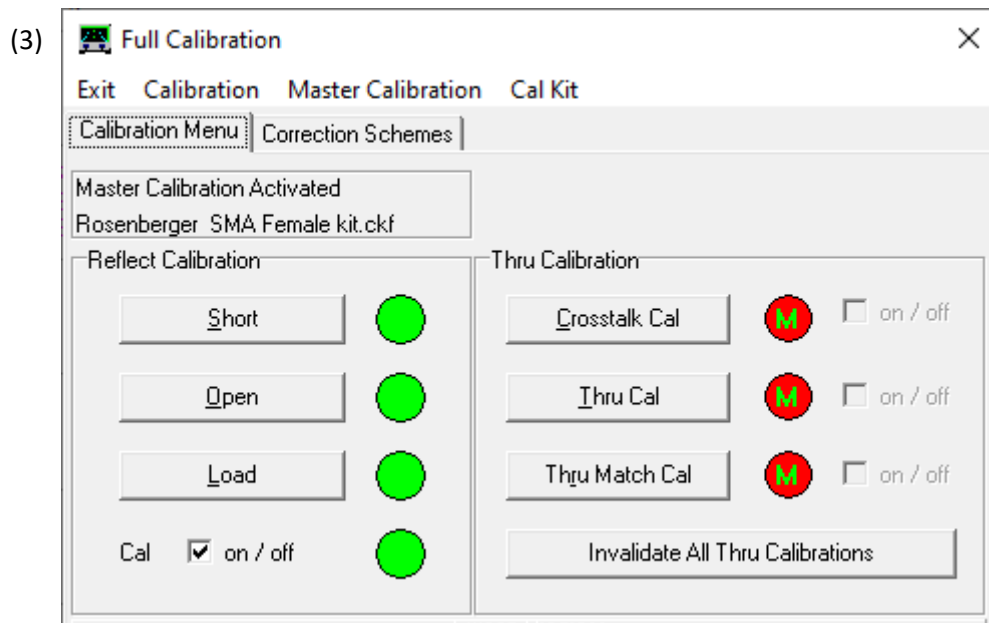


Figure 4.2 Female calibration step: (1) Set start and stop frequency, (2) Set number of datapoints and measurement time, and (3) Calibrate VNWA with Female SMA SOL 4 pcs Calibration Kit.

Secondly, we calibrate our tool with series RC circuit with VNWA Testboard Kit (figure 4.3). There one capacitor (68 pF) and three resistors (47 Ohms, 1 kOhms, and 10 kOhms). The results compared to RC circuit calculation both impedance and resistance-reactance signal are shown in figure 4.4-4.6.

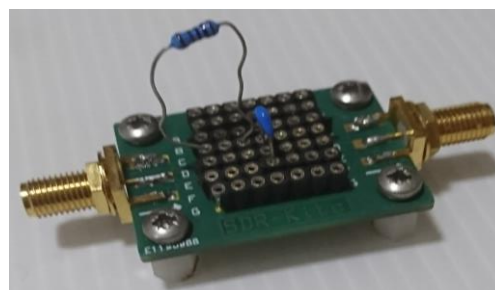
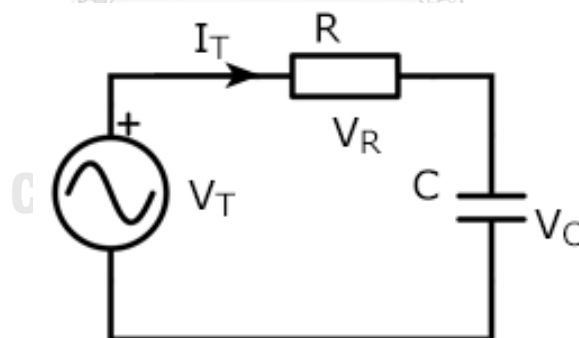


Figure 4.3 RC circuit with VNWA Testboard Kit.

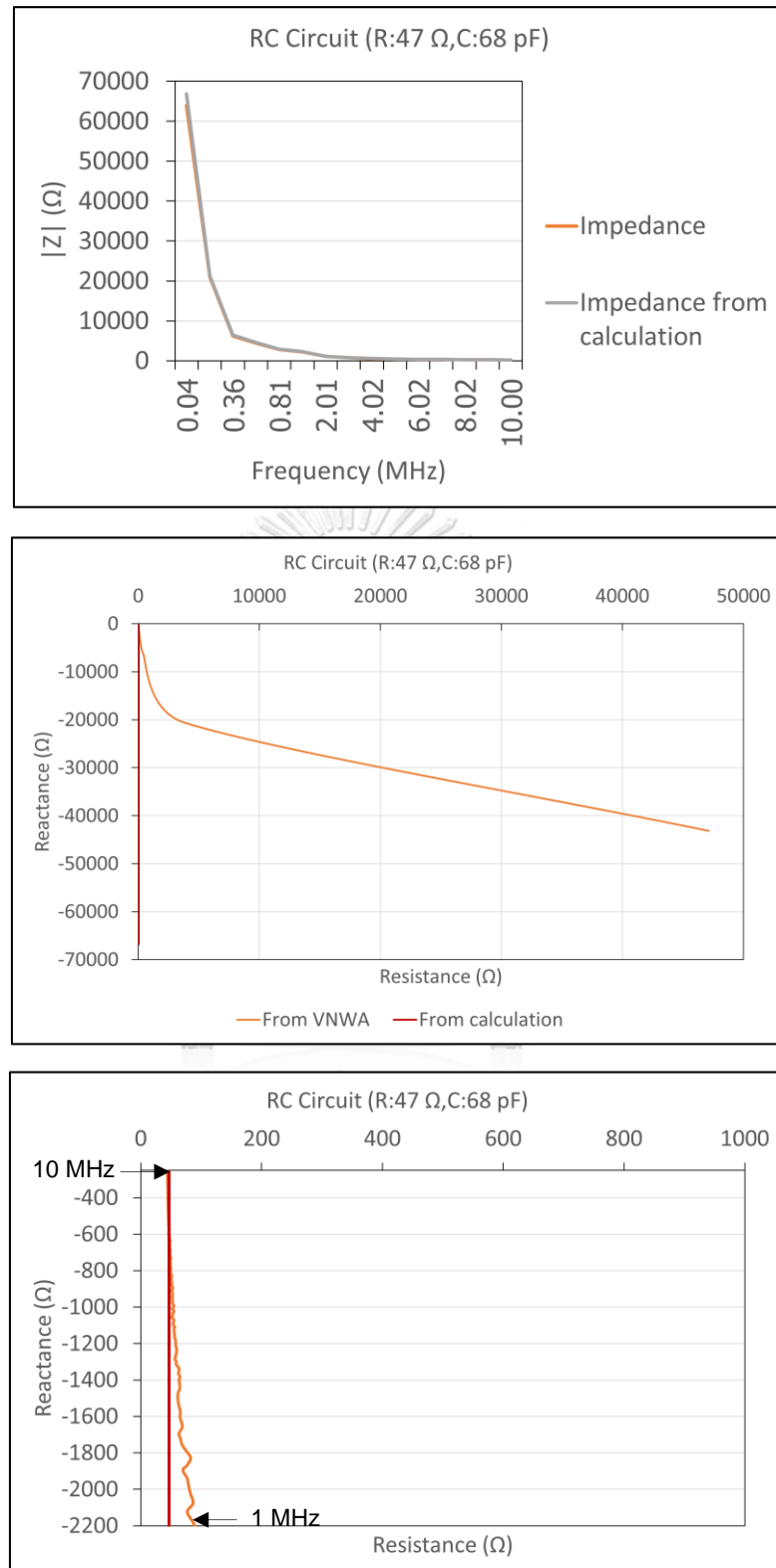


Figure 4.4 Impedance and Resistance-Reactance signal of resistor 47 Ohms and capacitor 68 pF.

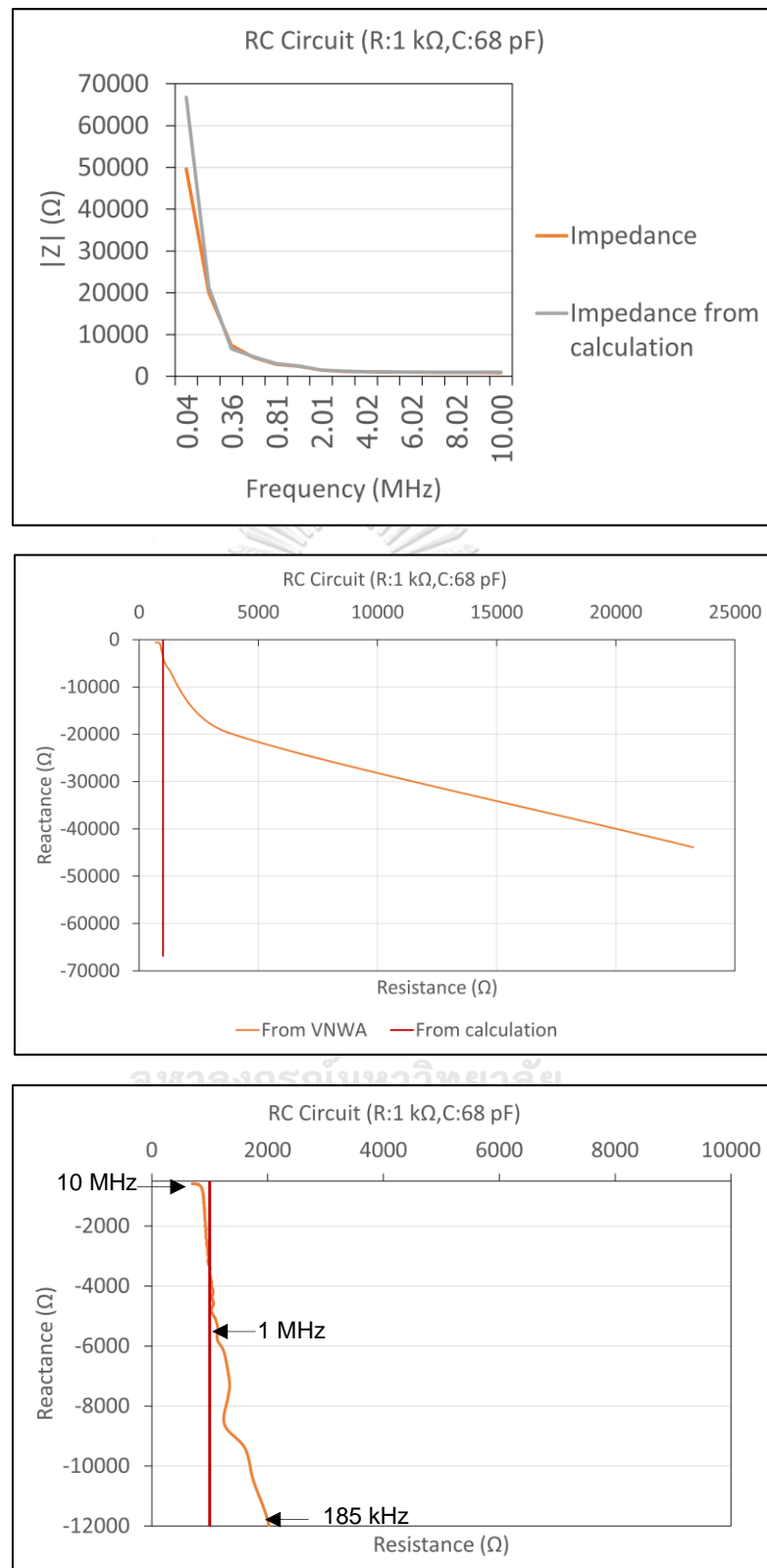


Figure 4.5 Impedance and Resistance-Reactance signal of resistor 1 kOhms and capacitor 68 pF.

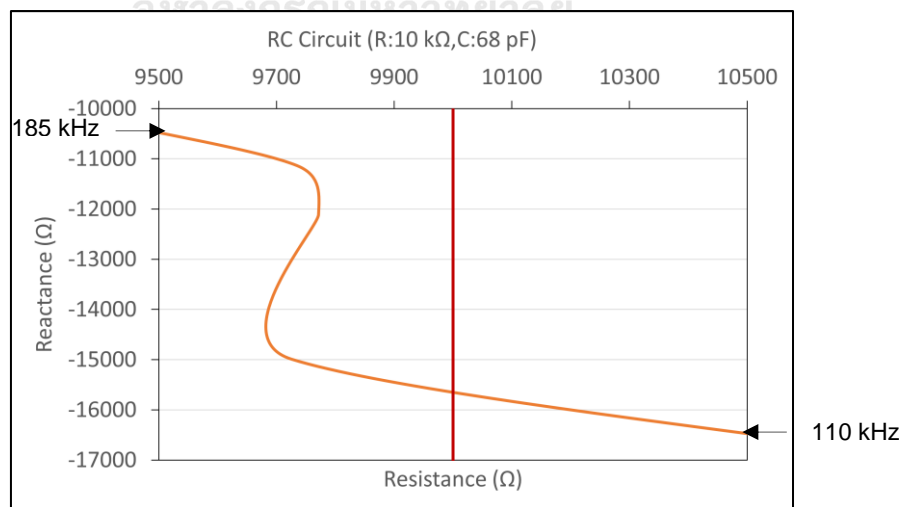
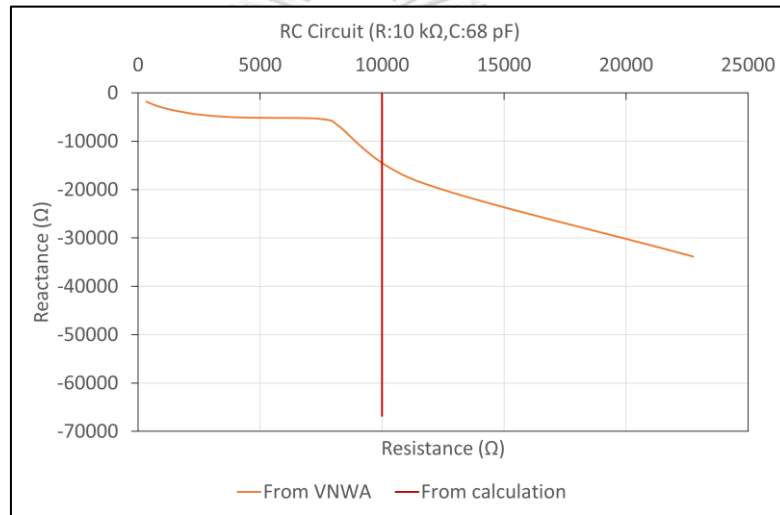
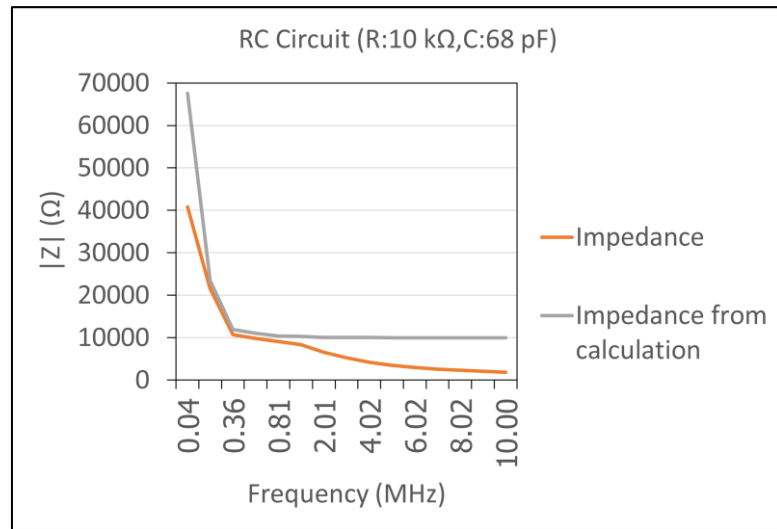


Figure 4.6 Impedance and Resistance-Reactance signal of resistor 1 kOhms and capacitor 68 pF.

Comparing to RC circuit calculator at 10 kHz–10 MHz, DG8SAQ Vector Network Analyzer can measure the similar value at different frequency in each case. In case of resistor 47 Ω and capacitor 68 pF, $|Z|$ is matched with the calculation at 10 kHz–10 MHz and Reactance–Resistance is matched with the calculation at 1 MHz–10 MHz. In case of resistor 1 k Ω and capacitor 68 pF, $|Z|$ is matched with the calculation at 100 kHz–10 MHz and Reactance–Resistance is matched with the calculation at 185 kHz–10 MHz. In case of resistor 10 k Ω and capacitor 68 pF, $|Z|$ is matched with the calculation at 100 kHz–1 MHz and Reactance–Resistance is matched with the calculation at 110 kHz–185 kHz.

4.2 Proof of concept

According to our concept to use the T-shape channel to be one inlet and two identical outlets, we must proof the functionality of system's enrichment part before we continue impedance measurement.

We combined all components, except PCB and VNWA, being one system (figure 4.7) for flowing two types of 10- μ m-diameter beads: polystyrene particles (plastic beads) which density is 650,000 beads/ml, and magnetic polystyrene particles (magnetic beads) 300,000 beads/ml. The experiment flow rate is 0.05 ml/min which is the optimized rate before leaking. Moreover, we applied electromagnet either side of system with providing 15V and 24V to generate electromagnetic field. The experiment is conducted three times repeating.

We assume that the microchannel will produce the symmetrical flow observed by the volume of sample we get in microcentrifuge tubes at both outlets and electromagnetic field will enrich only magnetic beads at the side that electromagnet located.

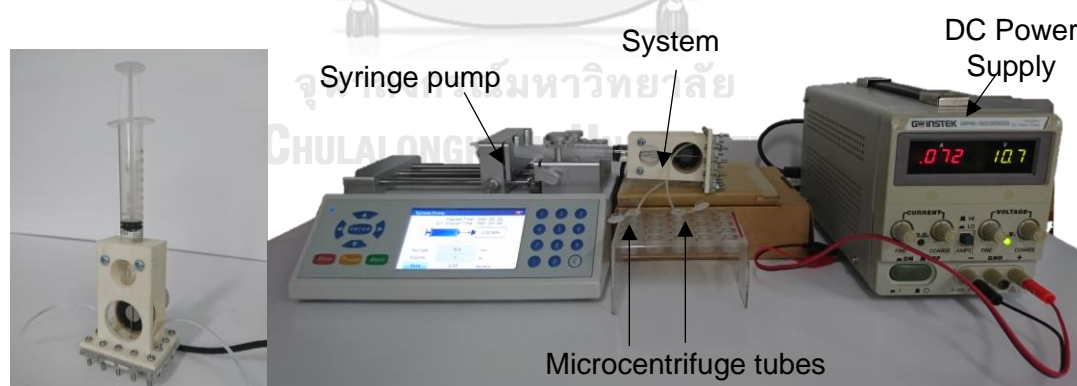


Figure 4.7 Proof of concept.

4.2 Preliminary Results

The proof-of-concept results showed that our microchannel is symmetrical flow with less than 33.33% difference of two outlets between the side that applied electromagnetic field and another side of 3 experiment batches as shown in figure 4.8. The electromagnet-applied side always had greater in volume than another side that

sum of both sides is similar to 1.5 ml input. Firstly, for plastic bead experiment, the applied side had 0.69 ml with $\pm 33.33\%$ uncertainty and another side had 0.58 ml $\pm 25.83\%$ uncertainty. Secondly, for magnetic bead experiments with 0V, 15V, and 24V supplied voltage, the applied side had 0.75 ml with $\pm 6.67\%$ uncertainty, 0.70 ml with $\pm 14.29\%$ uncertainty, 0.80 ml with $\pm 12.50\%$ uncertainty respectively. On the other hand, not applied side had 0.66 ml with $\pm 12.12\%$ uncertainty, 0.61 ml with $\pm 26.23\%$ uncertainty, 0.60 ml with $\pm 8.33\%$ uncertainty respectively. The results in number of beads of 3 experiment batches are shown in figure 4.9. In addition to number of particles both sides (the counting method is Appendix figure 3), the number of plastic beads is similar in both sides which had 65,000 beads/ml with $\pm 8.33\%$ uncertainty in not applied side and 63,000 beads/ml with $\pm 39.49\%$ uncertainty in applied side. There was not much different in number of beads in case of no supplied voltage of magnetic beads, that the applied side had 13,000 beads/ml with $\pm 1.64\%$ uncertainty and another side had 12,000 beads/ml $\pm 17.03\%$ uncertainty. On the other hand, the number of magnetic beads is increasing depending on the higher voltage we provide in electromagnet-applied side, and the number of magnetic beads is decreasing at the opposite side. In case of 15V supplied voltage of magnetic beads, the applied side had 26,000 beads/ml with $\pm 25.83\%$ uncertainty and another side had 12,000 beads/ml $\pm 0.43\%$ uncertainty. Lastly, in case of 24V supplied voltage of magnetic beads, the applied side had 31,000 beads/ml with $\pm 3.18\%$ uncertainty and another side had 8,000 beads/ml $\pm 26.32\%$ uncertainty. That is why we can make sure that our enrichment part is functional.

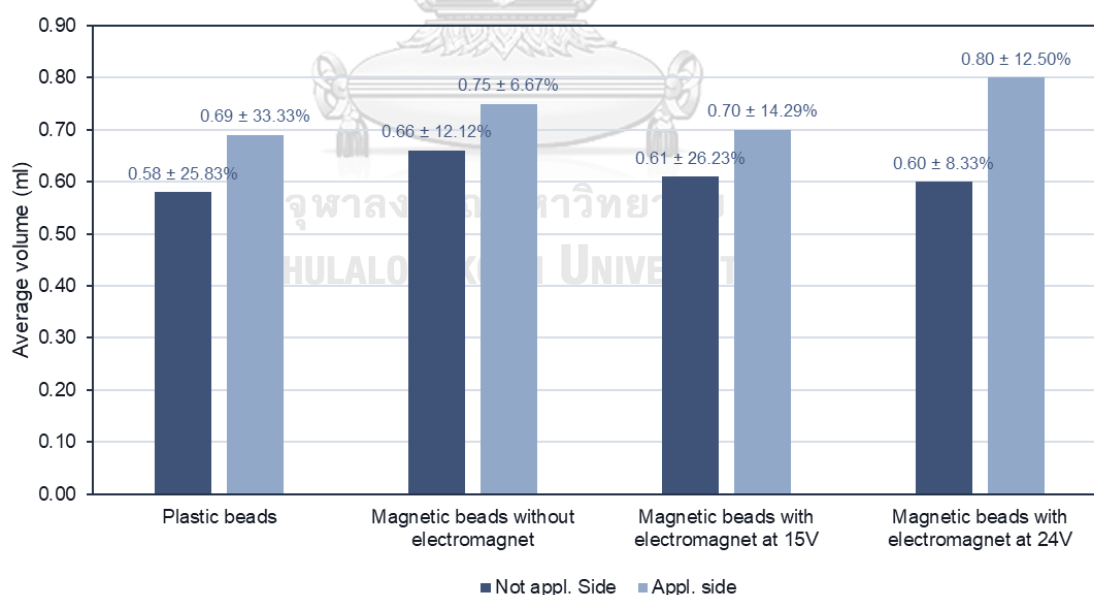


Figure 4.8 Results in volume of two sides (from repeating 3 times/condition).

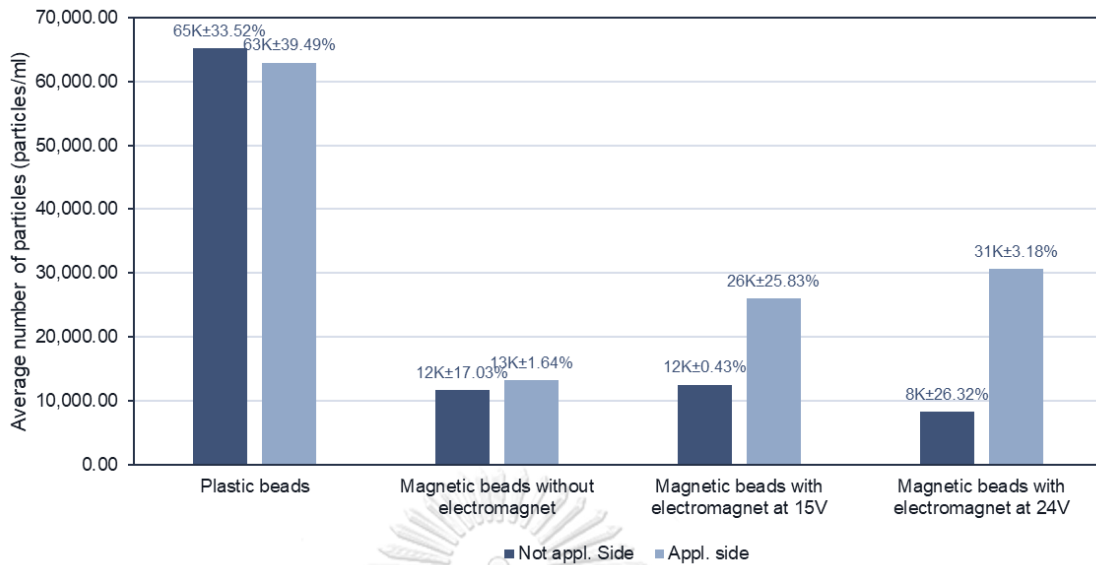


Figure 4.9 Results in number of two sides (from repeating 3 times/condition).

4.3 Summary

We calibrated DG8SAQ Vector Network Analyzer in range 10 kHz-10 MHz with compared between measurement and calculation of RC circuit using a capacitor 68 pF and 3 resistors: 47 Ω , 1 k Ω , and 10 k Ω . According to the results, the reliable impedance of measurement close to 47 Ω is in range 100 kHz-10 MHz and for resistance and reactance is in range 1 MHz-10 MHz. The reliable impedance of measurement close to 1 k Ω (similar to cells) is in range 100 kHz-10 MHz and for resistance and reactance is in range 185 kHz-10 MHz. The reliable impedance of measurement close to 10 k Ω (similar to beads) is in range 100 kHz-1 MHz and for resistance and reactance is in range 110 kHz-185 kHz.

Furthermore, we conducted the proof-of-concept experiment that using plastic beads as a representative of healthy red blood cells (hRBCs) and magnetic beads as a representative of malaria-infected red blood cells (iRBCs) to test the symmetrical flow and the functional of electromagnet to generate electromagnetic field for cell enrichment part. The results showed that our system is able to flow symmetrically with less than 33.33% difference in volume between both sides of 3 experiment batches. Moreover, electromagnetic field enriched magnetic beads to one side depending on provided voltage, but it did not affect plastic beads.

CHAPTER 5 RESULTS

According to chapter 4, we have already proved the reliability of DG8SAQ Vector Network Analyzer to be our tool to measure impedance and the magnetic particle enrichment of electromagnet at distinguished power supply. Then, we continued the impedance experiment. Firstly, we conducted two experiments: (1) static test and (2) dynamic test as shown in figure 5.1.

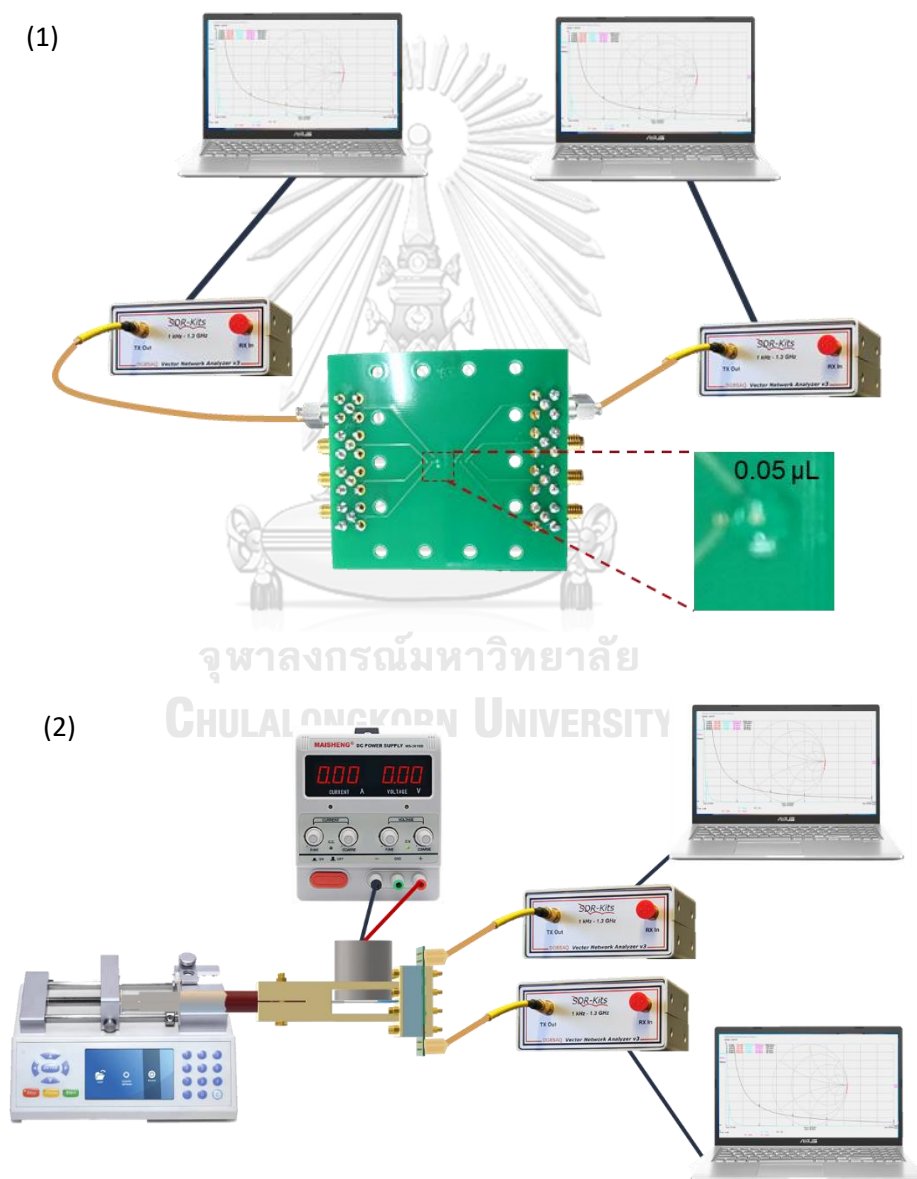


Figure 5.1 The impedance measurement part: (1) Static Test, and (2) Dynamic Test.

Secondly, we tested two kinds of sample: plastic beads and mouse blood. In static impedance test, we tested the effect of increasing density of both plastic beads and blood after 5 minutes and observed the changed signals in terms of resistance and reactance value. Similarly, the dynamic impedance test observed the signal in flowing environment. In case of plastic beads, we focused on how density affects the signal. On the other hand, in case of mouse blood, we focused on the different signals of normal mouse blood, 10% Malaria-Infected blood, and 44% Malaria-Infected blood after we applied the electromagnetic fields in the enrichment part. We used 0.05 ml/min flow rate that is capable for scan groups of particles before the same group came across the pair of electrodes.

5.1 Plastic test

5.1.1 Static impedance measurement

We prepared polystyrene beads (diameter 10 μm) at varied density: 200,000 beads/ml, 300,000 beads/ml, and 600,000 beads/ml. The test result is shown in figure 5.2-5.3.

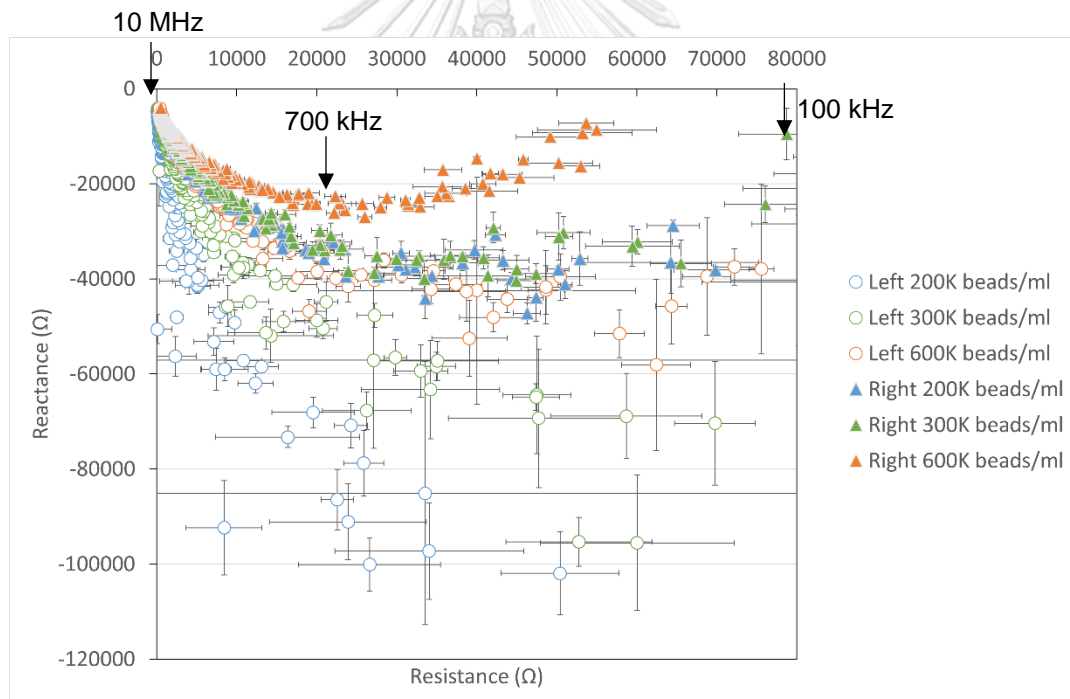


Figure 5.2 Resistance-Reactance of plastic static test at 100 kHz-10 MHz.

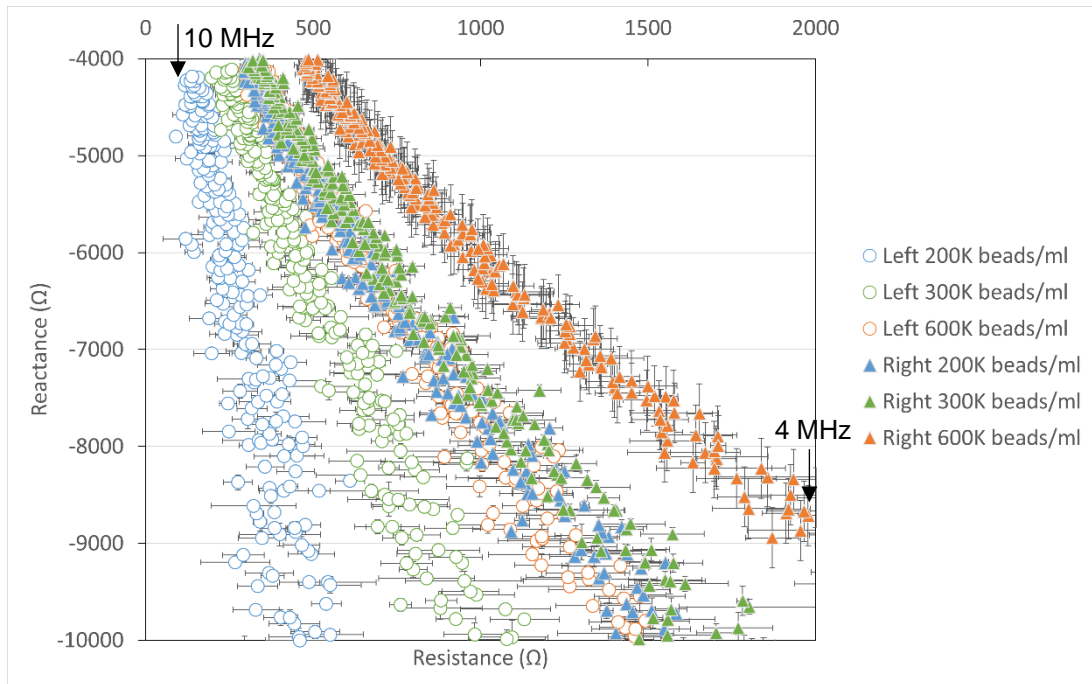


Figure 5.3 Resistance-Reactance of plastic static test at 4-10 MHz.

5.1.2 Dynamic impedance measurement

We prepared polystyrene beads (diameter 10 μm) at varied density: 600,000 beads/ml, 750,000 beads/ml, and 1,500,000 beads/ml. The test result is shown in figure 5.4-5.5.

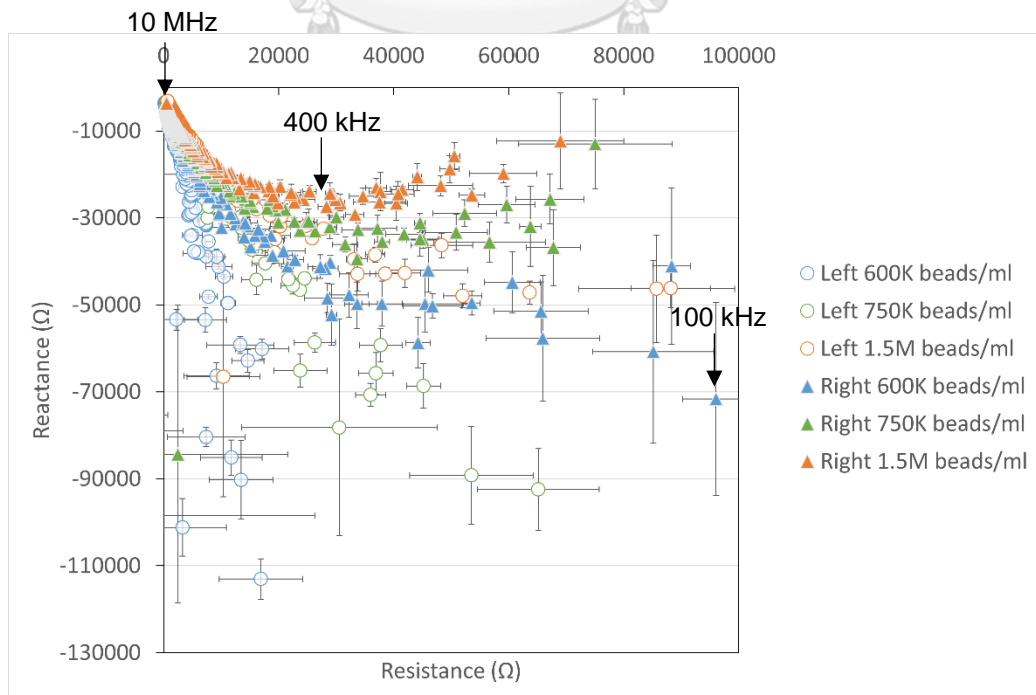


Figure 5.4 Resistance-Reactance of plastic dynamic test at 100 kHz-10 MHz.

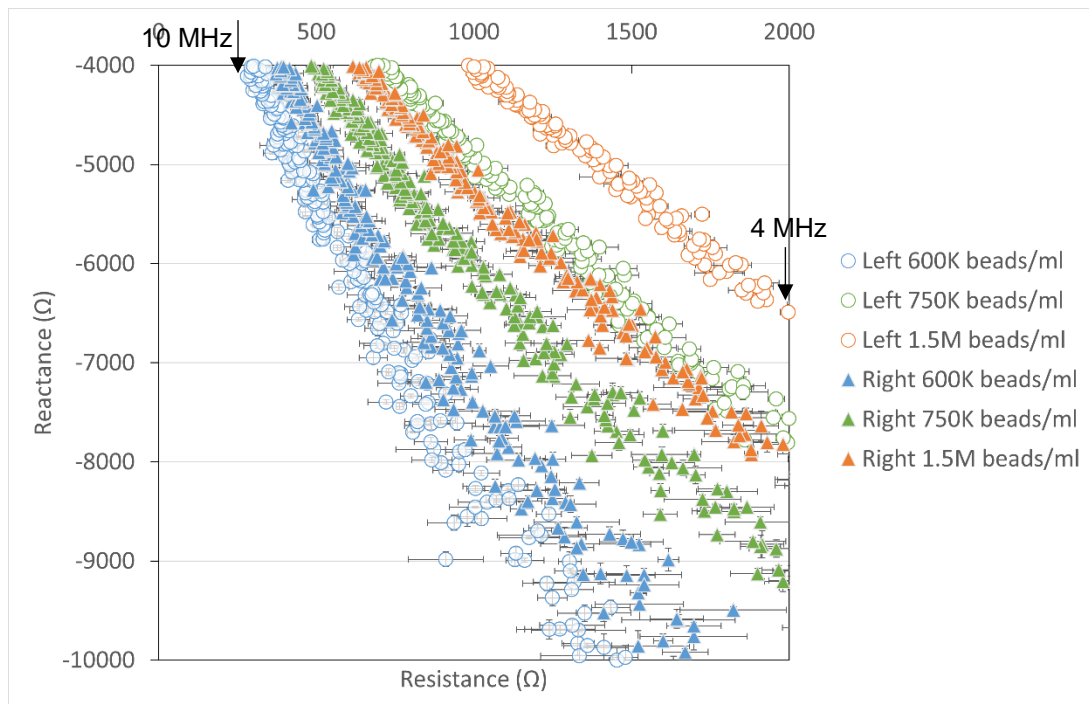
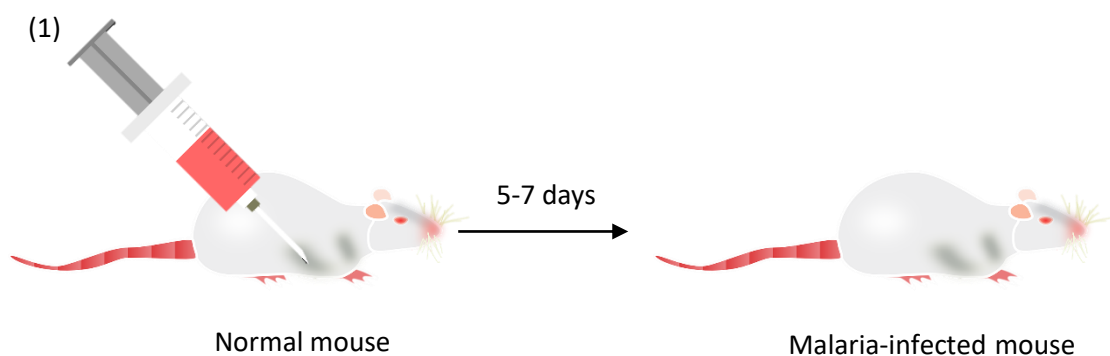


Figure 5.5 Resistance-Reactance of plastic dynamic test at 4-10 MHz.

According to test results when we increased the plastic density, the resistance was greatly increased. Because of the polarized effect of pair of electrodes, the reactance magnitude was increased until it reached the bottommost, after that it was decreased both in static and dynamic test at 100 kHz-10 MHz. The two sides of outlets had not much different and share the same trend.

5.2 Normal and malaria-infected mouse blood

For malaria-infected blood, we chose to test with *Plasmodium Yoelii* in mouse because we can induce the percentage parasitemia more than 30% (rarely found in human) by injected freeze parasite into abdominal cavity of laboratory mice and waited about 5-7 days up to individual mouse (figure 5.6). Because of the complexity of each mouse and the quality of freeze malaria-infected blood, the experiment control was difficult. Therefore, we collected only 10% parasitemia and 44% parasitemia malaria-infected blood to run the test.



(2)

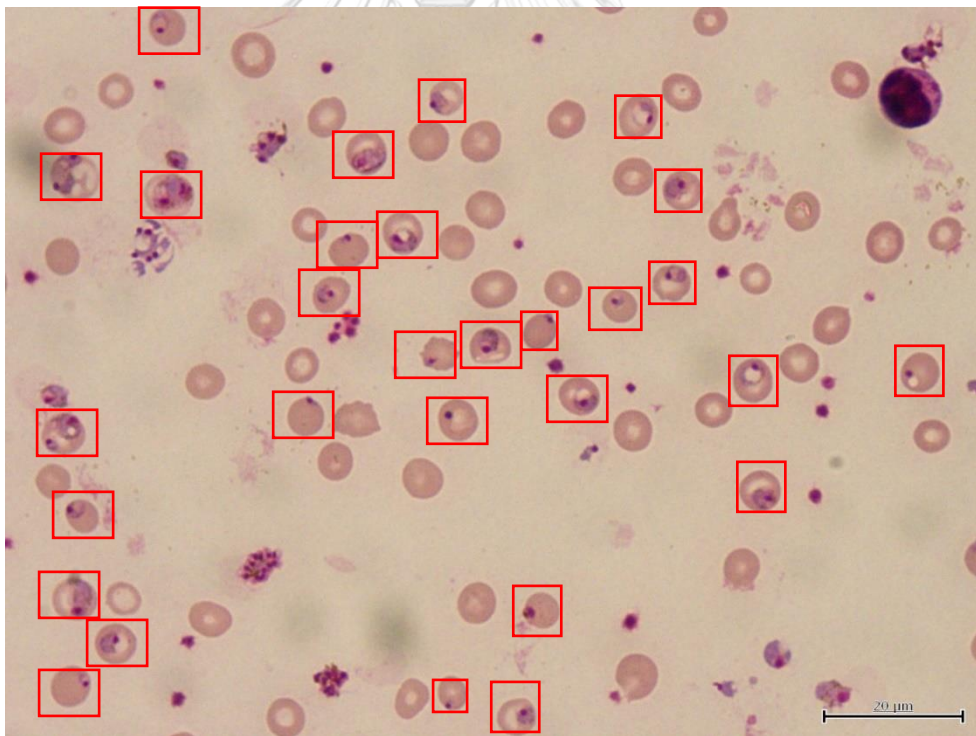
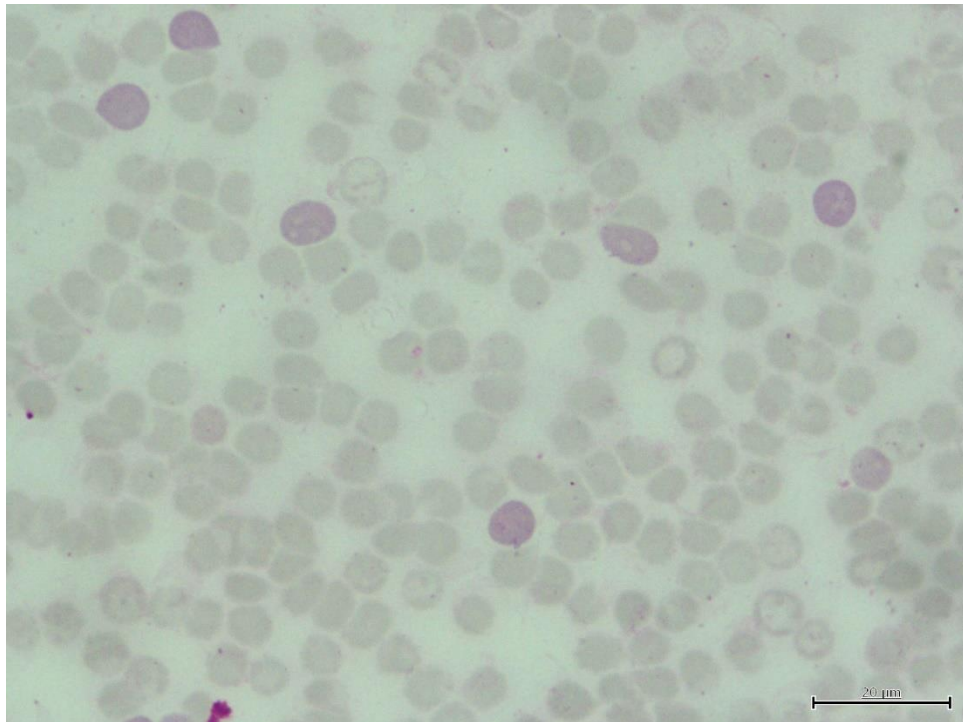


Figure 5.6 How to induce percentage parasitemia in mouse. (1) Injected malaria-infected blood. (2) Normal red blood cells and malaria-infected red blood cells (in red square).

We collected the blood sample for cutting the tip of mouse's tail and used thin smear technique with Giemsa stain to color blood cells (the procedure of Giemsa stain

is shown in Appendix Figure 4). For counting percentage parasitemia, we counted total number of malaria-infected red blood cells divided by total number of red blood cells multiplied by 100 (Eq. 15).

$$\% \text{ Parasitemia} = \frac{\text{Total number of infected RBCs}}{\text{Total number of RBCs}} \times 100 \quad (15)$$

In case of 10% parasitemia, we used 10 fields of thin smear to be counted (all picture is shown in Appendix Figure 5). We counted 87 malaria-infected red blood cells and 865 red blood cells. In case of 44% parasitemia, we used 10 fields of thin smear to be counted (all picture is shown in Appendix Figure 6). We counted 309 malaria-infected red blood cells and 693 red blood cells.

5.2.1 Static impedance measurement

5.2.1.1 Normal mouse blood

We prepared normal mouse blood at varied density: Not diluted, 5x diluted, and 10x diluted blood in PBS buffer. The test result is shown in figure 5.7.

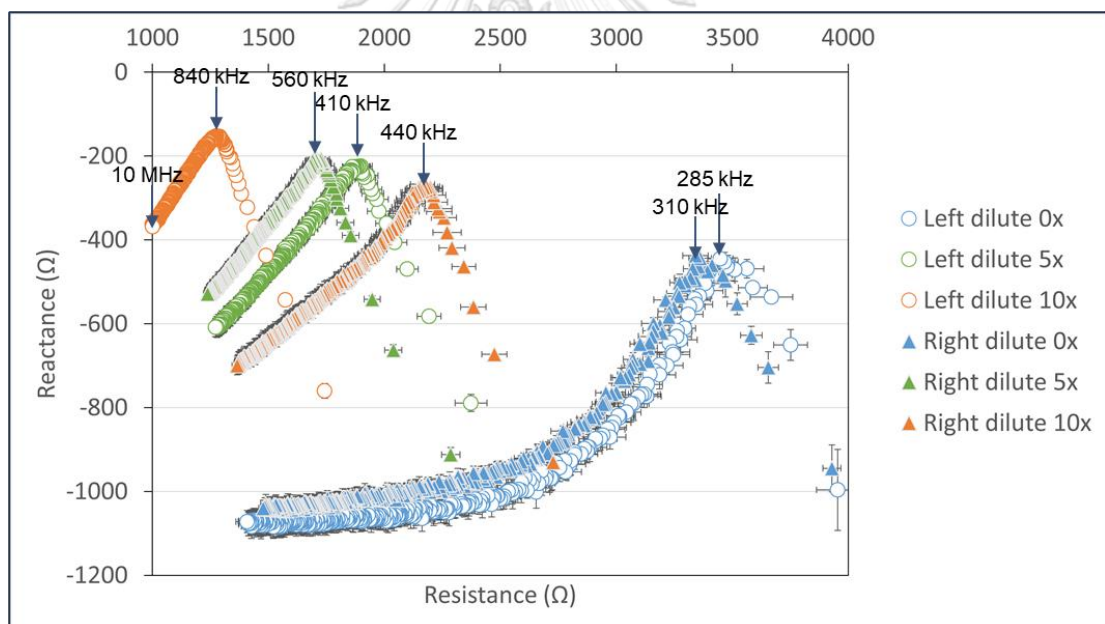


Figure 5.7 Resistance-Reactance of static test of normal mouse blood at 0x, 5x, and 10x dilution in PBS.

5.2.1.2 10% malaria-infected blood

We prepared 10% malaria-infected blood at varied density: Not diluted, 5x diluted, and 10x diluted blood in PBS buffer. The test result is shown in figure 5.8.

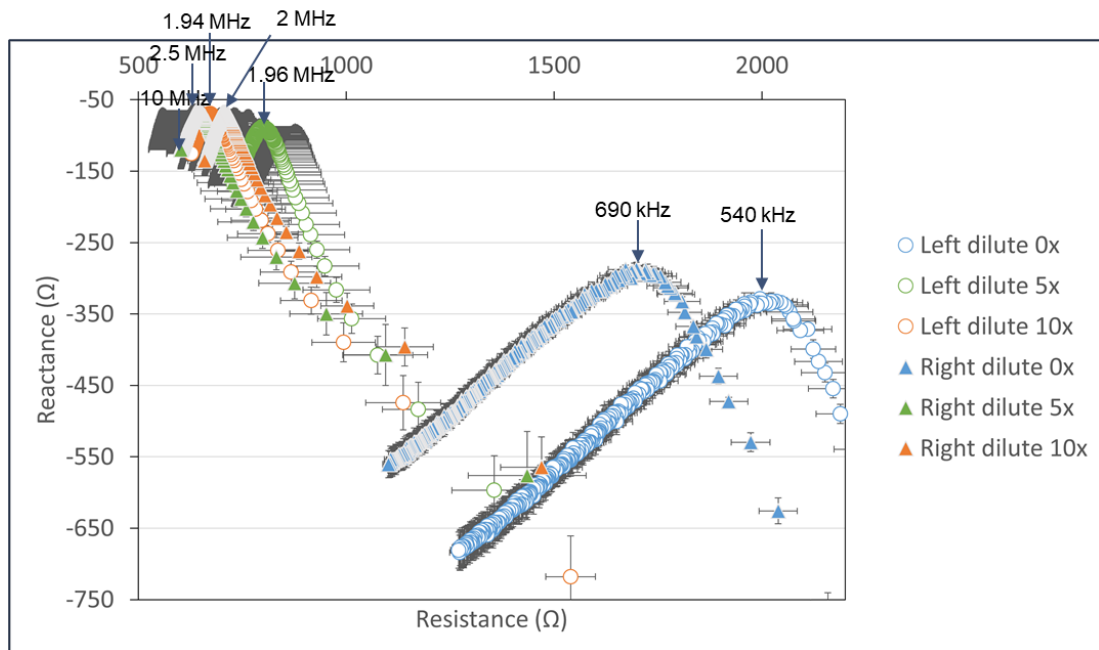


Figure 5.8 Resistance-Reactance of static test of 10% malaria-infected blood at 0x, 5x, and 10x dilution in PBS.

According to test results when we diluted the blood density, the resistance and reactance are greatly decreased in static test. Moreover, we can see the difference of signal between normal mouse blood, and 10% malaria-infected blood. The 10% malaria-infected blood had higher both the resistance and reactance compared to normal blood. In addition, PBS-diluted blood can sense the sediment of cells better than no dilution blood. The two sides of outlets had not much different and share the same trend.

5.2.2 Dynamic impedance measurement

For correcting the experiment in each condition, we let the system flow for 2 minutes before starting electromagnet. Moreover, we waited for 30 seconds after finished previous experiment to make sure that we measured the cells affected by electromagnet at different voltage.

5.2.2.1 Normal mouse blood

We applied electromagnetic field at 15V and 24V to test normal mouse blood. The test result is shown in figure 5.9.

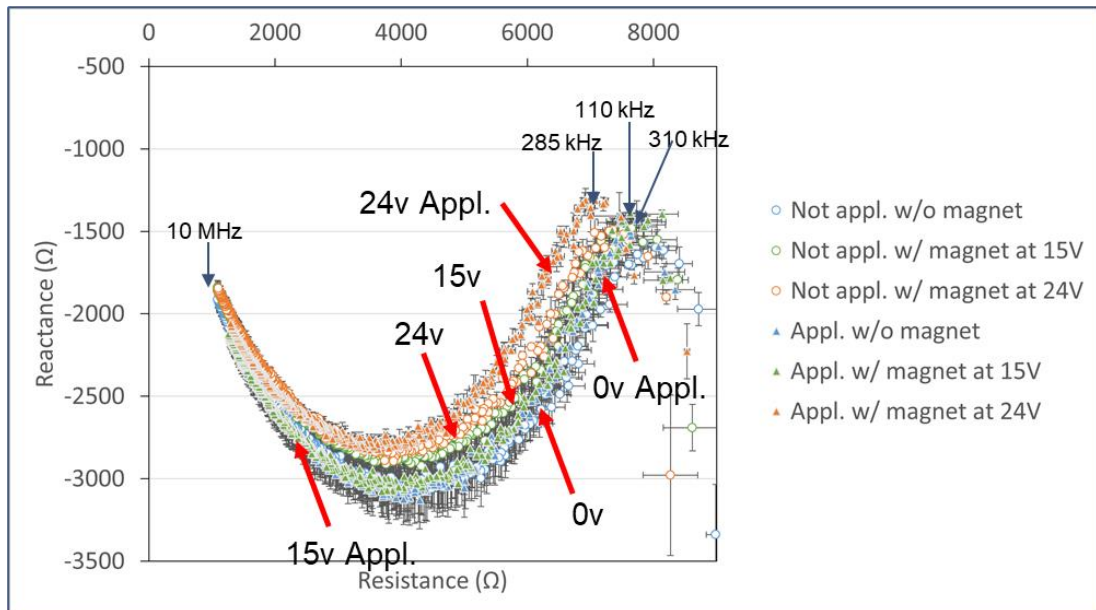


Figure 5.9 Resistance-Reactance of dynamic test of normal mouse blood at 0V, 15V, and 24V.

5.2.2.2 10% malaria-infected blood

We applied electromagnetic field at 15V and 24V to test 10% malaria-infected blood. The test result is shown in figure 5.10.

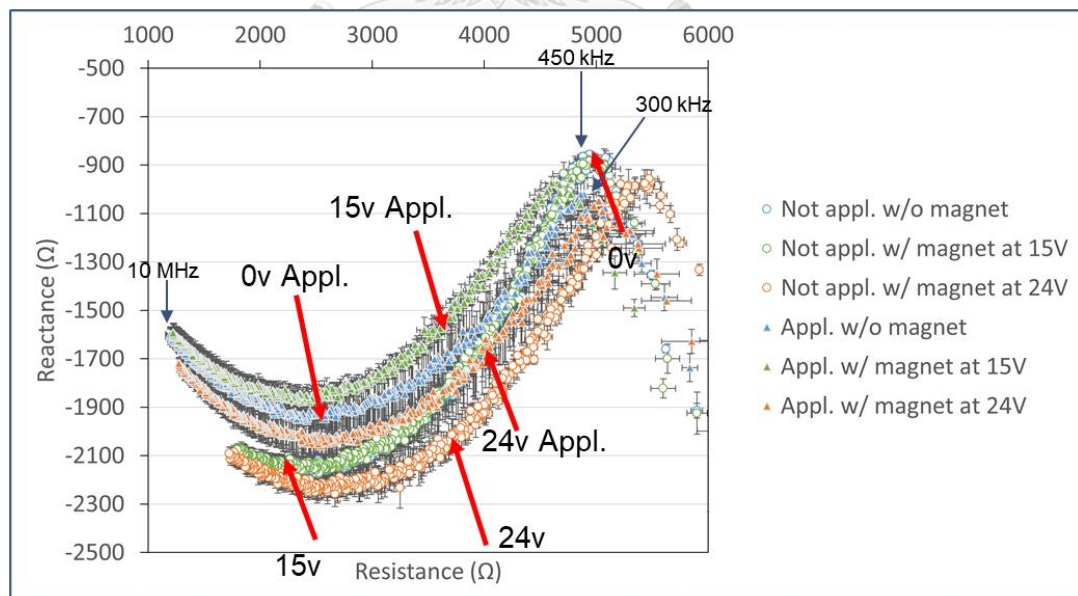


Figure 5.10 Resistance-Reactance of dynamic test of 10% malaria-infected blood at 0V, 15V, and 24V.

5.2.2.3 44% malaria-infected blood

We applied electromagnetic field at 15V and 24V to test 44% malaria-infected blood. The test result is shown in figure 5.11.

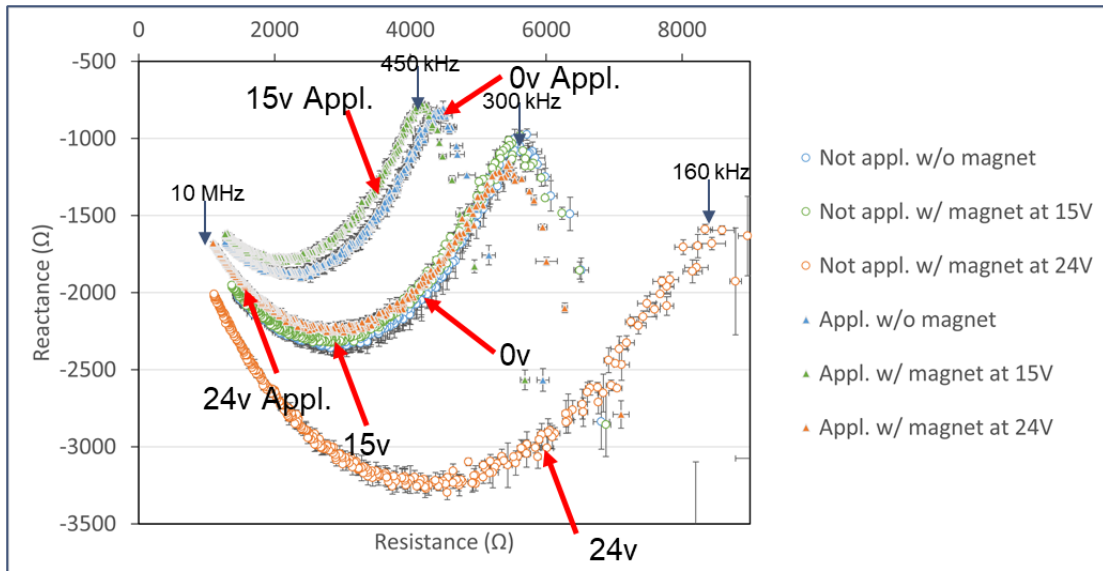


Figure 5.11 Resistance-Reactance of dynamic test of 44% malaria-infected blood at 0V, 15V, and 24V.

According to test results when we applied electromagnet at 15V and 24V, we can see the difference of signal between normal mouse blood, 10% malaria-infected blood, and 44% malaria-infected blood in dynamic test as shown in figure 5.12-5.14. The 10% malaria-infected blood and 44% malaria-infected blood have lower both the resistance and reactance compared to normal blood at 0V. In case of normal mouse blood and 10% malaria-infected blood, the resistance and reactance were not much changed by electromagnetic field (figure 5.12). In case of 15V, there was a small different as shown in figure 5.13. On the other hand, in case of 44% malaria-infected blood, it was obviously seeing the changes as shown in figure 5.14. The losing-cell side showed that resistance was greatly increased because infected cells had lower resistance than normal cells and less density of infected cells had higher resistance. While the enriching-cell side showed that resistance was slightly increased because infected cells had lower resistance than normal cells, but less density of normal cells had higher resistance, the result will be the countering effect of these two phenomena.

Unfortunately, we cannot make the applied side and not applied side produced the same signals when not applied electromagnetic field, because it was the mean of many cells flowing on electrode at measurement time and the effect of small difference flow in both outlets.

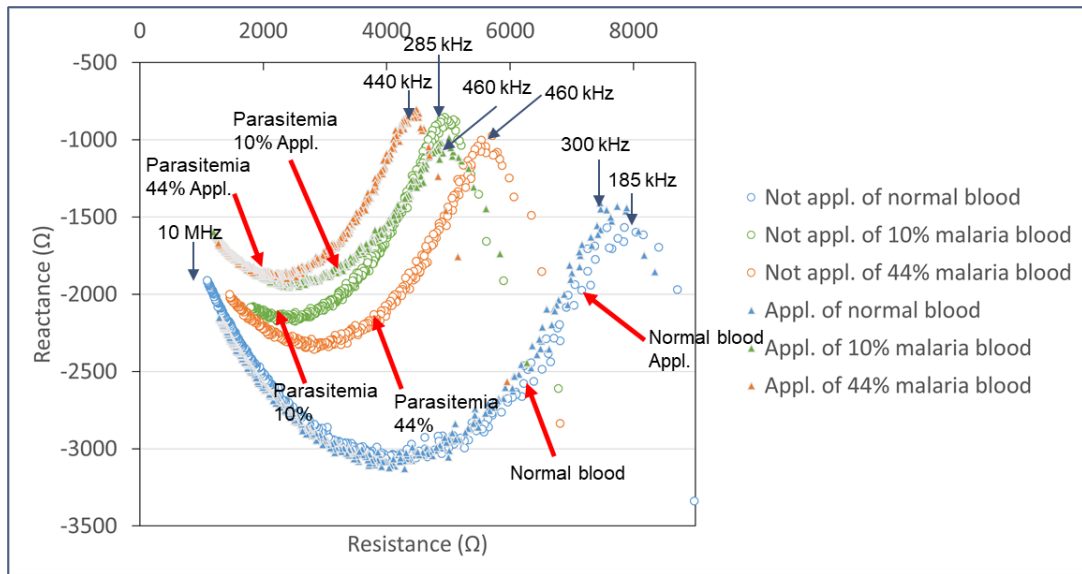


Figure 5.12 Comparison of normal mouse blood, 10% Malaria-Infected blood, and 44% Malaria-Infected blood when not applied electromagnetic field.

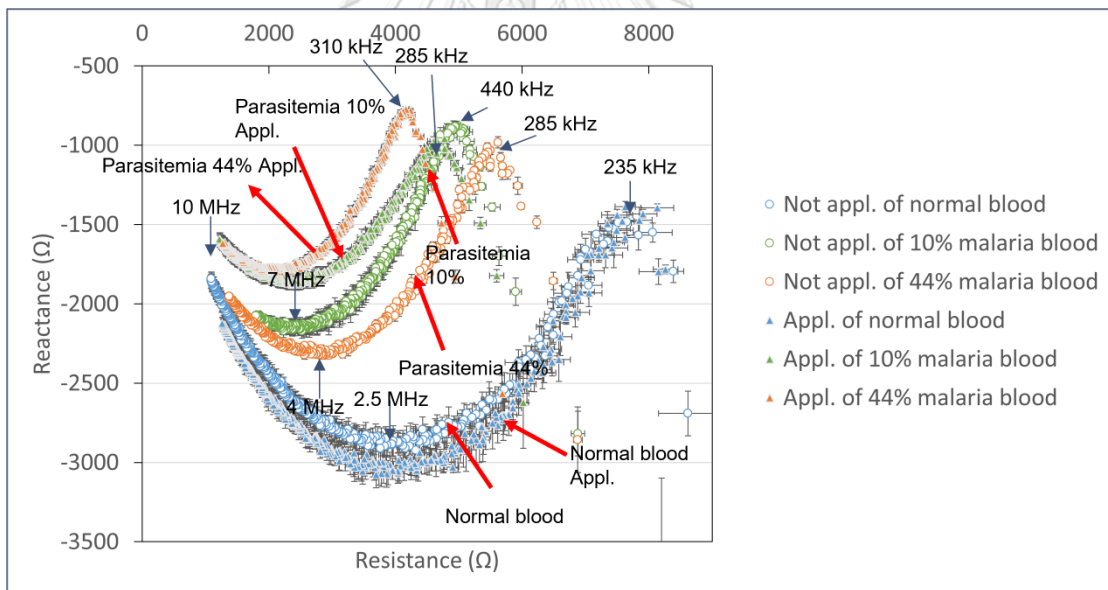


Figure 5.13 Comparison of normal mouse blood, 10% Malaria-Infected blood, and 44% Malaria-Infected blood when applied electromagnetic field at 15V.

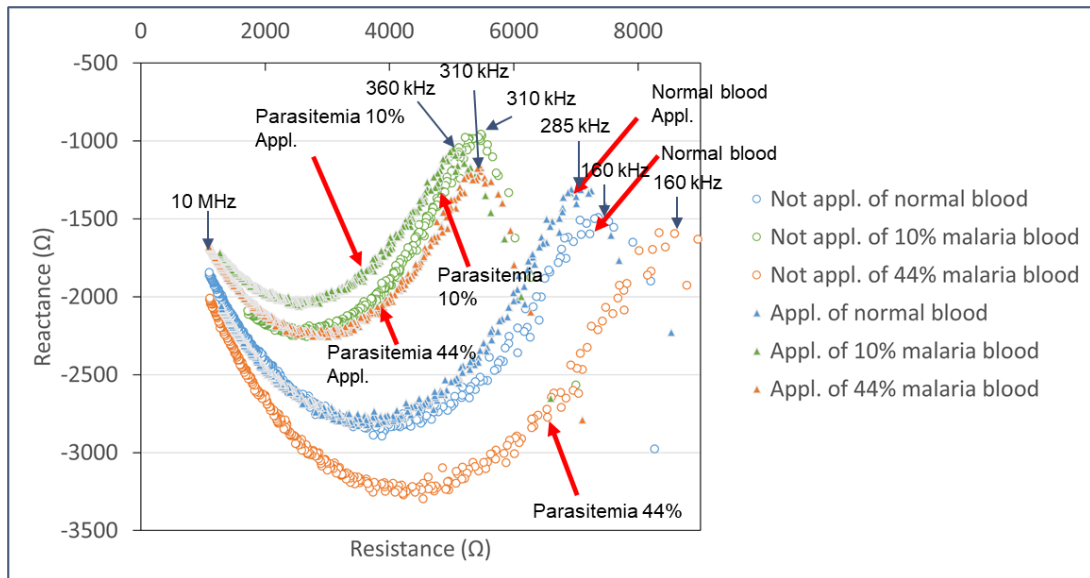


Figure 5.14 Comparison of normal mouse blood, 10% Malaria-Infected blood, and 44% Malaria-Infected blood when applied electromagnetic field at 24V.

5.2.3 Different ratio of infection

After we got all the experiment results, we need to find the different ratio of infection. In this research, we used two criteria to find the difference as follows:

- Normalized different between before applied electromagnetic field and after applied electromagnetic field of each outlet by finding difference of resistance and reactance at 0V and 24V compared each side (figure 5.15).

- Normalized different between two outlets by finding difference of resistance and reactance at 24V compared both sides with average resistance and reactance at 0V and normalized different between two outlets by finding difference of resistance (figure 5.16) and reactance at 15V compared both sides with average resistance and reactance at 0V (figure 5.17).

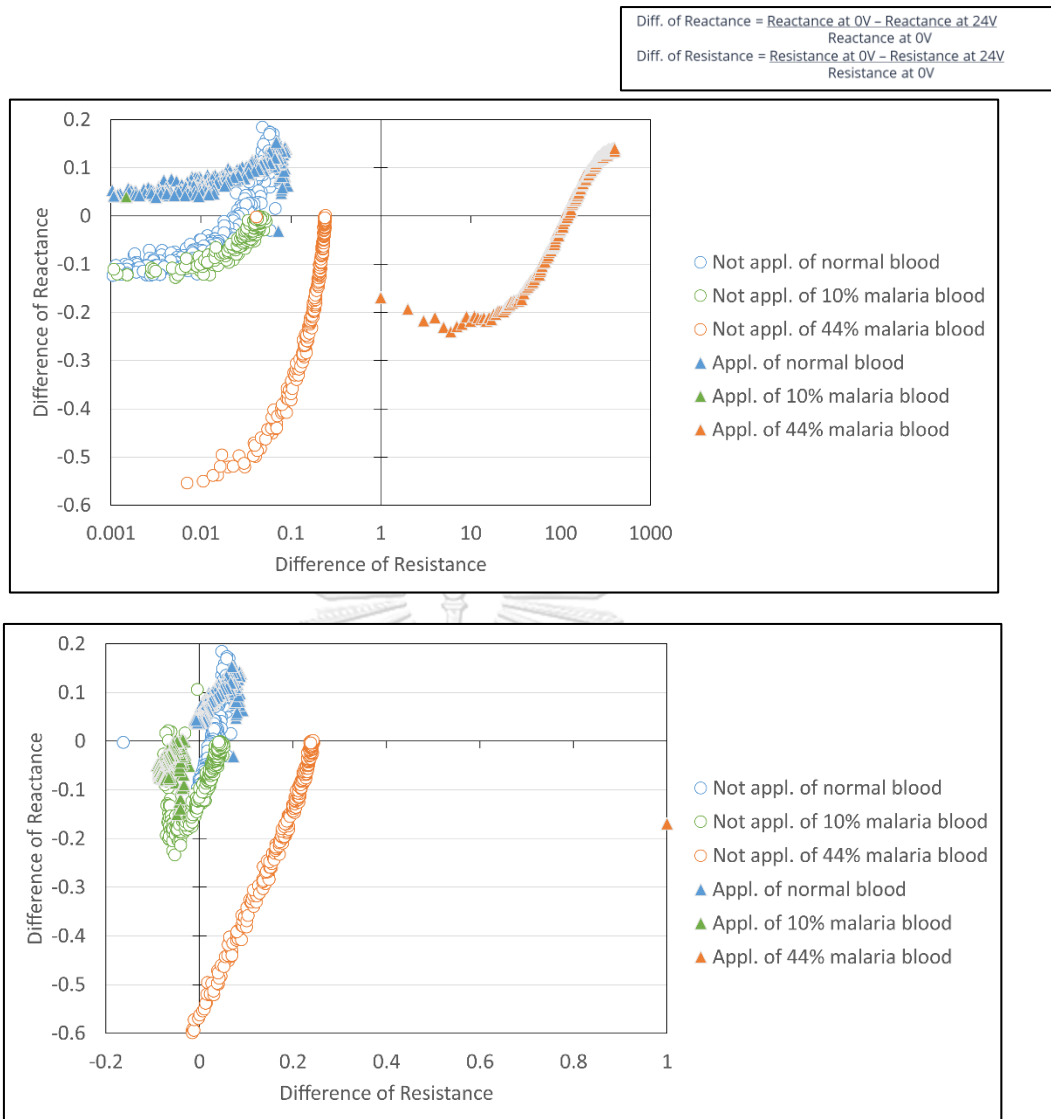


Figure 5.15 Difference of resistance and reactance at 24V compared each side with average resistance and reactance at 0V.

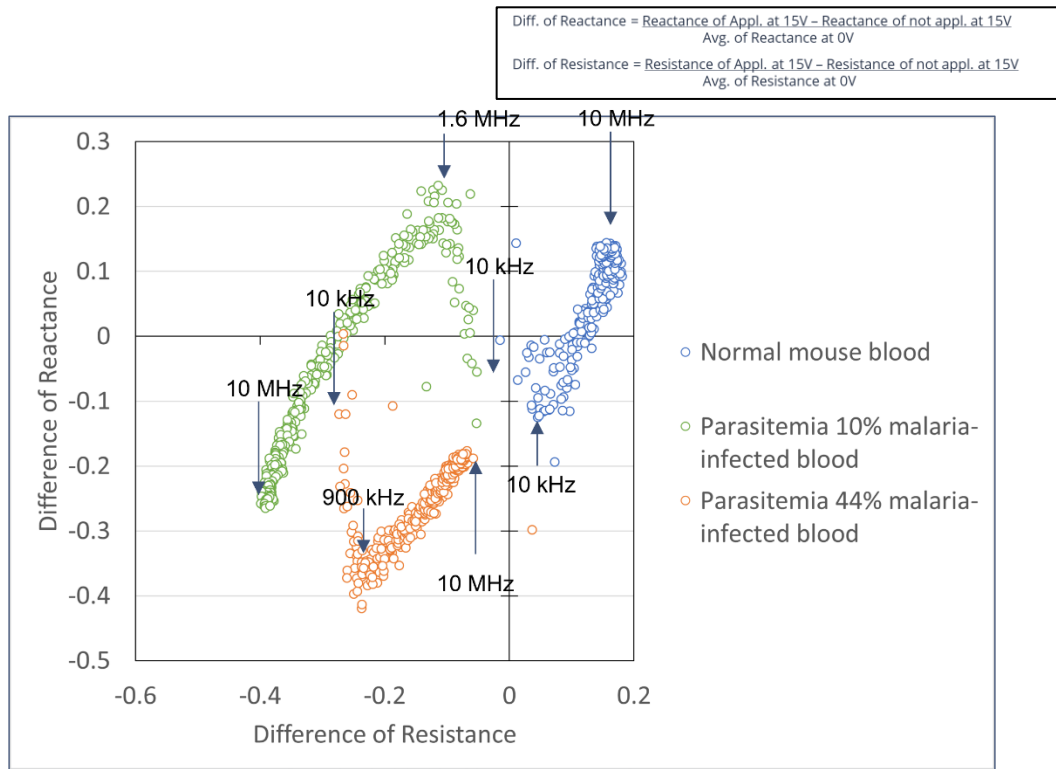


Figure 5.16 Difference of resistance and reactance at 0V and 15V compared both sides.

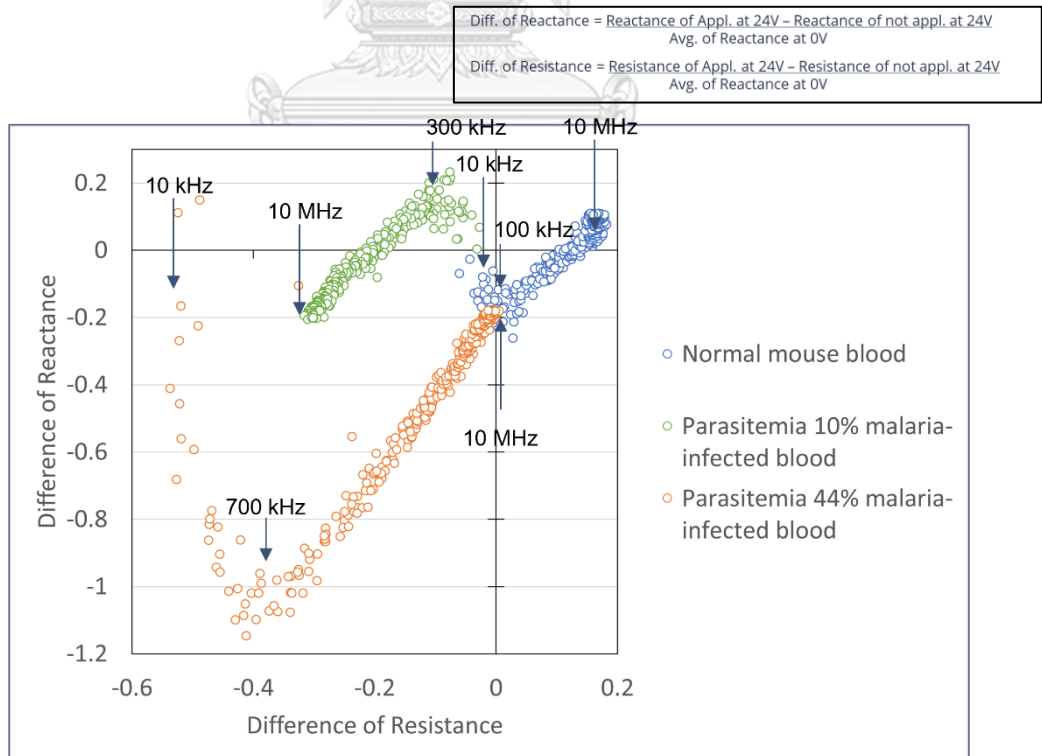


Figure 5.17 Difference of resistance and reactance at 0V and 24V compared both sides.

Following the ratio of different in these two criteria, we can see more change in case of parasitemia 44%, some change in case of parasitemia 10%, and small change in normal case. That means this research achieves the objectives in order to create the system that can differentiate percentage parasitemia by comparing impedance of two outlets coupled with cell enrichment.

5.3 Summary

We did experiments in two tests: plastic test and malaria-infected mouse blood test. In each test, we measured impedance for monitor the signal changes after 5 minutes in static method with dropping sample on electrodes, and dynamic method with flowing through system after 5 minutes. Firstly, in plastic test, we want to see the effect of particles at various density compared to DI water. As a result, both static and dynamic method, the resistance was greatly increased, as well as the reactance was slightly increased following by the increased density.

Secondly, in malaria-infected mouse blood test, we want to see the effect of particles at various density in static test and the cell enrichment phenomena, which had the clear difference in impedance signal, in case of dynamic test. Refers to results, in static test, the resistance and reactance are greatly decreased when we diluted the blood density. While, in dynamic test, we can see the difference of signal between normal mouse blood, 10% malaria-infected blood, and 44% malaria-infected blood when we applied electromagnet at 15V and 24V. It is observed that the 10% malaria-infected blood and 44% malaria-infected blood have lower both the resistance and reactance compared to normal blood at 0V. Especially, in case of 44% malaria-infected blood, it saw a lot of changes in resistance and reactance, that the losing-cell side showed that resistance was greatly, while the enriching-cell side showed that resistance was slightly decreased the countering effect of two phenomena: gathering infected cells (lower resistance) and increased cell density (higher resistance).

Finally, we can find ratio of different in these two criteria: normalized different between before applied electromagnetic field and after applied electromagnetic field of each outlet, and normalized different between two outlets. The results showed that 44% malaria-infected blood had the largest proportion. Next, 10% malaria-infected blood also had a larger proportion than case of normal blood.

CHAPTER 6

CONCLUSION AND FUTURE WORK

6.1 Conclusion

Malaria is a life-threatening disease caused by *Plasmodium* parasite. It is treatable and preventable depending on the time of diagnosis and regular ongoing examinations. Therefore, the diagnosis time is the key factor for patient's survive which affects severe malaria patients at most in order to response the treatment and adjust medicine in time. Nowadays, there are many techniques to replace traditional microscopic methods that integrated advanced technology for helping reduce diagnosis time such as microfluidics and impedance measurement. Recent research showed the good results, but it is still not suitable for using in field because of its complexity and control calibration. Therefore, we carried on Microfluidic System for Detecting Malaria-Infected Red Blood Cells Using Impedance Measurement Coupled with Electromagnetic Force to complete the uncomplicated and ready-to-use system for finding percentage parasitemia of malaria.

Our concept was to develop and improve the system that can differentiate percentage parasitemia by measuring impedance of two symmetrically located electrodes that we use electromagnetic field for cell enrichment in T-shaped microchannel. The reason, that we divided our system to be cell enrichment part and impedance measurement part, was reducing the complicated system. On the other hand, we compared two pair of electrodes with the same distance because of its cancellation of interference.

Our system contained many parts: 3D-printed connector, PDMS microchannel, PCB's electrodes, laser-cut acrylic plates, syringe, needle, and tubes to fix into one system connected to electromagnet with DC power supply for cell enrichment and DG8SAQ VNWA 3 for impedance measurement. The PDMS microchannel was created by pouring the PDMS into the aluminium mold and peel it out. Then, electrodes on PCB were created by designing the PCB and ordering custom-made PCB to get our desired electrodes. Next, a 3D-printed connector was created by plastic 3D printing and acrylic plates were created by a laser-cut technique to shape our system to be rigid. In addition, a syringe, a needle, and tubes was used to contain test sample, as well as be one inlet and two outlets. Once we combined all parts together, we connected electromagnet with DC power supply and DG8SAQ VNWA 3 and we were ready for an experiment.

Before we measured impedance signal, we had to clarify the reliable of the tool that we used. We calibrated DG8SAQ Vector Network Analyzer in range 10 kHz-10 MHz with compared between measurement and calculation of RC circuit using a capacitor 68 pF and 3 resistors: 47 Ω , 1 k Ω , and 10 k Ω . RC circuit calibration showed us that DG8SAQ Vector Network Analyzer was a reliable tool with resistor 47 Ω - 10 k Ω and capacitor 68 pF frequency range 100 kHz-10 MHz. We mostly used resistance and reactance with the range of 185 kHz-10 MHz, in case of resistor 1 k Ω

and capacitor 68 pF, that matched with the calculation to refer reliable measurement of cells.

Then, we conducted the proof-of-concept experiment that using plastic beads as a representative of healthy red blood cells (hRBCs) and magnetic beads as a representative of malaria-infected red blood cells (iRBCs). The proof-of-concept experiment showed us that our system was symmetrically flow with less than 33% difference comparing both sides of 3 experiment batches. Furthermore, the number of magnetic beads was increasing depending on the higher voltage we provided in electromagnet-applied side, and the number of magnetic beads was decreasing at the opposite side of 3 experiment batches. That was shown that our enrichment part can work well.

After that, we did experiments in plastic test to see the effect of particles at various density diluted in DI water. We measured impedance for finding out the signal changes after 5 minutes in static method by dropping sample on electrodes, and dynamic method by flowing through system after 5 minutes. The plastic samples had varied density which was at 200,000 beads/ml, 300,000 beads/ml and 600,000 beads in static test, and 600,000 beads/ml, 750,000 beads/ml, and 1,500,000 beads/ml in dynamic test. The plastic impedance test showed us that the resistance was greatly increased, and the reactance was gradually increased both in static and dynamic test if we increased the density in frequency 100 kHz-10 MHz.

Similarly, we did experiments in the normal and malaria-infected blood test to see the effect of cells at various density in static test and the cell enrichment phenomena, which had clarified differences in impedance signal, in case of dynamic test. We used normal mouse blood, 10% parasitemia malaria-infected blood, and 44% parasitemia malaria-infected blood to be our experiment samples. The normal and malaria-infected blood impedance test showed us that we can distinguish the signal between normal red blood cells, 10% parasitemia, and 44% parasitemia malaria-infected red blood cells in impedance measurement part and can see the different signal of the side that is near electromagnet and the other side. Moreover, we can find the ratio of infection from normalized different between before applied electromagnetic field and after applied electromagnetic field of each outlet, and normalized different between two outlets that tell us the proportion of each parasitemia.

This research was successful and fulfilled its objectives that was to develop a system to distinguish the state of malaria infection by using impedance of cell suspension and electromagnetic force for cell enrichment in order to detect the ratio of infection of malaria and tell us the severity of disease by finding percentage parasitemia. Moreover, we have done a lot of experiments to make our experiment reliable. Begin with RC circuit calibration, our impedance measurement equipment was reliable in the frequency range of measurement that matched both plastic test and malaria-infected blood. According to the results of plastic test and malaria-infected blood, we noticed the difference in density and types of cells, including the changed signal in terms of both resistance and reactance. Importantly, we can find the different ratio in order to be our criteria to find percentage parasitemia.

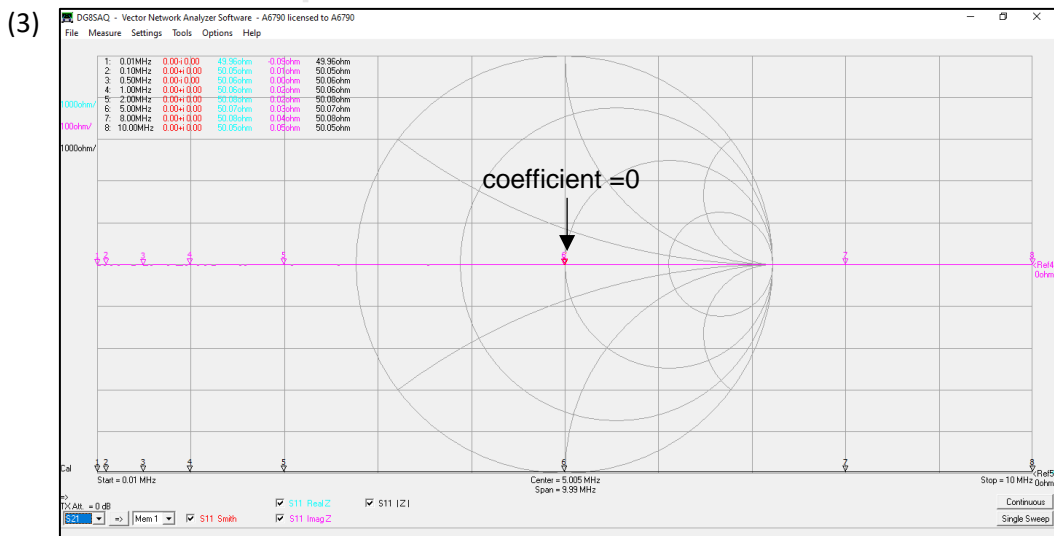
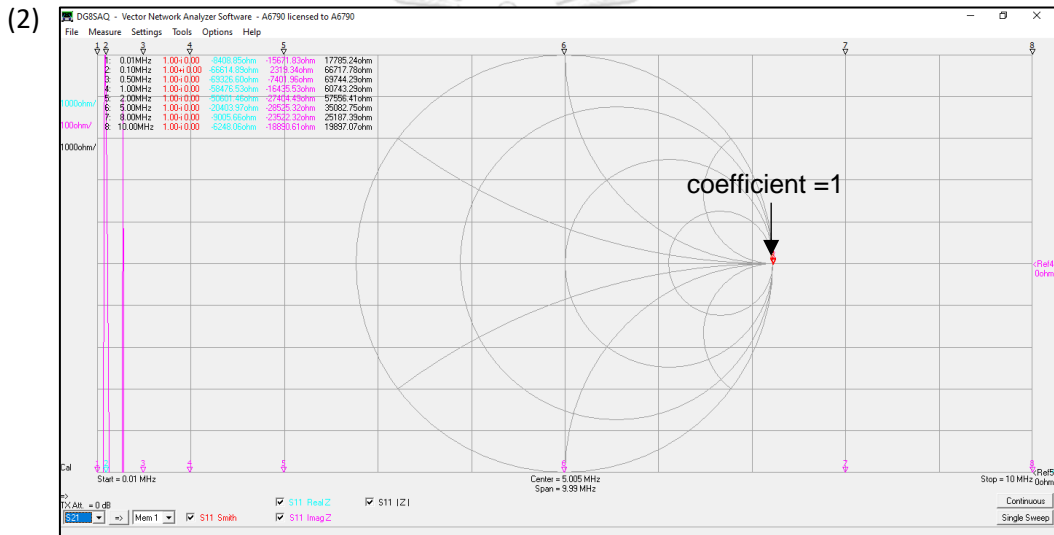
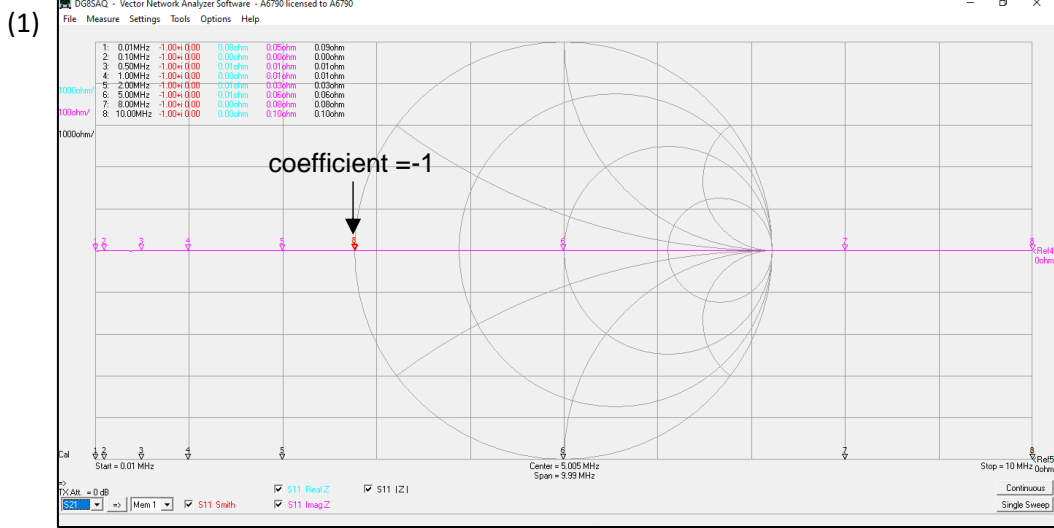
6.2 Future work

This research had a strong potential to be Point-of-Care percentage parasitemia detection to use in field because there is no need for training and additional sample preparation. However, we have to modify many parts of our system to downsizing the system to proper use with microliter blood testing and integrated automated embedded system with PCB design. If we can make our system flow symmetrically, we can investigate only the peak at frequency 100 kHz-10 MHz in order to be one of criteria to tell the distinguished percentage parasitemia.

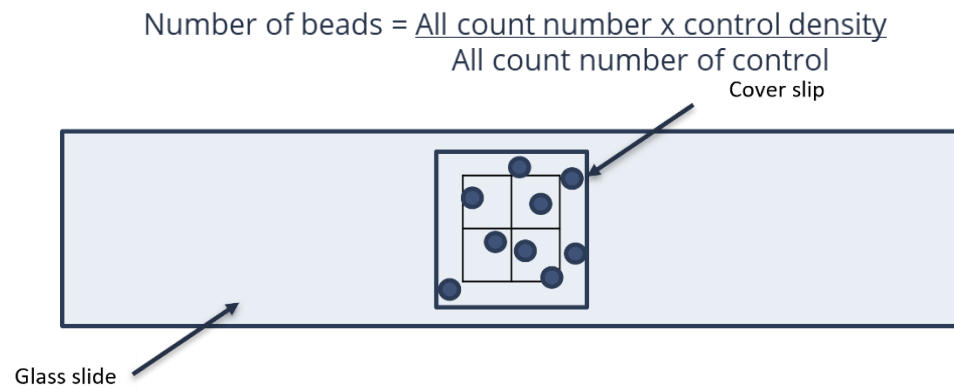


APPENDIX

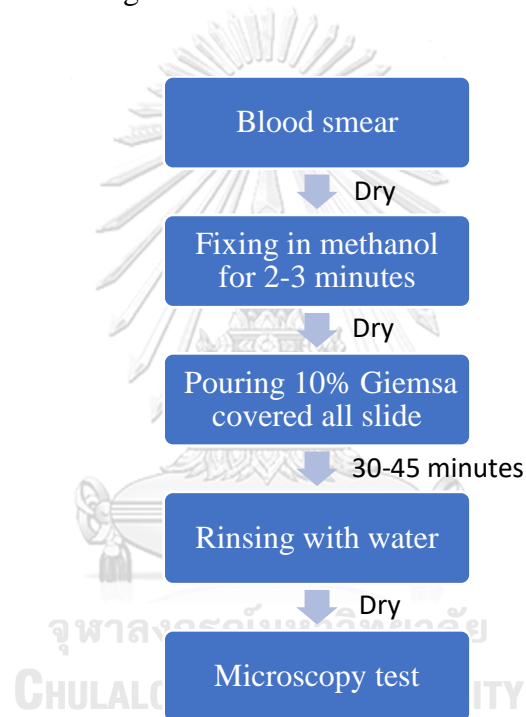
Appendix Figure 1 The previous version of connector.



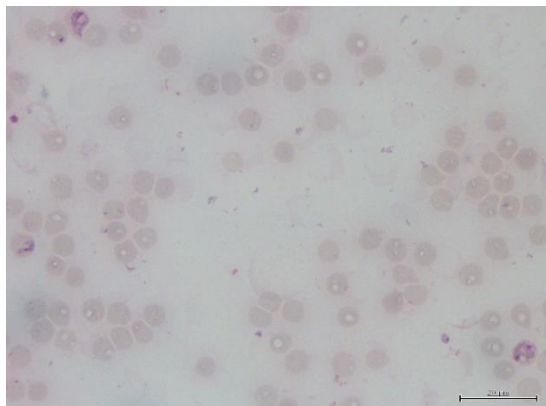
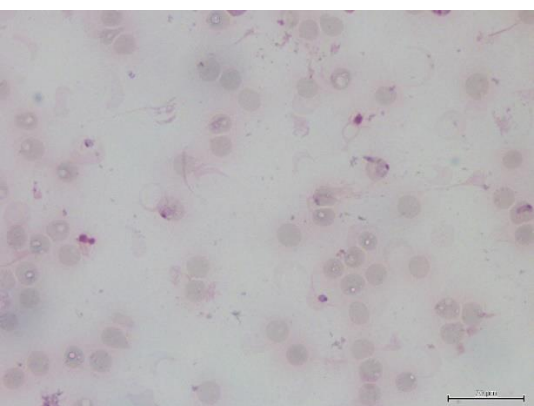
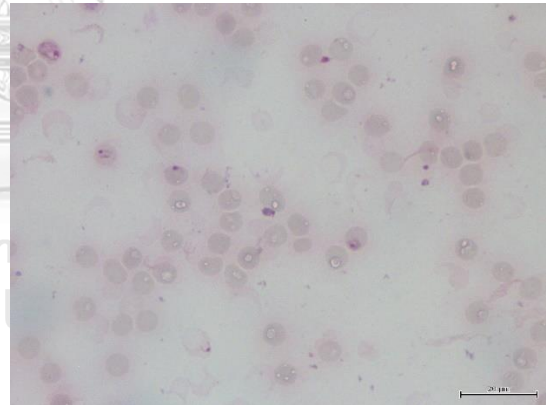
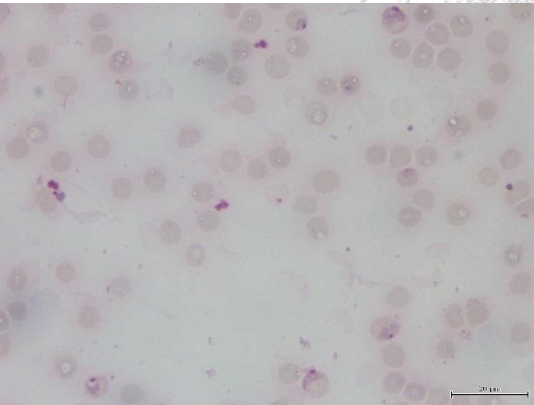
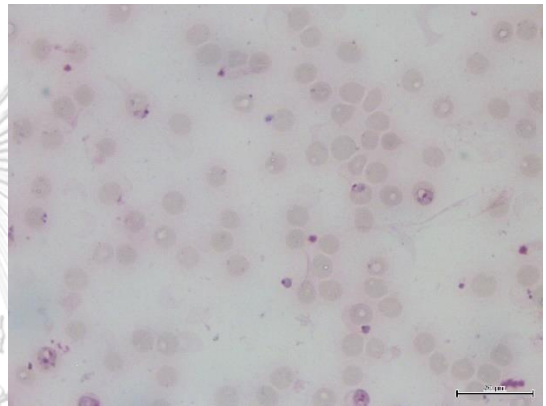
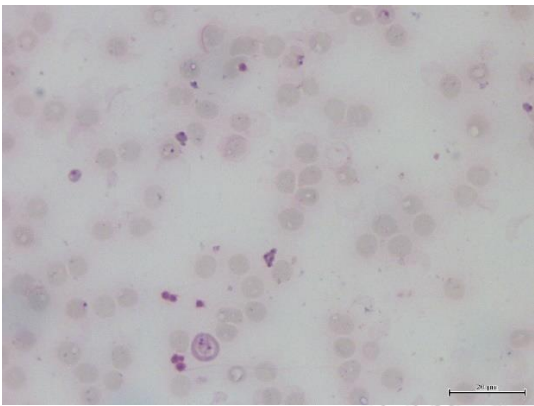
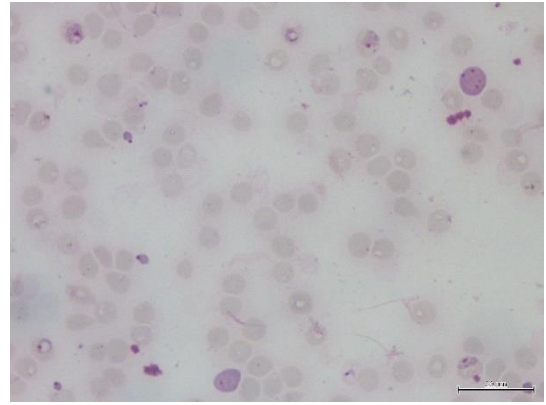
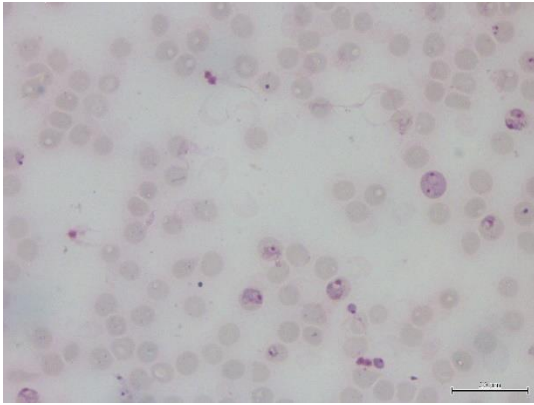
Appendix Figure 2 Smith chart of 10 kHz-10 MHz calibration. (1) Short calibration. (2) Open calibration. (3) Load calibration.

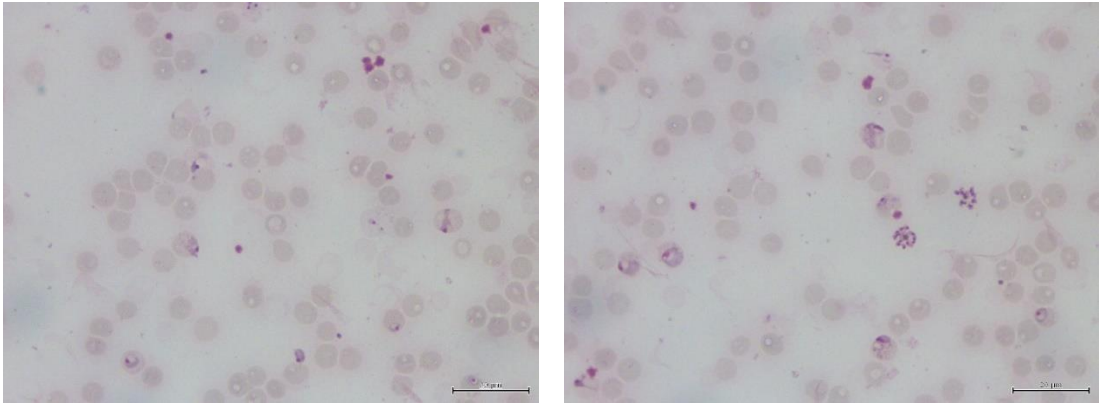


Appendix Figure 3 Counting number method.

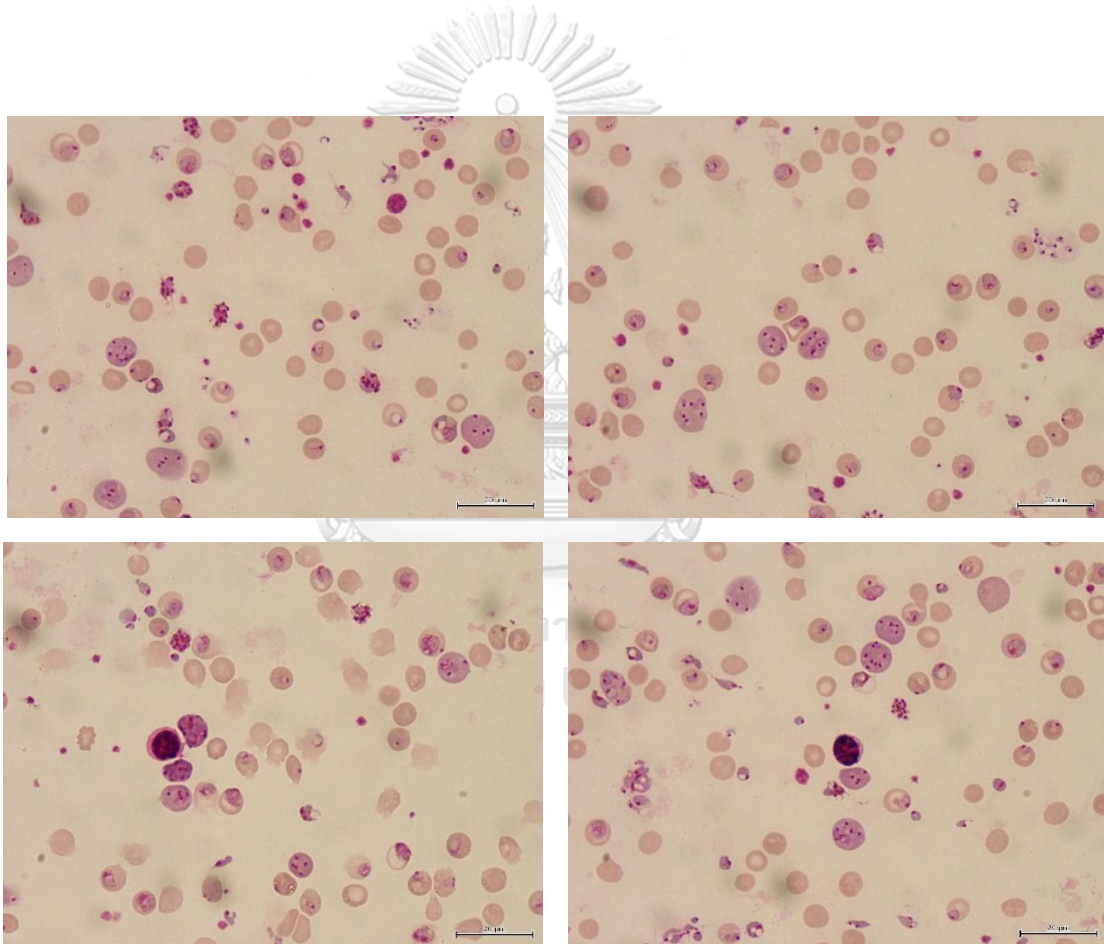


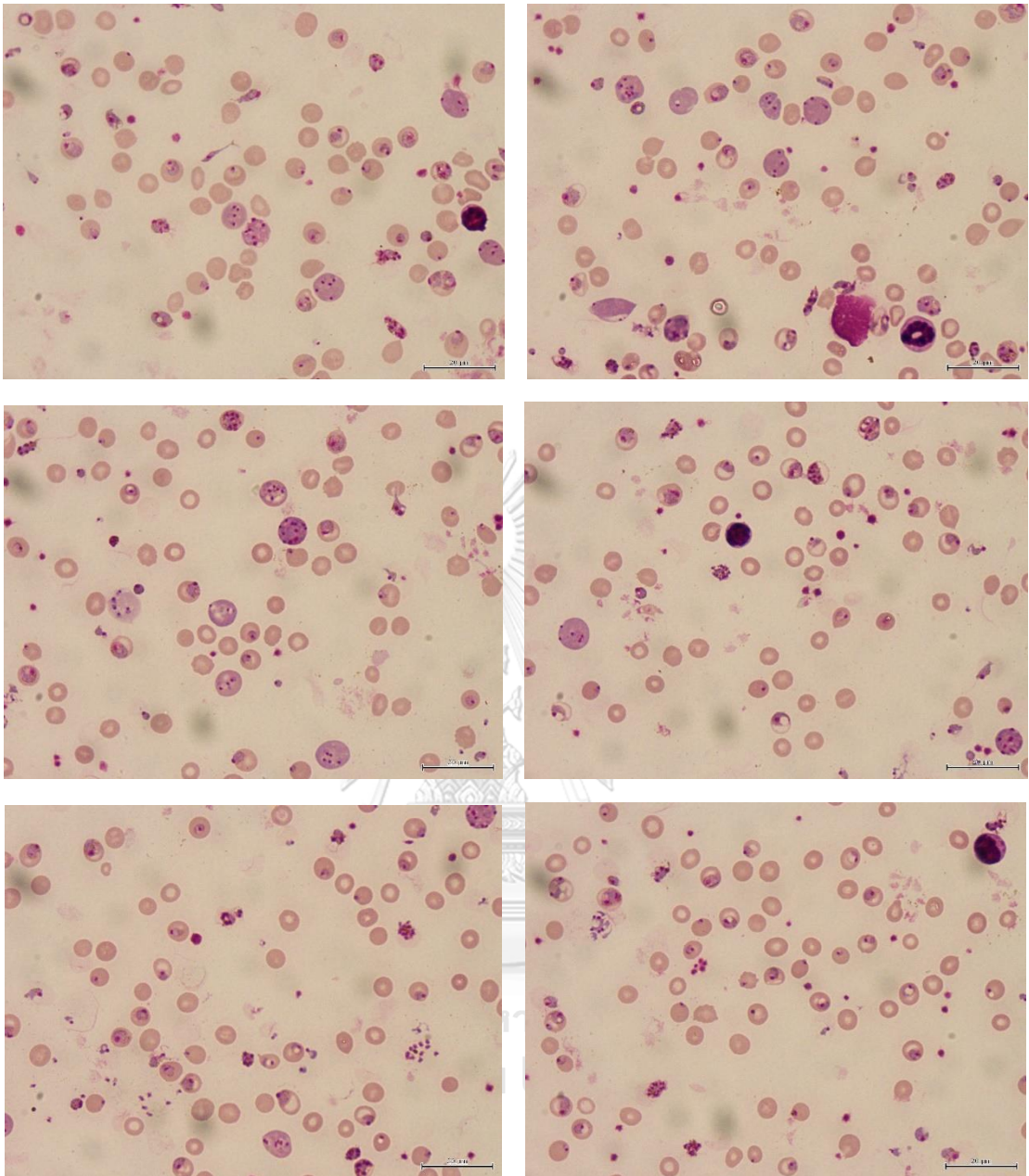
Appendix Figure 4 Giemsa stain procedure.





Appendix Figure 5 All fields of 10% parasitemia red blood cells.





Appendix Figure 6 All fields of 44% parasitemia red blood cells.

REFERENCES



จุฬาลงกรณ์มหาวิทยาลัย
CHULALONGKORN UNIVERSITY

- [1] U. S. D. o. H. H. Services. "Malaria." Centers for Disease Control and Prevention. <https://www.cdc.gov/malaria/about/biology/index.html> (accessed.
- [2] U. S. D. o. H. H. Services. "Malaria/Disease." Centers for Disease Control and Prevention. <https://www.cdc.gov/malaria/about/disease.html> (accessed.
- [3] M. C. D. INTERNATIONAL. "Diagnostic Finding Malaria." MEDICAL CARE DEVELOPMENT INTERNATIONAL. https://www.mcdinternational.org/trainings/malaria/english/DPDx5/HTML/Frames/M-R/Malaria/body_Malaria_MolDiag (accessed.
- [4] I. S. A. C. P. F. W. N. V. A. M. I. GREECE. " Laboratory diagnosis." MALWEST (Malaria-West Nile Virus). <http://www.malwest.gr/en-us/malaria/informationforhealthcareprofessionals/laboratorydiagnosis.aspx> (accessed.
- [5] C. W. Pirstill and G. L. Cote, "Malaria Diagnosis Using a Mobile Phone Polarized Microscope," *Sci Rep*, vol. 5, p. 13368, Aug 25 2015, doi: 10.1038/srep13368.
- [6] R. N. Deraney, C. R. Mace, J. P. Rolland, and J. E. Schonhorn, "Multiplexed, Patterned-Paper Immunoassay for Detection of Malaria and Dengue Fever," *Anal Chem*, vol. 88, no. 12, pp. 6161-5, Jun 21 2016, doi: 10.1021/acs.analchem.6b00854.
- [7] N. Kolluri, C. M. Klapperich, and M. Cabodi, "Towards lab-on-a-chip diagnostics for malaria elimination," *Lab Chip*, vol. 18, no. 1, pp. 75-94, Dec 19 2017, doi: 10.1039/c7lc00758b.
- [8] J. Wu, R. Kodzius, W. Cao, and W. Wen, "Extraction, amplification and detection of DNA in microfluidic chip-based assays," *Microchimica Acta*, vol. 181, no. 13-14, pp. 1611-1631, 2013, doi: 10.1007/s00604-013-1140-2.
- [9] L. M. Coronado, C. T. Nadovich, and C. Spadafora, "Malarial hemozoin: from target to tool," *Biochim Biophys Acta*, vol. 1840, no. 6, pp. 2032-41, Jun 2014, doi: 10.1016/j.bbagen.2014.02.009.
- [10] S. Kasetsirikul, J. Buranapong, W. Srituravanich, M. Kaewthamasorn, and A. Pimpin, "The development of malaria diagnostic techniques: a review of the approaches with focus on dielectrophoretic and magnetophoretic methods," *Malar J*, vol. 15, no. 1, p. 358, Jul 12 2016, doi: 10.1186/s12936-016-1400-9.
- [11] P. A. Zimmerman, H. Fujioka, J. M. Thomson, M. Zborowski, and W. E. Collins, "Diagnosis of Malaria by Magnetic Deposition Microscopy," *The American Journal of Tropical Medicine and Hygiene*, vol. 74, no. 4, pp. 568-572, 2006, doi: 10.4269/ajtmh.2006.74.568.
- [12] T. Sun and H. Morgan, "Single-cell microfluidic impedance cytometry: a review," *Microfluidics and Nanofluidics*, vol. 8, no. 4, pp. 423-443, 2010, doi: 10.1007/s10404-010-0580-9.
- [13] E. Du, S. Ha, M. Diez-Silva, M. Dao, S. Suresh, and A. P. Chandrakasan, "Electric impedance microflow cytometry for characterization of cell disease states," *Lab Chip*, vol. 13, no. 19, pp. 3903-3909, Oct 7 2013, doi: 10.1039/c3lc50540e.
- [14] M. Mansor, M. Takeuchi, M. Nakajima, Y. Hasegawa, and M. Ahmad, "Electrical Impedance Spectroscopy for Detection of Cells in Suspensions

- Using Microfluidic Device with Integrated Microneedles," *Applied Sciences*, vol. 7, no. 2, 2017, doi: 10.3390/app7020170.
- [15] *Management of severe malaria: a practical handbook*, 3rd edition ed. Geneva, Switzerland: World Health Organization, 2012.
- [16] N. Mohandas and X. An, "Malaria and human red blood cells," *Med Microbiol Immunol*, vol. 201, no. 4, pp. 593-8, Nov 2012, doi: 10.1007/s00430-012-0272-z.
- [17] X. Yang, Z. Chen, J. Miao, L. Cui, and W. Guan, "High-throughput and label-free parasitemia quantification and stage differentiation for malaria-infected red blood cells," *Biosens Bioelectron*, vol. 98, pp. 408-414, Dec 15 2017, doi: 10.1016/j.bios.2017.07.019.
- [18] C. Petchakup, K. Li, and H. Hou, "Advances in Single Cell Impedance Cytometry for Biomedical Applications," *Micromachines*, vol. 8, no. 3, 2017, doi: 10.3390/mi8030087.
- [19] B. Bhushan, *Encyclopedia of Nanotechnology*. 2012.
- [20] J. C. Maxwell, "Magnetic Problems," in *A Treatise on Electricity and Magnetism*, 2010, ch. Chapter v, pp. 56-73.
- [21] K. R. Foster and H. P. Schwan, "Dielectric properties of tissues and biological materials: a critical review," *Critical reviews in biomedical engineering*, vol. 17, no. 1, pp. 25-104, 1989.
- [22] C. Honrado, L. Ciuffreda, D. Spencer, L. Ranford-Cartwright, and H. Morgan, "Dielectric characterization of Plasmodium falciparum-infected red blood cells using microfluidic impedance cytometry," *J R Soc Interface*, vol. 15, no. 147, Oct 17 2018, doi: 10.1098/rsif.2018.0416.
- [23] M. I. Altaf and A. Ahmad, "Dielectric Properties of Malaria Parasite Infected Human Blood," *International Journal of Innovative Research in Science, Engineering and Technology*, vol. 6, no. 2, 2017, doi: 10.15680/IJIRSET.2017.0602071.
- [24] B. M. G. Rosa and G. Z. Yang, "Portable Impedance Analyzer as a Rapid Screening Tool for Malaria: An Experimental Study With Culture and Blood Infected Samples by Early Forms of Plasmodium Falciparum," *IEEE Trans Biomed Eng*, vol. 67, no. 12, pp. 3531-3541, Dec 2020, doi: 10.1109/TBME.2020.2990595.
- [25] M. Hejazian, W. Li, and N. T. Nguyen, "Lab on a chip for continuous-flow magnetic cell separation," *Lab Chip*, vol. 15, no. 4, pp. 959-70, Feb 21 2015, doi: 10.1039/c4lc01422g.
- [26] S. Huang, Y.-Q. He, and F. Jiao, "Advances of Particles/Cells Magnetic Manipulation in Microfluidic Chips," *Chinese Journal of Analytical Chemistry*, vol. 45, no. 8, pp. 1238-1246, 2017, doi: 10.1016/s1872-2040(17)61033-8.
- [27] J. Nam, H. Huang, H. Lim, C. Lim, and S. Shin, "Magnetic separation of malaria-infected red blood cells in various developmental stages," *Anal Chem*, vol. 85, no. 15, pp. 7316-23, Aug 6 2013, doi: 10.1021/ac4012057.

VITA

NAME Prapapan Sonridhi

DATE OF BIRTH 25 January 1996

PLACE OF BIRTH Bangkok

INSTITUTIONS ATTENDED Graduated from Sirindhorn International Institute of Technology (SIIT), Thammasat University, 2017.
Attending Biomedical Engineering Program, Faculty of Engineering, Chulalongkorn University, 2018.

HOME ADDRESS 45/45 LeabKlongSong32 rd,
BangChan Sub-district, KlongSamWa District, Bangkok,
Thailand 10510

PUBLICATION Design of Microfluidic System for Detecting Percentage Parasitemia of Malaria-Infected Red Blood Cells Using Impedance Measurement, published in Proceedings of The 11th TSME International Conference on Mechanical Engineering (ICoME 2020)